Space-time isogemetric methods for multi-field problems in mechanics

Christelle Saade

ED 353 SCIENCES POUR L'INGENIEUR : MECANIQUE, PHYSIQUE, MICRO ET NANOELECTRONIQUE

Spécialité : Mécanique des solides

Thèse

Pour obtenir le grade de

DOCTEUR DE L'ECOLE CENTRALE MARSEILLE

Par

Christelle SAADE

Méthodes isogéométriques espace-temps pour des équations multi-champs en mécanique

Soutenue le 03/12/2020 devant le jury suivant :

Thomas Elguedj	INSA de Lyon	Rapporteur
Piotr Breitkopf	CNRS, UTC	Rapporteur
Robin Bouclier	INSA de Toulouse	Examinateur
Raphaèle Herbin	Aix-Marseille Université	Examinateur
Pierre-Alain Boucard	ENS Paris-Saclay	Examinateur
Pierre Lamy	Smac Toulon	Invité
Roy Saad	Université Libanaise Fanar	Invité
Dominique Eyheramendy	Ecole Centrale de Marseille, LMA	Directeur
Stéphane Lejeunes	CNRS, LMA	Co-directeur

Numéro national de thèse : 2020ECDM0011

I, undersigned, Christelle Saadé, hereby declare that the work presented in this manuscript is my own work, carried out under the scientific direction of Dominique Eyheramendy and Stéphane Lejeunes, in accordance with the principles of honesty, integrity and responsibility inherent to the research mission. The research work and the writing of this manuscript have been carried out in compliance with both the french national charter for Research Integrity and the Aix-Marseille University charter on the fight against plagiarism.

This work has not been submitted previously either in this country or in aother country in the same or in a similar version to any other examination body.

Marseille, 03 December 2020

Christelle Saadé

Acknowledgements

This dissertation was written between 2017 and 2020 during my PhD years at the LMA (Laboratoire de Mécanique et d'Acoustique), Marseille, France.
It was done under the hospice of the SMAC company based in Toulon which manufactures elastomer parts for the aerospace industry. This work is the result of a very enriching experience sculpted by various people that I would like to thank here.

I would like first to sincerely thank my first supervisor Prof. Dominique Eyheramendy for giving me the opportunity to work with him during this PhD. I would also like to thank my second supervisor, Dr. Stéphane Lejeunes, for his huge help during these 3 years. If not for him, I would not have been able to get along with understanding the important skills of numerical computing and programming. The patience, assistance and inspiration that my two supervisors gave me is very much appreciated, they were a large contribution to the work included in this thesis.

I would also like to thank the ECM (Ecole Centrale Marseille) and the Région Sud Provence Alpes Côte d'Azur for the funding of the PhD. Their funding is gratefully acknowledged.

Furthermore, I would like to thank the members of my examining jury Prof. Thomas Elguedj and Prof. Piotr Breitkopf. I would like to also thank Dr. Robin Bouclier and Prof. Raphaèle Herbin for taking part of the jury panel.

Finally, I would like to thank my parents Elias and Ghada Saadé for their continuous encouragement and support.

Christelle Saadé

Marseille, France
December, 2020

Abstract

In this work, we introduce different weak formulations based on time continuous Galerkin methods for several types of problems, governed by partial differential equations in space and time. Our approach is based on a simultaneous and arbitrary discretization of the space and time. The Isogeometric Analysis (IGA) is employed instead of the classical Finite Element Method (FEM) in order to take advantage of the continuity properties of B-splines and NURBS functions. A detailed state of the art is narrated first to introduce the concept of both of these methods and to show the work already done in literature regarding the space-time methods on a first basis, and the IGA on a second basis. Then, the methods are applied to different types of mechanical problems. These problems are mainly engineering problems such as elastodynamics, thermomechanics, and history dependant behaviors (viscoelasticity). We compare different types of variational formulations and different discretizations. We show that in the case of problems having discontinuous solutions such as impact problems, the use of both a formulation with derived in time test functions and additional least square terms makes it possible to avoid the spurious numerical oscillations often observed for these type of problems. Furthermore, we introduce a new stabilization technique that can be used easily for non-linear problems. It is based on the consistency condition of the acceleration, so we call it Galerkin with Acceleration Consistency (GAC). The problems investigated take both linear and non-linear forms. We solve elastodynamics, thermomechanics and viscoelatic type problems at small and finite strains. Both compressible and incompressible materials are considered. The convergence of the method is numerically studied and compared with existing methods. We verify, where applicable, the conservation properties of the formulation and compare them to the conservation properties of the classical methods such as the FEM equipped with an HHT scheme for the time discretization. The numerical results show that space-time methods are more energy conserving than classical methods for the elastodynamic problems. Different convergence tests are leaded and optimal convergence rates are obtained, showing the efficiency of the method. We show furthermore that heterogeneous and asynchroneous schemes can be built in a very simple manner, opening up many possibilities while dealing with space-time methods. Finally, the performances observed on different problems and the versatility of the approach suggest that ST IGA methods have a strong potential for advanced simulations in engineering.

Keywords: Space-time methods, isogeometric analysis, coupled multiphysics, viscoelastic wave equation, thermomechanics, continuous Galerkin method, optimal rates of convergence

Résumé

Dans ce travail, nous introduisons différentes formulations faibles basées sur des méthodes de Galerkin continues en temps pour plusieurs types de problèmes, pilotés par des équations aux dérivées partielles dans l'espace et le temps. Notre approche repose sur une discrétisation simultanée et arbitraire de l'espace et du temps. L'analyse isogéométrique (IGA) est utilisée comme outil de discrétisation à la place de la méthode classique des éléments finis (FEM) afin de bénéficier des propriétés de continuité des fonctions B-splines et NURBS. Un état de l'art détaillé est présenté pour introduire le concept de ces deux méthodes et pour montrer les travaux déjà réalisés dans la littérature concernant les méthodes espace-temps d'une part, et l'IGA d'une autre part. Les méthodes seront combinées et appliquées à différents types de problèmes mécaniques. Ces problèmes sont principalement des problèmes d'ingénierie tels que l'élastodynamique, la thermomécanique et les problèmes viscoélastiques. On compare différents types de formulations variationnelles et différentes configurations de discrétisation. On montre que dans le cas de problèmes ayant des solutions discontinues en temps comme les problèmes d'impact, l'utilisation conjointe d'une formulation avec des fonctions test dérivées en temps et des termes de stabilisation de type moindres carrés permettent de contrôler les oscillations numériques souvent observées pour ce type de problèmes. De plus, nous introduisons une nouvelle stratégie de stabilisation qui peut être utilisée facilement pour des problèmes non linéaires. Celle-ci est basée sur la condition de consistence de l'accélération, nous l'appelons donc Galerkin avec consistence sur l'accélération. Les problèmes étudiés prennent donc à la fois des formes linéaires et non linéaires. Nous résolvons des problèmes en petites et en grandes déformations: que ce soit pour l'élastodynamique, la thermomécanique ou pour les problèmes de type viscoélatique. Des matériaux compressibles et incompressibles sont considérés. La convergence de la méthode est étudiée numériquement et comparée aux méthodes existantes. Nous vérifions autant que possible les propriétés de conservation de la formulation et les comparons aux propriétés de conservation des méthodes classiques telles que la FEM équipée d'un schéma HHT en temps. Les résultats numériques montrent que la méthode espace-temps est plus conservative en énergie que les méthodes classiques pour les problèmes d'élastodynamique. Différents tests de convergence sont menés et des taux de convergence optimaux sont obtenus à chaque fois, montrant l'efficacité de la méthode. Nous montrons en outre que des schémas hétérogènes et asynchrones peuvent être construits d'une manière très simple, ouvrant à de nombreuses possibilités avec les méthodes espace-temps. Enfin, les performances observées sur différents problèmes et la polyvalence de l'approche suggèrent que les méthodes IGA espace-temps ont un fort potentiel dans le domaine de la simulation numérique en ingénierie.

Mots clés: Méthodes espace-temps, analyse isogéométrique, problèmes multiphysiques, problèmes viscoélastiques, thermomécanique, méthode de Galerkin continue, taux optimaux de convergence

Contents

List of Figures

List of Tables

Introduction

Engineering problems are encountered in everyday's life and concern the design, building, and use of engines, machines, and structures. These problems are modelled and simulated by advanced numerical models that mostly consider space and time as separate variables. The space discretization is done with FEM or Finite Volume Method (FVM) in most of the commercial softwares available, and the time discretization is done with time advancing scheme, such as the Hilber-Hughes-Taylor (HHT) method, the explicit central difference method, implicit Crank–Nicolson schemes, etc. While these modelling strategies are robust in most cases, they nevertheless have limitations or drawbacks. The first drawback is due to the fact that time advancing can be only done in a sequential manner. Therefore, if one needs to compute the full history of a part with a time dependent nonlinear material for a high cycle fatigue conditions, the computational power of even an hpc system might be of no help. A second drawback appears in the case of multiphysics problems where each physics may have a huge difference in its characteristic times while being strongly coupled. In this case, if one adopts a fully coupled resolution, the global time step will be constrained by the shortest characteristic time. And if one uses a staggered scheme, divergence from the fully coupled problem may be observed. These typical problems occur, for example, in the case of elastomer-based structures for which we can have very complex material models (viscoelasticity, damage, dynamic softening, etc) and strongly coupled multiphysics (thermo-mechanical or thermo-chemo-mechanical, etc). In this work, we propose to explore a more original method for solving different engineering problems, including elastodynamics and thermomechanics. The originality is the combination of the so-called space-time method, with the Isogeometric Analysis. This combination may offer great potential in the solving of engineering problems and may help to overcome the difficulties mentionned above caused by traditional methods.

The space-time methods are very promising for the resolution of many types of problems. They may be efficient in the resolution of inverse type problems, where the solution is known at the final time and is to be computed at the initial one. These methods may also be promising for the treatment of problems having internal variables (viscoelasticity, for example). Moreover, parallel methods not only in space but also in time are possible as well due to space-time methods.

Our aim in this work is to investigate the efficiency of the space-time methods together with the isogeometric analysis for different kinds of problems. These problems are mainly mechanical ones where multi-fields are used in the variational

formulations. In this manuscript, the space-time isogeometric method was compared to classical methods such as the finite element method equipped with a classical time solver such as an HHT scheme. We show that this method may help gain more stability in numerical schemes compared to explicit solvers where the CFL condition is necessary to be fulfilled. Moreover, space-time methods are more energy conservative than traditional schemes. It was also proven in the literature that it allows to control numerical oscillations encountered while solving complex problems having discontinuous solutions such as impact problems. In such problems, classical methods fail to provide accurate solutions, often giving solutions with numerous oscillations and therefore a larger numerical error. But classical variational formulations in the context of space-time methods could not solve these types of problems and additionnal terms should be added to the formulation to reduce the oscillations.

We investigate the choice of the test functions employed in the variational formulations. Instead of using classical test functions, we use test functions that are derived in time (Petrov-Galerkin type formulations). This choice of replacing regular test functions with derived ones is discussed, and different examples are provided in the discussion for problems where a comparison between using both types of functions was made.

In the context of thermomechanical models, we investigate the choices of discretization for multi-field formulations : we employ a grid that is finer in time for some fields, displacement and velocity, and coarser for others, the temperature. On a second basis, we test the use of a smaller degree for the temperature field in comparison with the displacement and velocity fields. This shows the possibility of using heterogeneous (using multiple patches in space-time) and asynchroneous (using multi-grids in time) schemes when space-time methods are employed. For time dependent behaviors with internal variables as the case of viscoelasticity, we propose new formulations for which the treatment of the internal variables is made as regular variables that are discretised over the space-time domain. This allows to get rid of the global/local paradigm that is mainly used in standard models. We show that promising results can be obtained with this approach, opening lots of new possibilities and applications.

This thesis lies within the following context : in a previous work [102], IGA was implemented in an in-house code, femJava, that allows to straightfowardly treat multi-field and multiphysics problems with FE. Elemental and material formulations are independent of the approximation field and the same code can be solved with either B-splines or NURBS approximation, or classical Lagrange polynomial approximations. In [102], the focus was done on convergence properties of IGA and the implementation of nonlinear thermoelastic couplings and nearly incompressible hyperelastic behaviors with IGA. In [5], nonlinear thermochemomechanical problems in rubbers have been investigated. These problems lead to complex numerical formulations and the time integration scheme is clearly a limiting aspect of standard

methods in these cases. Therefore, our ambition in this thesis is to develop new tools that will help to overcome current limits for complex nonlinear and multiphysics evolution problems in mechanics.

In chapter 1, a state of the art is provided for space-time methods and IGA and basic principles for both methods are discussed. Numerous references for which space-time methods are adapted in the resolution of engineering problems are observed. The authors used finite elements discretization or a richer discretizaton such as the IGA. The interest of using such methods is discussed and examples taken from literatures are shown proving the true interest behind the use of such methods in numerical analysis. Comparisons between these methods and classical ones such as the Implicit Euler method or the trapezoidal rule are provided. Only few references exist where the space-time isogeometric method is employed, but this method could nowadays be used without any impediment due to the efficiency of modern softwares and hardware systems. In Chapter 2, the space-time isogeometric method was employed in the resolution of elastodynamics equation. In Chapter 3, the method was used for the resolution of multiphysics equations, more precisely for thermomechanics, and in Chapter 4, the method was applied for solving viscoelastic problems. Optimal convergence rates were obtained for several applications, including elastodynamics or thermomechanics. All the problems were solved at small and finite strains, showing the efficiency of the method for linear and nonlinear cases. To our knowledge, it is the first time that the space-time method is employed for solving finite strains elastodynamics, thermomechanics and viscoelastodynamics including compressible and nearly incompressible cases.

1. State of the art of isogeometric and space-time methods

This chapter is dedicated to the description of the state of art of space-time methods and the isogeometric method. In the literature, one can see that the space-time method or the isogeometric analysis can be applied for the resolution of a wide range of problems such as elastodynamics problems, heat propagation problems, contact problems, shell and plate problems, structural dynamics problems, etc. The results taken from literature show the differences between IGA and the FEM on one hand, ST methods and semi-discrete ones on the other hand. These comparisons emphasis the interest of the ST IGA method. Moreover, we cite examples where stability and convergence analysis were proposed for different kinds of space-time formulations, whether it's in a continuous or in a discontinuous Galerkin context, showing that the space-time formulations possess a strong mathematical firm. We explain as well our point of view and the reason that made us use these specific methods in our numerical study.

1.1. Isogeometric Analysis: A global overview

Engineering and applied mathematics problems are mostly modelled by a set of PDEs to be solved numerically. The finite element method is one of the most widely adopted methods used for solving such problems. The main idea of this method is to solve boundary value problems based on a variational formulation and to approximate the domain and the solution on adequate polynomial space. This leads to a system of simple algebraic equations. The domain of definition of the PDE is decomposed into simple shapes called elements (triangles, squares, rectangles, hexahedra, tetrahedral, etc). In [45], this method is detailed and applied to statics and dynamics. While the finite element method is widely used and proved to be efficient in lots of mathematical physics and engineering problems, it has also some limitations. First, the solution is built with a low order of continuity, typically C^0-continuous interpolation on the boundary of the element. In some cases, higher orders are used; these cases are the construction of thin shells, for example, or thin plates. Second, inter-element low order continuity and low order polynomial approximation have a negative impact on the accuracy of the shape. The IGA was introduced in 2005 by Hughes and al. in [43] as a numerical method that offers real perspectives in the integration of geometric and computational models. The isogeometric method is linked to the finite element method given that both are based on the same variational frame. The fundamental concept of the IGA is to

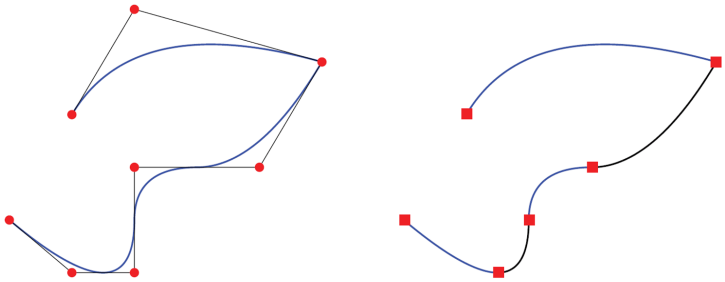

(a) Curve and control points (b) Curve and mesh denoted by knot locations

Figure 1.1. – B-spline, piecewise quadratic curve in $\mathbb{R}^2$. The knots are denoted by red squares, control points by red dots (figure taken from [23])

employ the basis functions used for geometric description as a discretization tool for analysis as well: the same basis functions (B-splines and NURBS) are used for both describing the geometry of the computational domain and approximating the solution. This method has shown very good numerical qualities even with coarse meshes (numerical accuracy, capacity in supporting large deformations...). It allows, on one hand, to exactly represent complex geometries, and on the other hand, to enrich the approximation basis compared to classical Lagrange polynomials (higher order of continuity between elements) which is highly important due to the fact that complex geometries can be made and represented in CAD design tools. Spline functions are widely used in computer graphics to manage surfaces and geometries. Via these functions and the control points, complex shapes and surfaces can be approximated through curve fitting. Splines are popular and simple to build (see Figure 1.1 for an example of a B-spline curve). In numerical analysis, B-spline interpolation is considered better than polynomial interpolation because it can keep the interpolation error small without the need of high degree polynomials, avoiding in this way the Runge's phenomenon, that states that oscillation problems can be occurred at the edges of an interval when using polynomial interpolation with polynomials of high degree.

1.1.1. B-splines or NURBS for IGA

B-Spline functions are defined from a knot vector which is a set of points, a sequence of ordered numbers, defined in a parametric space (the parametric space has the same dimension as the physical space). A knot vector is written by $E = \{\xi_1, \xi_2, ..., \xi_{n+p+1}\}$, where:

- $\xi_i \in \mathbb{R}$ is the i^{th}element of the sequence
- i is the knot index, $i = 1, 2, ..., n + p + 1$
- p is the polynomial order
- n is the number of basis functions used to construct the B-spline curve

(1.1)

The interval $[\xi_i, \xi_{i+1}]$ is called the i^{th} knot span. One knot may appear more than once in a knot vector. The number of times this knot is present in the knot vector is called the order of multiplicity of the knot. A uniform knot vector is where all the knots are equidistant, e.g. $E = \{0, 1, 2, 3, 4, 5\}$. An open knot vector is where the first and last knots are repeated $p + 1$ times. In this case, the corresponding basis functions are interpolating at the boundaries, but not in the middle of the parameter space. In the middle, this phenomenon can be occurred only if the order of multiplicity of the knot in question is equal to the degree of the polynomial, unlike in finite element analysis where the basis is interpolating at each node. For a specified knot vector, the relation between the number of knots m, the degree of basis function p and the number of basis functions n is:

$$m = n + p + 1 \tag{1.2}$$

This equality states that once the knot vector and the degree of the functions are chosen, the number of basis functions is automatically defined. In one dimension, if $E = \{\xi_1, \xi_2, ..., \xi_{n+p+1}\}$, is a knot vector (where p is the polynomial order and n is the number of basis functions), B-Splines functions are recursively defined by the Cox–de-Boor formula:

$$\begin{aligned} &\text{For } p = 0 \\ &N_{i,0}(\xi) = \begin{cases} 1 & \text{if } \xi_i \leq \xi < \xi_{i+1} \\ 0 & \text{otherwise} \end{cases} \\ &\text{For } p > 0 \\ &N_{i,p}(\xi) = \frac{\xi - \xi_i}{\xi_{i+p} - \xi_i} N_{i,p-1}(\xi) + \frac{\xi_{i+p+1} - \xi}{\xi_{i+p+1} - \xi_{i+1}} N_{i+1,p-1}(\xi) \end{aligned} \tag{1.3}$$

Let's consider a trial example based on a simple uniform knot vector that contains 6 knots ($m = 6$), $E = \{0, 1, 2, 3, 4, 5\}$. For degree $p = 0$, the number of basis functions is $n = 5$. For degree $p = 1$, the number of basis functions is $n = 4$. For degree $p = 2$, there are 3 quadratic basis functions, $n = 3$. These basis functions are plotted in Figure 1.2.

Basis functions of order p have $p - m_i$ continuous derivatives across knot ξ_i, where m_i is the multiplicity of the value of ξ_i in the knot vector. When the multiplicity of a knot value is exactly p, the basis is interpolating at that knot. When the multiplicity is $p + 1$, the result is "C^{-1}"-continuity, that is, the basis is fully discontinuous, naturally terminating the domain. Consider the open knot vector given by $E = \{0, 0, 0, 1, 1, 3, 3, 3\}$, the quadratic basis functions ($p = 2$) are drawn in Figure 1.3. The knot vector has 8 knots ($m = 8$). Hence, the number of basis functions is $n = 5$. The first and last knots have both a multiplicity order of $p + 1$, the knot vector is open. The knot value $\xi = 1$ is repeated twice, thus the basis functions are C^0 across knot $\xi = 1$.

NURBS (Non-Uniform Rational B-Splines) is a type of mathematical model

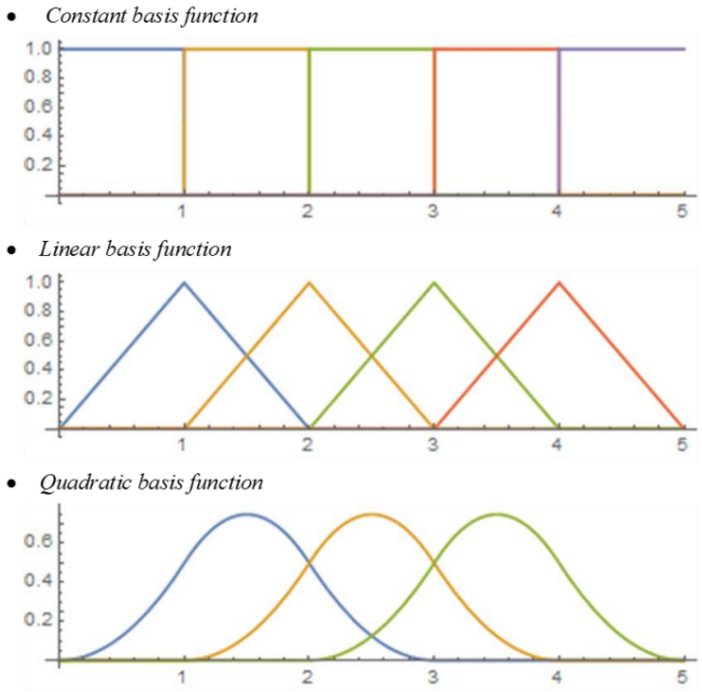

Figure 1.2. – B-Spline basis functions of degrees $p = 0, 1$ and 2 using the knot vector $E = \{0, 1, 2, 3, 4, 5\}$

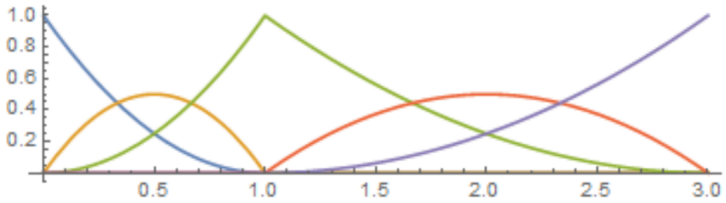

Figure 1.3. – An example of B-spline basis functions

that helps in representing all conic sections, complex forms of curves, surfaces and solids, such as circles, cylinders, spheres, ellipsoids, contrarily to B-splines. They are commonly used in industrial CAD software. From B-Spline functions, NURBS functions can be defined such that:

$$R_i^p(\xi) = \frac{N_{(i,p)}(\xi)\omega_i}{W(\xi)} = \frac{N_{(i,p)}(\xi)\omega_i}{\Sigma_{j=1}^{n} N_{j,p}(\xi)\omega_j} \tag{1.4}$$

where ω_i denotes the weight of the i^{th} B-Spline function. This rational basis degenerates the B-spline basis functions when $\omega_i = 1$ for every control point because B-Spline functions have the partition of unity property. For the description of the geometry, a tensorial construction of the approximation basis is used. For a

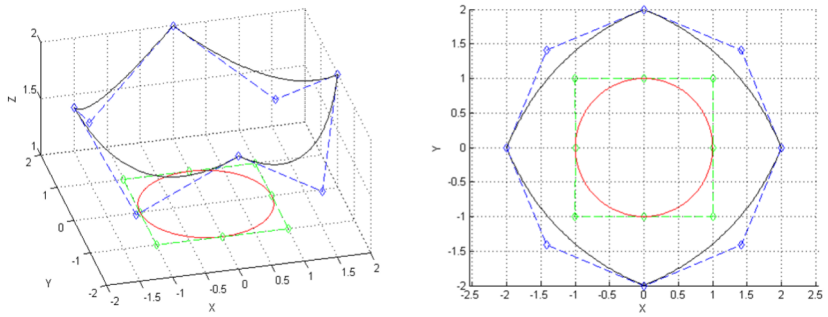

Figure 1.4. – Projection from a B-spline based spatial curve to a NURBS based perfect circle

1D problem in space, one has:

$$\mathbf{u}_h(\xi,\eta) = \sum_{i}^{n}\sum_{j}^{m} R_{i,j}^{p,q}(\xi,\eta)\mathbf{B}_{i,j} \tag{1.5}$$

where $\mathbf{B}_{i,j}$ are called control points (similar to nodes dofs for finite elements) and $R_{i,j}^{p,q}$ corresponds to a 2D NURBS basis of orders p in direction ξ and q in direction η such that:

$$R_{i,j}^{p,q}(\xi,\eta) = \frac{N_{i,p}(\xi)M_{j,q}\omega_{i,j}}{\sum_{k=1}^{n}\sum_{l=1}^{m} N_{k,l}(\xi)M_{l,q}(\eta)\omega_{k,l}} \tag{1.6}$$

Approximation basis for 2D and 3D cases can be derived in the same manner. As an example, consider the construction of a plane circle based on NURBS functions. The plane circle is in $\mathbb{R}^2$, hence we need a spatial curve based on B-spline in $\mathbb{R}^3$ (see Figure 1.4). The spatial B-spline is represented by the black curve in Figure 1.4 with its control points indicated by the blue points. A radial projection on the plane $z = 1$ leads to define the red circle, and the projected control points are denoted by green points. The circle is exactly constructed based on NURBS.

As mentionned before, the IGA uses the same basis functions to approximate the geometry and to calculate the solution. Figure 1.5 illustrates this difference between IGA and FEM, which is the fact that in the IGA, the CAD functions are used as basis functions for the variational framework approximation, whereas in the case of the finite element method, the domain generated from CAD is discretized, and then the solution is calculated on this discretized domain.

A comparison between FEM and IGA concerning the inter-element continuity is shown in Figure 1.6: B-spline basis functions (left) and Lagrange basis functions (right) are plotted, both of degree $p = 2$ and consisting of 3 unidimensional elements $[0, 1], [1, 2]$ and $[2, 3]$. The inter-element continuity of the B-spline functions is higher, and it can be controlled by simply repeating the knots in the parametric space. Due to the fact that basis functions of order p have $p - m_i$ continuous derivatives across knot ξ_i, when the multiplicity of each knot value is exactly $p = 2$, the two sets of basis functions become similar. The ability of controlling the inter-element continuity of the basis functions is a major advantage of the IGA compared to

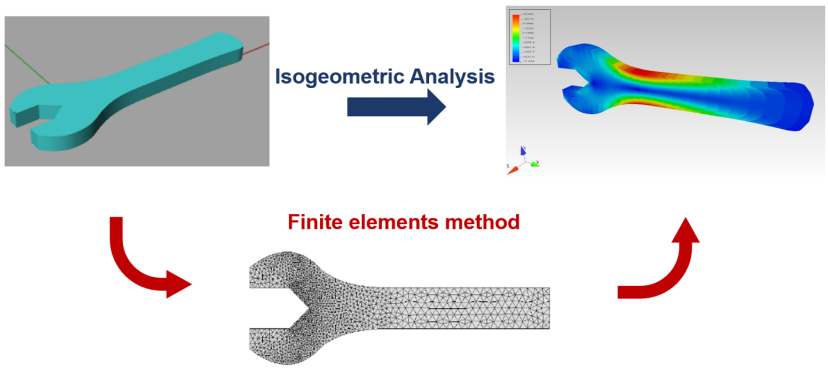

Figure 1.5. – Difference in conception between IGA and FEM

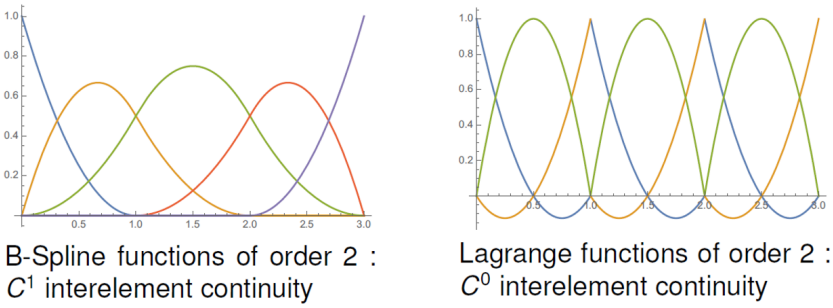

Figure 1.6. – B-Spline basis functions vs. Lagrange basis functions for degree $p = 2$ and based on 3 elements

the FEM and may have an influence on the convergence for some formulations. Not only it makes the IGA capable of representing complex geometries and shapes that cannot be represented using Lagrange polynomials, but also gives better convergence results.

1.1.2. Mesh refinement strategies

The IGA allows refinement strategies available for B-spline basis. These strategies may look similar at first to those of the finite element method but they are in fact much richer: we have control over the element size and the order and continuity of the basis. The refinement strategies that can be used are the knot insertion, the order elevation and the k-refinement. The insertion of knots can take place without bringing any changes on the geometric curve itself. So, if we consider the knot vector $E = \{\xi_1, \xi_2, ..., \xi_{n+p+1}\}$, we add m knots into it and we have a new knot vector $\bar{E} = \{\bar{\xi}_1 = \xi_1, \bar{\xi}_2, ..., \xi_{n+m+p+1} = \xi_{n+p+1}\}$, such that $E \subset \bar{E}$. This knot insertion will lead to a larger number of basis functions, due to the relation $m = n + p + 1$ explained before. Knot values already present in the knot vector may be repeated in this way, thereby increasing their multiplicity, but as described before, the continuity of the basis will be reduced. An example of knot insertion for a simple, one-element, quadratic B-spline curve is presented on the upper left of Figure 1.7. The knot vector of the original curve is $E = \{0, 0, 0, 1, 1, 1\}$. A

new knot $\bar{\xi}$ is inserted such that $\bar{\xi} = 0.5$. There is one more control point, one more element, and one more basis function compared to the unrefined case. The h-refinement strategy in finite element analysis is similar to the knot insertion; they both consist of splitting new elements into new ones. The continuity of the basis functions in the finite element method being C^0 across boundaries against C^{p-1} in the IGA, inserting p times the new knot allows to replicate h-refinement. The difference between the two mechanisms is the fact that the inter-element continuity in the FE analysis cannot be controlled by knot insertion as it is the case in IGA, the continuity across boundaries being always C^0.

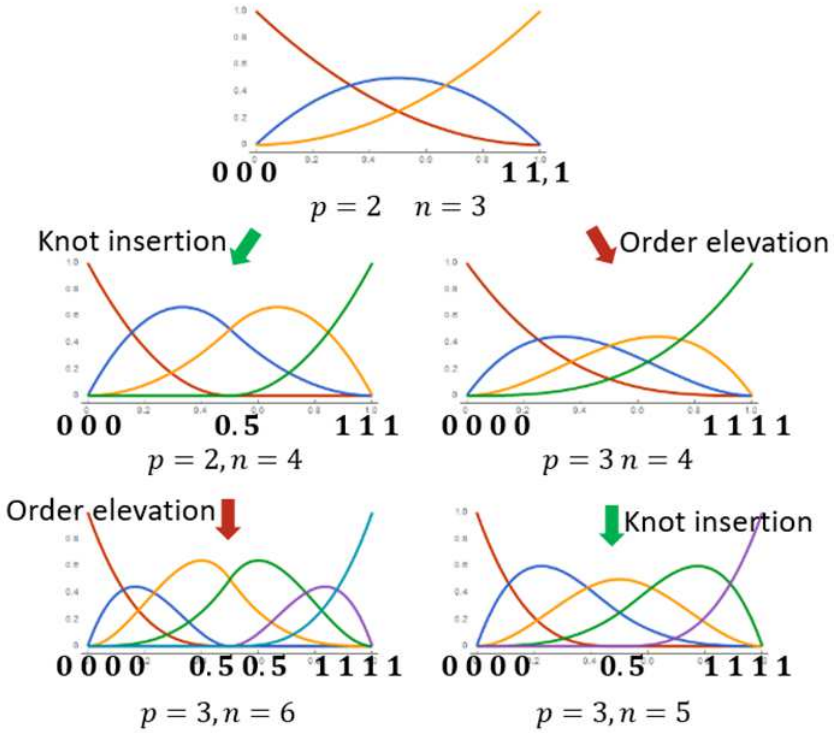

Figure 1.7. – Different refinement mechanisms

Order elevation, or degree elevation, is the second mechanism that allows to enrich the B-spline basis. Obviously, it is based on raising the value of the degree of the basis functions used to represent the geometry. As we've seen in Section 1.1.1, the basis has $p - m_i$ continuous derivatives across element boundaries. To change the value of p, we will also have to change that of m_i by increasing the order of multiplicity of each knot value by 1, in order to keep the number of continuous derivatives of the basis functions the same. An example of order elevation for a one-element curve is depicted on the upper right of Figure 1.7. The order of multiplicity of the knots is increased by one but, as stated above, no new knot values are added. For this simple case, the number of control points and the number of basis functions each increase by one. There are now four cubic basis functions. Order elevation clearly resembles to the classical p-refinement strategy in finite element analysis, since both mechanisms rely on the augmentation of the

polynomial order of the basis to refine it. When both the knot insertion and degree elevation are employed to perform refinement on a B-spline geometry, the order of combination changes the resulting description since these two processes do not commute. Consider a p^{th} degree spline curve as the geometry that we would like to refine. Applying the knot insertion first then degree elevation will result in a curve whose basis functions are C^{p-1} at knot ξ, see the lower part on the left of Figure 1.7 for an example. Degree elevation first then knot insertion give a curve in which the basis functions have C^{q-1} continuity order at knot ξ, see the lower part on the right of Figure 1.7 for an example. Since $q > p$, the second scheme leads to basis functions with higher order continuity. This scheme is referred as k-refinement and has no analogous in finite element analysis.

1.1.3. Beyond B-splines/NURBS

Despite all, B-splines and NURBS may cause some difficulties in numerical simulations. In order to topologically model complex geometries, one has to deal with multi-patch. A knot insertion refinement on B-splines/NURBS requires the insertion of an entire row of control points because of the B-splines/NURBS tensor product structure, so mesh refinement has global effects. Adaptive and local refinement on single patch of B-splines/NURBS is not possible. Alternative spline forms are developed in order to overcome these difficulties, that are Hierarchical B-splines, T-splines, Subdivision Surface and Spline forest. Hierarchical B-splines introduced in [31, 32] allow to localize the effect of refinement through the use of overlays. These overlays are hierarchically controlled subdivisions. Hierarchical B-splines rely on two things: the principle of B-spline subdivision, which allows to maintain linear independence throughout the refinement process, and on a local tensor product structure. However, just like B-splines/NURBS, hierarchical B-splines suffer from topological limitations due to their hierarchically tensor-product structure. T-spline basis functions were initially introduced in [11]. They possess a local refinement property that allows to obtain an acurate numerical solution with less control points compared to B-splines/NURBS basis functions, thus less degrees of freedom. Hence, a row of T-spline control points is allowed to to be added and yet not include the entire surface. This property can drastically reduce the numerical cost. Subdivision schemes [19], Splines forest [86], polynomial splines over T-meshes [24] and LR B-splines [26, 80] are also powerful computational geometry techniques in surface modeling. They allow geometry refinement with a well-chosen approximation scheme.

IGA has been widely applied in different fields of computational mechanics. For example in [23], various examples of applications of this method in different fields are given such as structural mechanics, solid mechanics, fluid-structure interaction problems and contact problems, fluid flows, wave propagation problems...

The Isogeometric Analysis has been applied for solving shell and plate problems [61, 60, 13, 12, 14]. The IGA was also used for solving problems with incompressible or nearly incompressible materials, which is of high importance in many engineering applications to consider for example rubber, elastomers and elasto-plastic materials.

Elguedj & al. were the first to apply the IGA to nearly-incompressible elasticity problems in [28] and in [29] on problems of large strain plasticity. In [94], Taylor used a three-field mixed formulation in an isogeometric context to solve problems in finite deformation solid mechanics in which compressible and nearly incompressible behaviors may be encountered. Later, Galerkin Least Squares terms were added to the formulation to stabilize it in [20] and [57]. In [58], Kadapa & al. used the IGA to propose a two-field mixed variational formulation at small and large strains to solve solid mechanics problems in order to deal with the issues of incompressibility. The authors employed the subdivision property of NURBS to develop an inf–sup stable displacement–pressure combination. Numerical examples involving nearly incompressible and incompressible elastic and elasto-plastic materials at both small and large strains regimes confirmed the accuracy of the formulation and the inf-sup stability. The IGA was also used in fluid mechanics for solving Stokes and incompressible Navier-Stokes problems [10, 79, 18] and contact problems [95, 56, 96, 25]. The fact that the NURBS basis functions allow higher inter-elements continuity enables to have better convergence results for contact problems compared to Lagrange polynomials that are only C^0 inter-element continuous. More smooth contacts surfaces are obtained, leading to more physically accurate stress. The IGA was also used for solving structural vibration problems [10, 44, 100], optimization problems [99, 84, 70] and others problems. Today, the isogeometric analysis is being widely used for solving many types of problems as it allows to attain high order space interpolation in an easy and straightforward manner. It is therefore employed in various fields.

1.2. Space-time methods

1.2.1. Historical point of view

In the resolution of partial differential equations, the finite element method is widely applied in the discretization of space: the system of partial differential equations is then transformed into a system of ordinary differential equations in time. Then, the resulting initial value problem is solved with a time stepping method such as the finite differences for the time resolution, a so-called semi-discrete method (see [38] for an example of a time-stepping method), leading to a sequential calculation in time. This is called the vertical method of lines. The Rothe Method discretizes in reverse order: it first discretizes in time and then solves the PDE. Space-time discretization consists of considering time dependence as spatial dependence. Time is considered to be an extra dimension and so the time variable t is treated in the same way as the spatial coordinates, and a space-time variational principle is used.

The very first publications on space-time methods began to show in the late 60s for solving elastodynamics problems: Argyris and Scharpf [7] and Oden [81] were the first to develop the so-called space-time method. In [7], the authors proposed a standard finite element formulation for space for solving an elastody-

namics problem. The corresponding discrete time-dependent problem was handled using a second finite element interpolation over a time interval. They used a Hamiltonian formulation considering both velocities and displacements; in fact, for elastodynamics problems, using the Hamiltonian principle constitutes a common approach and has been used by many authors both for displacement and displacement-velocity formulations. Clearly, the drawback of using a two-field formulation (e.g. a displacement-velocity formulation) is the increase of the number of unknowns in the resulting system. On another side, such formulation allows the authors to impose straightforwardly velocity boundary and initial conditions. It also gives the possibility of considering different approximation functions for the displacement and the velocity and reduce the order of the PDE. Argyris and Scharpf then showed that the elastodynamics problem leads to the resolution of sequential linear problems. This approach implies a separation of time and space (always structured mesh). In [81], Oden proposed an alternative approach for solving the elastodynamics problem for which space and time are considered as an augmented dimensional finite element problem. He proposed the concept of meshing the space-time domain with finite elements in a more general manner. In this approach, polynomial approximations should be the same for space and time as the finite element can be positioned arbitrary in the space-time mesh. This type of methods didn't gain immediate popularity because employing it means having one extra dimension in the problem to be solved, and, at the same time, robust and efficient implicit algorithms, such as the HHT [38], were developed during the 70's that could be applied to engineering problems with an acceptable numerical cost for the ressources that were available back then. But since, the technology of computers has far developed, not only in number of cores but also in speed, and from our point of view, the space-time method might today be an interesting alternative for solving complex problems.

1.2.2. Space-time finite element methods

Authors have proposed different numerical applications since the space-time method was proposed, mainly in elastodynamics. Consider the space-time cylinder $Q = \Omega \times [0, T]$, where $\Omega \subset \mathbb{R}^d$ is a closed domain and d is the number of space dimensions, T is the final time. The boundary of Ω is denoted by Γ. Let Γ_u and Γ_σ denote the non-overlapping subregions of Γ such that : $\Gamma = \Gamma_u \cup \Gamma_\sigma$, $\Gamma_u \cap \Gamma_\sigma = \phi$. The equation of elastodynamics is given by:

$$\rho \ddot{\mathbf{u}} - \mathrm{div}_{\mathbf{x}} \boldsymbol{\sigma} = \mathbf{f} \quad \forall (\mathbf{x}, \mathbf{t}) \in Q \tag{1.7}$$

where $\rho(\mathbf{x})$ is the material density, $\mathbf{u}(\mathbf{x}, t)$ is the displacement field, $\boldsymbol{\sigma}(\mathbf{x}, t)$ is the stress tensor and $\mathbf{f}(\mathbf{x}, t)$ is the applied body load.

Literature shows that the space-time formulation can be used both in continuous and discontinuous finite element methods, and the difference relies on whether continuous or discontinuous basis functions are used inside a space-time slab. One can find formulations based on a single field (the displacement). Another

approach is to transform the original problem into a system of first-order equations, rendering a two field formulation, displacement and velocity. One of the pioneering works on time-discontinuous Galerkin methods is that of Hughes and Hulbert [46] and Hulbert and Hughes [48], in which the authors developed an unconditionally stable formulation for elastodynamics using space-time unstructured meshes while allowing discontinuities in the principal unknowns at finite time intervals. In [46], the method employed was based on the natural framework of second-order hyperbolic equations, while in [48], a single-field formulation was employed. This means that the displacement field is chosen as the single unknown in the problem. Figure 1.9 shows a comparison between a 2D space-time discretization arising from the semi-discrete approach and a 2D space-time finite element mesh, accomodating unstructured meshes in the space-time domain for a two-material elastic 1D bar problem in dynamics (see Figure 1.8), where non-uniform traction is applied near the material interface at the initial time. A relatively sharp stress distribution propagates throughout the bar, and the interest of this problem is tracking it. The unstructured mesh shown in Figure 1.9 and accomodated from the space-time finite element method may be considered to arise from an adaptive mesh refinement strategy: fine mesh can be employed in regions near the stress wave fronts and a coarser mesh is used where the solution is smooth, and in this way, a uniformly-refined and computationally expensive mesh is not necessarily needed to obtain an accurate solution.

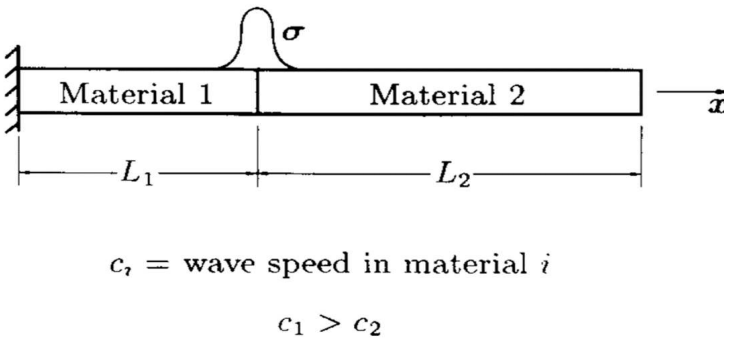

Figure 1.8. – Bimaterial elastic bar problem. (figure taken from [48])

In [48], the authors were interested in solving the impact problem of a 1D elastic bar shown in Figure 1.10.

Linear stabilizing dissipative Galerkin Least Squares (GLS) type terms and non-linear discontinuity capturing operators are added to the formulation in order to reduce the oscillations in the computed response and achieve stability. In elastodynamics, these terms follow the form:

$$\sum_e \int_{Q_e} (\rho \ddot{\mathbf{u}}_h - \mathrm{div}_x \boldsymbol{\sigma} - \mathbf{f}_h)\rho^{-1}\tau(\rho\delta\ddot{\mathbf{u}}_h - \mathrm{div}_x(\mathbf{C} : \boldsymbol{\varepsilon}(\delta\mathbf{u}_h))dQ \tag{1.8}$$

where τ is a stabilization parameter and $\mathbf{C}$ is the 4th order elasticity tensor. Being evaluated elementwise, these additional terms do not affect the continuity of the

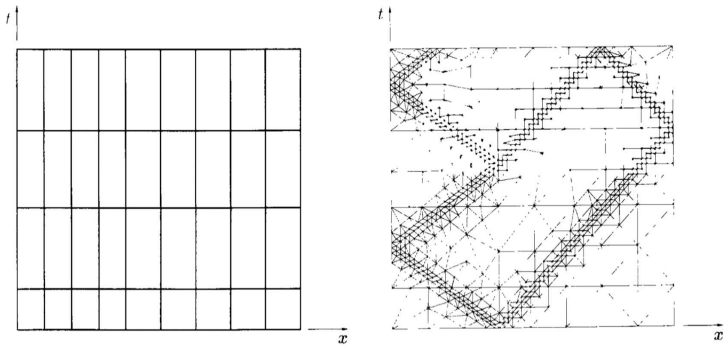

Figure 1.9. – Comparison between semidiscrete space-time structured mesh (left) and space-time finite element non-structured mesh (right) (figure taken from [48])

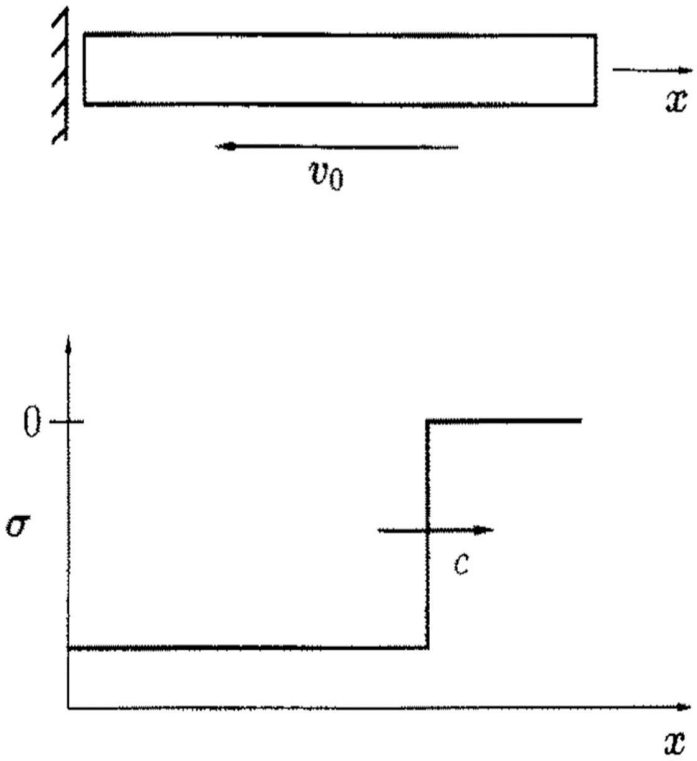

Figure 1.10. – One-dimensional elastic bar impact problem: exact solution (figure taken from [48])

original variational formulation. Moreover, they are based on residual forms, hence the exact solution satisfies the formulation, meaning that the consistency condition is satisfied. The authors showed that the computed response using discrete methods such as trapezoidal or HHT methods exhibits oscillations in the solution (see Figure 1.11 for an example of the solution obtained using the HHT method). As a matter of fact, the authors explained that the semi-discrete approach has a disadvantage which is the difficulty in offering algorithms that accurately capture discontinuities

or sharp gradients in the solution.

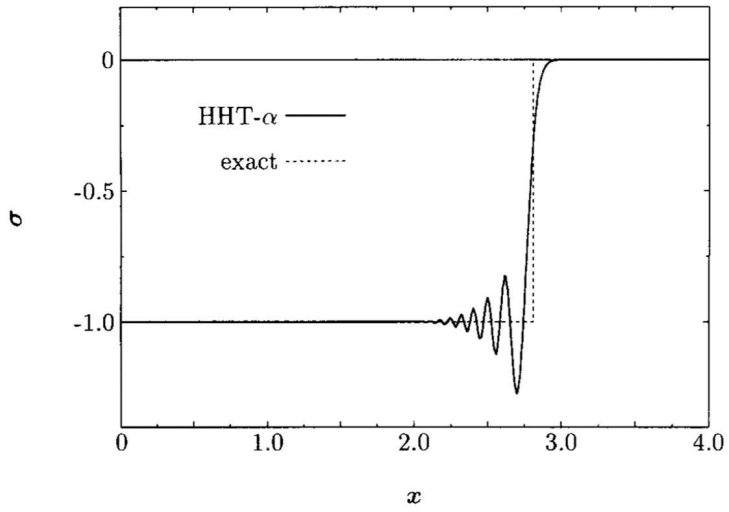

Figure 1.11. – Stress distribution in the bar calculated using the HHT algorithm (figure taken from [48])

For this reason, they adopted the time-discontinuous Galerkin method and added the dissipative terms (least-squares type terms) to the formulation, further reducing by that the oscillations in the solution, see Figure 1.12. They proved stability and convergence of the method, showing the firm mathematical foundation that this method possesses.

In [47], Hulbert & al. give further results of a dispersion and dissipation analysis. The authors proved that their method possesses high accuracy properties.

French, in [34], used the discontinuous Galerkin space-time FE methods for

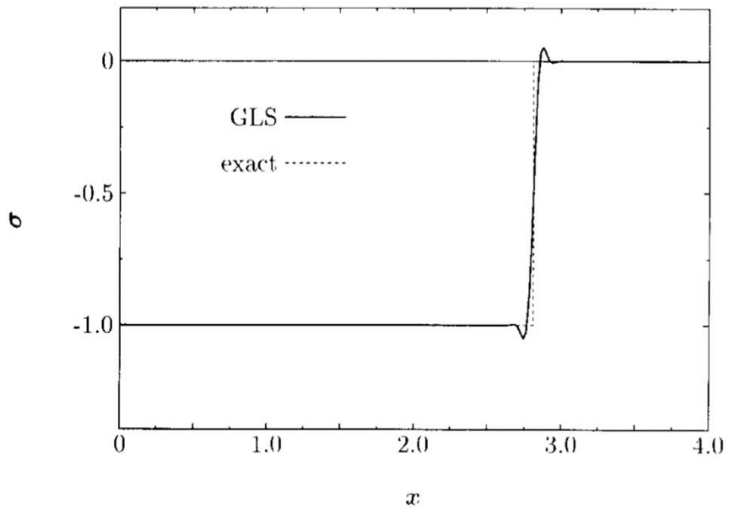

Figure 1.12. – Stress distribution in the bar calculated using Galerkin/least-squares algorithm (figure taken from [48])

solving the wave equation using a single-field formulation with test functions derived with respect to time. His formulation is very similar to the one developed in [48] but no least-square terms were added. He gave stability and convergence theorems, where no restriction on the time slab thickness should be taken, in contrast to the case in [48] where the thickness of each time slab is proportional to the size of the element domain. An error analysis for the scheme was presented. the author showed that for the case of piecewise linear basis functions, the asymptotic rate of convergence of the approximation to the exact solution in an H^1-norm is $O(h^{\frac{1}{2}})$, and is $O(h^{p+1})$ for degree $p > 1$.

In [55] and [53], mesh-dependent norms were introduced and a priori error estimates were derived in such norms for first-order hyperbolic systems concerning fluid mechanics and conservation laws. In [53], the capacity of the time-discontinuous Galerkin methods to conveniently represent discontinuities when the problem to be treated has a discontinuous solution was shown. The time-discontinuous Galerkin method allows higher order A-stable time stepping schemes. Optimal or nearly optimal a priori and a posteriori error estimates were given. A generalization to second order hyperbolic problems was done in [54]: a priori and a posteriori error estimates were given for a finite element method for linear second order hyperbolic equations based on a two-field (displacement and velocity) time- discontinuous Galerkin finite element discretization using linear basis functions in time and space. It can be proved that the a priori and a posteriori error estimates are nearly optimal. The authors gave general structures of the proofs of both the a priori and a posteriori error estimates. These error estimators yield upper and lower bounds for the error. In literature, one can see that the discontinuous Galerkin approach was used in spatial discretization as well as in temporal discretization of partial differential equations, allowing discontinuities at the element interfaces. Researchers used the discontinuous Galerkin method for a wide range of applications. In particular, the discontinuous Galerkin method was applied for solving shock wave propagation problems, because of its good stability properties. The authors in [6] used a discontinuous Galerkin formulation in space and time and compared the solution with these obtained using the Newmark method, showing that the space-time method is more performant for bar impact problems. The authors also proposed a bi-material bar impact problem and a suddenly loaded axi-symmetric circular plate to further prove the accuracy of the method used. Huang in [42] used the time-discontinuous Galerkin method for solving shock wave propagation problems for solid dynamics including both stationary and moving material interfaces. He adopted the single-field formulation proposed by [48], meaning that the displacement field is the primary unknown field, for the study of dynamic solid–solid phase transitions, and Galerkin least square terms were added to the formulation. He compared the solution obtained with the theoretical one in order to prove the accuracy of the method. The authors also presented a unicity and stability analysis of the solution, describing the conditions needed for the solution to be unique and unconditionally stable. In [22], a modification of the formulation of [42] was presented, making it become unconditionally stable. This means that

no restriction on the grid topology has to be considered. A two-field space-time discontinuous Galerkin formulation was adopted in [68, 69]. The authors applied the time-discontinuous Galerkin method for 2D structural dynamic and elastodynamic problems using linear interpolation functions in time for unknown displacement and velocity. In [90], an efficient predictor-multicorrector iteration algorithm was presented which is implicit, unconditionally stable and capable of filtering the effects of high spurious modes. In [69], the authors extended the algorithm to the analysis of continuum problems. Moreover, they proposed an h-adaptive procedure using the time-discontinuous Galerkin method capable of updating the spatial mesh and the time step size automatically. Thus, the estimated errors could be controlled within specified tolerances. The authors concluded from the accuracy of their numerical results (the time- discontinuous ST method is of second-order accuracy in space in the L^2-norm and third-order accuracy in time) that time-discontinuous Galerkin finite element method is well suited for structural dynamic analysis. Abedi & al. [2] introduced a novel space–time discontinuous Galerkin method, allowing for displacement discontinuities across every inter-element boundary. Stability and a-priori error estimates were given and proven, showing the effectiveness of their space-time formulation. They showed that their formulation can accurately capture shocks and can be used with fully unstructured non-conforming space-time grids.

Beside discontinuous formulations, authors have worked on continuous Galerkin formulations (time-continuous Galerkin). The use of a Galerkin continuous formulation is similar to the strategy adopted by Oden in [81], i.e. no separation of space and time is made and a space-time mesh that can be either structured or non-structured is used on the entire space-time domain. In [9], triangular and tetrahedral ST elements based on the principle of virtual work were used for vibration analysis. Hou & al. in [41] applied the ST method using Hamilton's weak principle and triangular elements were adopted for solving 1D elastodynamics problems. They showed that there is an interest of using the p-version of finite element in space and time by showing the accuracy of the numerical results obtained concerning the wave propagation in a rod and in a Timoshenko beam. In [27], Dumont & al. developped a 4D ST formulation for elastodynamics, established a stability and convergence analysis and compared it to a Newmark integration scheme, proving by that the effectiveness and accuracy of their space-time finite element formulation for 4D elastodynamics. A numerical example of a problem of mobile loading was given. Idesmann in [49] introduced a new form of weighting functions, that is $\lambda(t)(w + a\dot{w})$ where w is the standard test function used. The author used this form of test functions with different values of λ's and a's forming a Petrov-Galerkin variational formulation to control the numerical dissipation in the resolution of linear elastodynamics 1D elastic bar impact problem using structured and unstructured meshes. He compared time-continuous Galerkin with time-discontinuous Galerkin methods using both standard test functions and his proposed test functions, showing that the convergence of the time continuous Galerkin is faster than the one of the time-discontinuous Galerkin using the new form. The time continuous Galerkin method developed is unconditionally stable

and numerial results showed that it has a higher order of accuracy by the factor of two than the standard time continuous Galerkin method due to the additional terms $a\dot{w}$. For the same number of degrees of freedom, the accuracy of the new implicit time continuous Galerkin method is one order higher than the accuracy of the standard implicit time-discontinuous Galerkin method. The accuracy and stability of the approach were analytically analyzed for structured meshes, proving that the theoretical results that were obtained are in agreement with analytical estimations, thereby showing the effectiveness of space–time elements on structured and unstructured meshes.

Beyond elastodynamics, other applications were proposed such as free surface problems [15], compressible fluid flows [52], heat transfer problems [1, 21], advection-diffusion equations [78], contact problems [3, 4]. Time-discontinuous Galerkin methods were used in the domain of fluid mechanics [91, 93]. The space-time method was employed for solving the Navier-Stokes equations in compressible and incompressible regimes. High-performance computing implementations were developed in the context of ST formulations. The authors showed that accurate large scale problems can be solved within this framework. In [87], additional terms of least-square type were added to the variational formulation of a time-dependent linear scalar advective-diffusive model problem. A Fourier stability and accuracy analysis were proven as well. A Galerkin least-squares formulation was also developed in [71] for the Navier-Stokes equations for moving domain problems in a space-time FE context. An interesting feature of the ST method is its capacities to compute the solution of problems having deforming boundaries. The STFE method has also been adopted for solving acoustic problems [98, 97]. Podhorecki was among the first authors who used this method for linear viscoelasticity in [83] for solving a 1D problem. He introduced general forms for the stifness matrices concerning different types of viscoelastic models, like Maxwell's, Kelvin voigt's, Burger's and Zener's. In [17], the authors used the continuous Galerkin method for the treatment of symmetric and non-symmetric formulations of two different viscoelastic three-parameter models: the Malvern Model (generalized Maxwell Model) in 1D and the generalized Kelvin-Voigt Model in 3D. The authors gave numerical results that underline the advantage of this method compared to the semi-discrete one. The numerical results also show both the effectiveness of parallel computation and adaptive refinement in time and space. Moreover, the efficiency of the p-adaptation was shown and yielded a higher rate of convergence than h-adaptation. In [50], a modification of the variational formulation, the discrete system of equations and the solver of [17] was done allowing the use of an iterative solver within parallel computations, showing by that high parallel effectiveness of simultaneous space-time finite element calculations. The authors used the continuous and discontinuous Galerkin space-time for the viscoelastic Malvern model. Numerical examples were given for both methods showing optimal convergence rates for a coupled adaptive refinement in space and time for viscoelastic problems with smooth boundary and initial conditions. Moreover, the effectiveness of the discontinuous Galerkin method in the case viscoelastic problems with discontinuous boundary conditions was

underlined. In [51], a generalization of the work done in [51] was done to the case of the generalized viscoelastic Maxwell Model in which several Maxwell elements are assembled in parallel. Li & al. [67] worked on space-time viscoelasticty in 2D and introduced a continuous Galerkin two-field formulation (displacement and velocity). The authors stated that space-time continuous Galerkin finite element method retains energy conservation properties. They proved existence, uniqueness and stability of the ST continuous FE solution of the viscoelastic wave equation. The authors also showed optimal convergence rates for different norms including the L^2 and H^1 norms. In [76], the finite element method was employed in space and time simultaneously to establish the space-time variational formulation of the heat equation. The space-time finite element method was used for the numerical solution of parabolic evolution problems in moving spatial computational domains. The authors employed C^0 continuous basis functions and used a time upwind test function of the form $v_h + \theta h \partial_t v_h$ where θ is a positive constant to derive the discrete bilinear form, elliptic on a mesh-dependent norm that they introduced. Moore then proved boundedness and consistency of the bilinear form and use the ellipticity, boundedness and consistency results to derive a priori discretization error estimates in the discrete norm. Finally, numerical results are given for moving spatial domains with unstructured mesh and optimal convergence rates are obtained. The stability of Petrov–Galerkin discretizations with application to parabolic evolution problems in space-time weak form was discussed in [74]. In [8], the authors presented the formalism of using time-derivatives of the space–time continuous test functions for the resolution of the heat equation with the space-time continuous Galerkin method. This means that they replaced the test function $\delta\theta$ by its derivative in time, for it to become $\dot{\delta\theta}$. They showed numerical results concerning a simple 2D example and concluded from the results the fact that a given accuracy of solution is obtained more rapidly by a higher-order method, and proved the fact that, for at least this smooth example, as the order of the method increases, the time necessary for a given accuracy of solution decreases. In [37], different problems were treated: the thermal conduction problem, a non-linear elasticity problem and a fluid system. The authors presented many numerical results including convergence studies that show the accuracy of space-time methods compared to standard time-stepping schemes, see Figure 1.13. The authors compared the efficiency of the space-time method to the trapezoidal and the implicit Euler methods for the heat conduction equation. The second example concerned a non-linear elasticity test applied to a continuum body having the form of an L-shaped block. The authors compared using a convergence analysis the space-time method to a midpoint rule and an implicit Euler formulation. The convergence results showed the better accuracy of space-time methods compared to traditionnal time-stepping schemes, see Figure 1.14.

The space-time method was also used for solving problems in multiphysics. For example in [65], the authors used a space–time finite element method for the linear thermo-elasticity problem and established an exact a posteriori error representation formula using the standard Galerkin method in space and the

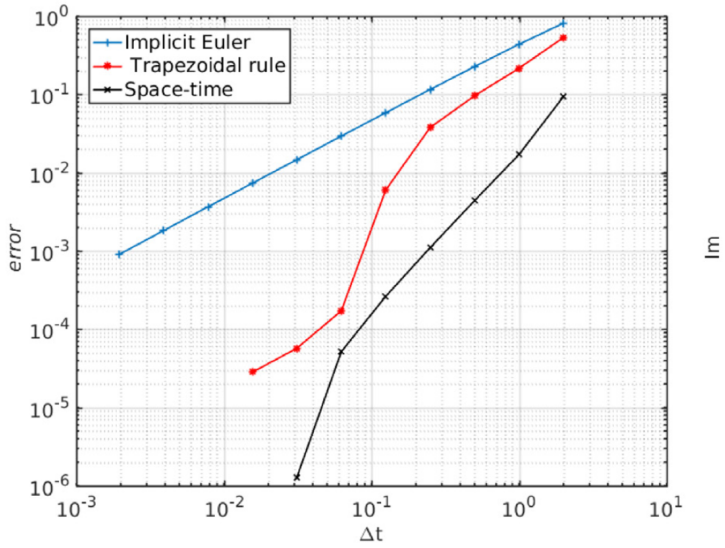

Figure 1.13. – Convergence curves for heat conduction equation (figure taken from [37])

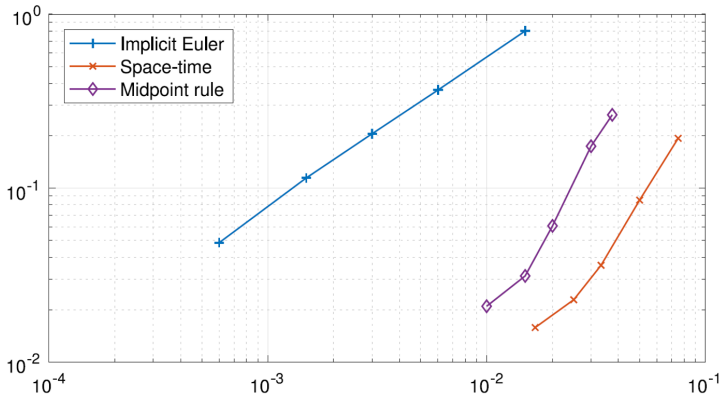

Figure 1.14. – Convergence curves for non-linear elasticity equation (figure taken from [37])

discontinuous Galerkin method in time. Moreover, in [59], a space-time finite element method was employed to solve the thermoelasticity equation at finite strains. Time-discontinuous Galerkin methods have also given rise to other original methods such as the TX-FEM (Time Extended Finite Element Method) [85] or the combination of time-discontinuous Galerkin and PGD (Proper Generalized Decomposition) [16].

1.2.3. Space-time isogeometric methods

ST-IGA methods (continuous of discontinuous) can be an attractive alternative to ST-FEM methods. References in literature dealing with the Galerkin space-time method in an isogeometric framework are very recent. In [64], the space-time

isogeometric method was adopted for solving the heat equation in fixed and moving spatial computational domains using a continuous Galerkin formulation. They used a time upwind test function of the form $v_h + \theta h \partial_t v_h$, where θ is a positive constant, to derive the discrete bilinear form, elliptic on a mesh-dependent norm $\|.\|_h$ that they introduced. They proved boundedness and consistency of the bilinear form and used the ellipticity, boundedness and consistency results to derive a priori discretization error estimates in the discrete norm $\|.\|_h$. Numerical examples for fixed and moving spatial computational domains were given for polynomial degrees $p = 1, 2, 3$ and 4 in 3D showing optimal convergence rates obtained with respect to the norm $\|.\|_h$ and with respect to the $L^2 - norm$. The authors also showed results in 4D for polynomials of degrees $p = 1$ and 2 for both of the norms as well. In all of these cases, optimal convergence rates were obtained, that are $O(h^p)$ with respect to $\|.\|_h$ and $O(h^{p+1})$ for the L^2 norm. These results are for fixed domains, and the authors showed convergence rates for the case of moving domains as well, reflecting the interest of using space-time methods even though it means having one large space–time system of linear algebraic equations instead of many smaller systems like in traditional time-stepping methods. As a matter of fact, parallel computers with many cores can allow to overcome the sequentiality of time. Langer & al. [63] introduced a posteriori error estimates for the same initial boundary value problem. These a posteriori error estimates were proven to be efficient and reliable, in the sense that different forms of a posteriori error majorants were established and proven equivalent to the energy error norm. They are also flexibile with respect to several free parameters. Using these parameters, it is possible to obtain estimates for different error norms and minimise the respective majorant in order to find the best possible bound of the error. According to the authors, full space-time approach combined with IGA technologies means having efficient fully-adaptive and heavily parallelised schemes and is a major step for solving industrial problems. Moreover, the error estimates that the authors made provide guaranteed, sharp, and fully computable upper bound of the error $e = \|u_{exact} - u_h\|$, where u_{exact} is the exact solution of the problem and u_h is the approximated solution computed with the space-time isogeometric method. These majorants provide reliable and efficient upper bounds of the total energy error and a quantitatively sharp indicator of local errors.

These massively parallel computers have made parallel time integration methods a possible and easy thing over the last decade and a domain-decomposition can be applied by modern multigrid solver. An overview of time parallel methods is made in [35] and the methods are classified into four groups: methods based on multiple shooting, methods based on domain decomposition and waveform relaxation, space-time multigrid methods and direct time parallel methods. The author explained the history and the core ideas of each technique.

In [39, 77], the authors generalized the results of [64] from the single-patch to the multipatch Galerkin space-time IGA schemes considering the same initial boundary value problem of the heat conduction equation. As a matter of fact, in most industrial applications, the computational domain involves several patches.

Hence, the IGA enables a multipatch discretizations that can involve several domains. Hofer & al [39] established the communication of the discrete solution across the time patch interfaces using time-discontinuous Galerkin techniques with time-upwind fluxes. They defined appropriate discontinuous B-spline spaces and a related discrete norm. They proved that the produced discrete bilinear form is coercive (elliptic) with respect to this norm, which ensures uniqueness and existence of the IGA solution. They then gave boundedness and consistency results of the discrete bilinear form, and finally estimated the discretization error with respect to this discrete norm. The authors showed that the sequentiality inherited from classical time-stepping methods could be overcomed even though a huge linear system should be solved. They proved that this could be possible by adopting a space-time multigrid method that solves the complete system in parallel. Numerical results verified the A-priori error estimate that was made for high order B-Splines in case of a 2D space-time cylinder. The convergence curves exhibit optimal convergence rates, i.e. the defined discrete norm behaves like $O(h^p)$, where p is the B-Spline degree. The authors also showed numerical examples including optimal convergence rates for norms in L^2 and the discrete norm in case of a 4D space-time cylinder for degree $p = 1$, where the IGA coincides with the FEM, proving the accuracy of their technique for generating and solving the large system of IGA equations on massively parallel computers. In [77], the author proposed a discontinuous Galerkin method in both space and time and derived a stable scheme. The author gave accurate numerical results concerning two and three dimensional space-time domains. He showed that optimal convergence rates are obtained for the discrete norm that was defined and for the L^2-norm in the case of a moving 2D spatial domain. The convergence rates are $O(h^p)$; $p \geqslant 2$ for the defined discrete norm and $O(h^{p+1})$; $p \geqslant 2$ for the L^2-norm. In [75], the space-time isogeometric method was applied for the parabolic problem and least square terms were added to the variational formulation. A-priori error estimates were given and confirmed. Moreover, the authors proposed a preconditioning strategy and showed its performance using numerical results.

In [37], a space-time isogeometric method was used for solving the Kuramoto–Sivashinsky equation in 3D. The authors compared the solution obtained using the space–time approach to the one obtained using a classical time stepping scheme, which is the midpoint time integration scheme. They used quadratic NURBS functions in space and time showing thereby the possibility of the application of higher-order shape functions in time as well. Recently, Takizawa and Tezduyar [92] used a NURBS interpolation with continuous representation in time for solving fluid equations in order to enhance the accuracy and obtain a temporally smooth, NURBS-based solution. In [62], the authors described different aspects of space-time methods, among them the ST IGA, concerning tire aerodynamics. They advocated the use of higher-order basis functions in time and the benefit of using higher-order basis functions in space. The authors also pointed out that the ST-IGA allows to make a more accurate representation of the motion of the solid surfaces, a more efficient temporal representation of the motion and deformation of the

volume meshes, and more efficient remeshing. The benefits of using IGA in space (as it was described before in the IGA section) was pointed out in this paper: the authors explained that ST-IGA with IGA basis functions in space allows to have more accurate representation of the geometry, especially in the cases where the geometry to be described is not so simple, such as the one of a tire. Lastly, the authors mentioned the fact that ST-IGA enables the use of larger time-step sizes while keeping the Courant number at a desirable level for good accuracy.

1.3. Conclusion

In this chapter, a state of art was given for the space-time method based on FE and IGA schemes. Space-time methods seem to guarantee less numerical dissipation, more stability and versatility in computed responses. Comparisons were provided between the FEM and the IGA on one side, and space-time methods and semi-discrete methods on the other side. Stability, convergence and error analysis concerning space-time formulations were developed in many references of the literature. The idea of solving one huge linear system instead of smaller ones with incremental equations may look disadvantageous, but the power of massively parallel computers available nowadays may overcome this difficulty. In semi-discrete methods, only one spatial problem can be solved in parallel at a certain time step. So in the case where many time steps are necessary together with a relatively small number of degrees of freedom for the spatial discretization, the parallel efficiency becomes very low. Hence, for an efficient parallelization, it would be better to be able to compute the whole problem in a distributed way. The total algebraic equation system in space and time could be parallelized efficiently in the case of the space-time methods. Many techniques of parallel time integration started to emerge for over a decade ago, and therefore space-time methods could be used without any impediment with the emergence of space-time multigrid methods that solve the complete system in parallel. Moreover, both h- and p-adaptation can be realized. It became quite natural to treat time as another dimension in space in the evolutionary equations. As seen in this chapter, very few applications are found in literature where the space-time method is combined with the IGA for the resolution of mechanical problems. Hence we would like in the next chapter to examine and evaluate the numerical performance of continuous ST-IGA for elastodynamics problems, in both linear and non-linear cases, at both small and finite strains. We also apply the ST IGA to compressible and incompressible material behaviors. We introduce a simple and robust variational form compared to other formulations found in literature. This form can be straightforwardly extended to non-linear cases. We compare the numerical results obtained using our ST-IGA formulations to continuous ST-FEM ones and semi-discrete FEM simulations with the HHT scheme for transient dynamic problems with and without discontinuities. The work provided by literature will serve as a reference to our work.

2. Space-Time for Elastodynamics

Chapter Contents

2.1. Introduction

The classical method for solving elastodynamics problems is to discretize first the space domain using the finite element method, and then the time using a time-stepping method (trapezoidal method, HHT method...). An alternative of this classical method can be the so-called space-time method where the full space-time problem is solved without iteration. This method may have many advantages compared to classical time-stepping methods. For instance, it may help gain more stability in numerical schemes compared to explicit solvers where

the CFL condition is necessary to be fulfilled. Moreover, space-time method may be more energy conservative than traditional schemes. As seen in the previous chapter, these methods may also allow to control numerical oscillations that can be encountered while solving problems having discontinuous solutions such as impact problems. In this chapter, we propose alternative space-time isogeometric formulations for elastodynamics problems. We use IGA in order to take benefit from its numerical qualities, taking advantage of higher inter-element continuity. Least-square terms are added to the space-time formulations for problems at small and finite strains for stabilizing purpose. In the literature, there are very few references where the space-time isogeometric methods are used for the resolution of the elastodynamics problem, at small or at finite strains. We focus on two points: stabilized formulations, and the interest of using continuous Galerkin schemes in space and time with higher order and higher continuity approximation basis. We illustrate the numerical performance of these methods through typical impact or vibration problems commonly encountered in the field of elastodynamics of solids. For compressible elasticity, we adopt a two-field formulation (displacement/velocity) with additional least square terms. We adopt a simpler form than the ones found in the literature, that can actually be straightforwardly extended to non-linear cases. This form can be interpreted as a penalized formulation with a consistency condition on the acceleration field. It makes sense with high continuity order of the NURBS-based approximations compared to piecewise Lagrange polynomials. The proposed formulation leads to optimal rates of convergence on trial problems and we show that the additional stabilization terms play a fundamental role in controlling numerical oscillations that occur in problems with discontinuities, such as impact problems. We compare the numerical results obtained using our space-time isogeometric formulations to continuous space-time finite elements formulations and semi-discrete FEM simulations with the HHT scheme for transient dynamic problems with and without discontinuities. An important property of our formulation is that space-time isogeometric formulations allow us to obtain more conservative solutions than semi-discrete methods.

2.2. Small-strain formulation

We consider the space-time cylinder $Q = \Omega \times [0, T]$, where $\Omega \subset \mathbb{R}^d$ is a closed domain, d is the number of space dimensions and T is the final time. The boundary of Ω is denoted by Γ. Let Γ_u and Γ_σ denote the non-overlapping subregions of Γ such that : $\Gamma = \Gamma_u \cup \Gamma_\sigma$, $\Gamma_u \cap \Gamma_\sigma = \phi$. The conservation of the linear momentum on Q takes the following form in the small strain case:

$$\rho\ddot{\mathbf{u}} - \mathrm{div}_{\mathbf{x}}\boldsymbol{\sigma} = \mathbf{f} \quad \forall(\mathbf{x}, \mathbf{t}) \in Q \tag{2.1}$$

where $\rho(\mathbf{x})$ is the material density, $\mathbf{u}(\mathbf{x}, t)$ is the displacement field, $\boldsymbol{\sigma}(\mathbf{x}, t)$ is the stress tensor and $\mathbf{f}(\mathbf{x}, t)$ is the applied body load. Assuming linear isotropic elasticity, the stress tensor can be related to the strain field, $\boldsymbol{\varepsilon}(\mathbf{x}, t) = \frac{1}{2}(\nabla_{\mathbf{x}}\mathbf{u} + \nabla_{\mathbf{x}}^T\mathbf{u})$,

by the following standard constitutive equation

$$\boldsymbol{\sigma} = 2\mu\boldsymbol{\varepsilon} + \lambda tr(\boldsymbol{\varepsilon})\mathbf{1} \tag{2.2}$$

where $\lambda(\mathbf{x}, t)$ and $\mu(\mathbf{x}, t)$ are Lamé elasticity parameters and $\mathbf{1}$ is the second order identity tensor. The problem's boundary and initial conditions are the following:

$$\begin{aligned}
&\mathbf{u} = \mathbf{g}(\mathbf{x}, t) \text{ for } \mathbf{x} \in \Gamma_u, t \in [0, T] \\
&\boldsymbol{\sigma}.\mathbf{n} = \mathbf{T}(\mathbf{x}, t) \text{ for } \mathbf{x} \in \Gamma_\sigma, t \in [0, T] \\
&\mathbf{u}(\mathbf{x}, t = 0) = \mathbf{u}_0(\mathbf{x}) \text{ for } \mathbf{x} \in \Omega \\
&\dot{\mathbf{u}}(\mathbf{x}, t = 0) = \mathbf{v}_0(\mathbf{x}) \text{ for } \mathbf{x} \in \Omega
\end{aligned} \tag{2.3}$$

where $\mathbf{n}(\mathbf{x})$ is the normal to the boundary Γ_σ, $\mathbf{g}$ is the prescribed displacement at the boundary Γ_u, $\mathbf{T}$ is the prescribed traction at the boundary Γ_σ, $\mathbf{u}_0(\mathbf{x})$ and $\mathbf{v}_0(\mathbf{x})$ are respectively the initial displacement and velocity fields.

2.2.1. Two-fields variational formulations

First, we define the Sobolev spaces $H^{l,k}(Q) = \{u \in L^2(Q) : \partial_x^\alpha u \in L^2(Q)\ \forall\ \alpha \text{ with } 0 \leq |\alpha| \leq l, \partial_t^i \in L^2(Q), i = 0, ..., k\}$ of functions defined in the space-time cylinder Q, where $L^2(Q)$ denotes the space of square-integrable functions, $\alpha = (\alpha_1, ..., \alpha_d)$ is a multi-index with non-negative integers $\alpha_1, ..., \alpha_d$, $|\alpha| = \alpha_1 + ... + \alpha_d$, $\partial_x^\alpha u := \partial^{|\alpha|}/\partial x_1^\alpha = \partial^{|\alpha_1|}...\partial x_d^{\alpha_d}$ and $\partial_t^i u := \partial^i u/\partial t^i$.

In order to obtain a 2-field weak form, we first introduce the velocity field, $\mathbf{v}(\mathbf{x}, t) = \dot{\mathbf{u}}$, then we transform the second order problem of eq. (2.1) to a first order system, such that:

$$\begin{aligned}
&\begin{cases} \rho\dot{\mathbf{v}} - \text{div}_{\mathbf{x}}\boldsymbol{\sigma} - \mathbf{f} = 0 \\ \rho(\mathbf{v} - \dot{\mathbf{u}}) = 0 \end{cases} \quad \forall(\mathbf{x}, \mathbf{t}) \in Q \\
&\mathbf{u} = \mathbf{g}(\mathbf{x}, t) \text{ for } \mathbf{x} \in \Gamma_u, t \in [0, T] \\
&\boldsymbol{\sigma}.\mathbf{n} = \mathbf{T}(\mathbf{x}, t) \text{ for } \mathbf{x} \in \Gamma_\sigma, t \in [0, T] \\
&\mathbf{u}(\mathbf{x}, t = 0) = \mathbf{u}_0(\mathbf{x}) \text{ for } \mathbf{x} \in \Omega \\
&\mathbf{v}(\mathbf{x}, t = 0) = \mathbf{v}_0(\mathbf{x}) \text{ for } \mathbf{x} \in \Omega
\end{aligned} \tag{2.4}$$

Thus, we obtain a two-field form of the problem. This form allows us to impose velocity initial and boundary conditions as Dirichlet conditions. We would like to show in the following how the choice of the test functions can affect the solution of the problem to be solved. For that, we first consider the classical form where we use test functions defined in appropriate spaces. We weight the first two equations of the system (2.4) by these test functions and we integrate them over the space-time cylinder Q. We then obtain:

$$\begin{aligned}&\text{Find } (\mathbf{u}(\mathbf{x},t),\mathbf{v}(\mathbf{x},t)) \in \mathcal{H}^u \times \mathcal{H}^v, \text{ such that } \forall\, (\delta\mathbf{u}(\mathbf{x},t),\delta\mathbf{v}(\mathbf{x},t)) \in \mathcal{H}_0^u \times \mathcal{H}_0^v \\ &\int_Q \left(\rho\dot{\mathbf{v}} - \mathrm{div}_{\mathbf{x}}\boldsymbol{\sigma} - \mathbf{f}\right)\delta\mathbf{u}dQ + \int_Q \rho\left(\mathbf{v}-\dot{\mathbf{u}}\right)\delta\mathbf{v}dQ = 0\end{aligned} \tag{2.5}$$

where $\mathcal{H}^u = \{\mathbf{u} \in (H^{1,1}(Q))^d,\ \mathbf{u} = \mathbf{g} \text{ on } \Gamma_u, \mathbf{u}(x,t=0) = \mathbf{u}_0(x)\}$, $\mathcal{H}^v = \{\mathbf{v} \in (H^{0,1}(Q))^d\ \mathbf{v} = \dot{\mathbf{g}} \text{ on } \Gamma_u, \mathbf{v}(x,t=0) = \mathbf{v}_0(x)\}$, $\mathcal{H}_0^u = \{\mathbf{u} \in (H^{1,1}(Q))^d, \mathbf{u} = \mathbf{0} \text{ on } \Gamma_u, \mathbf{u}(t=0) = \mathbf{0}\}$, $\mathcal{H}_0^v = \{\mathbf{v} \in (H^{0,1}(Q))^d, \mathbf{v} = \mathbf{0} \text{ on } \Gamma_u, \mathbf{v}(t=0) = \mathbf{0}\}$. After integrating by parts the divergence operator and using traction boundary conditions, the weak variational formulation of eq (2.5) becomes:

Form 1

$$\begin{aligned}&\text{Find } (\mathbf{u}(\mathbf{x},t),\mathbf{v}(\mathbf{x},t)) \in \mathcal{H}^u \times \mathcal{H}^v, \text{ such that } \forall\, (\delta\mathbf{u}(\mathbf{x},t),\delta\mathbf{v}(\mathbf{x},t)) \in \mathcal{H}_0^u \times \mathcal{H}_0^v \\ &\int_Q \rho\dot{\mathbf{v}}\delta\mathbf{u}dQ + \int_Q \boldsymbol{\sigma} : \boldsymbol{\varepsilon}(\delta\mathbf{u})dQ - \int_P \mathbf{T}\delta\mathbf{u}dP - \int_Q \mathbf{f}\delta\mathbf{u}dQ \\ &\qquad + \int_Q \rho\left(\mathbf{v}-\dot{\mathbf{u}}\right)\delta\mathbf{v}dQ = 0\end{aligned}$$

where $P = \Gamma_\sigma \times [0,T]$ is the space-time boundary where external forces apply. We therefore obtain a form similar to the principle of virtual work that can also be obtained by considering the stationarity of a Hamiltonian form. Consider for instance the following Lagrangian $\mathcal{L}$:

$$\mathcal{L}(\mathbf{u},\dot{\mathbf{u}},\mathbf{v}) = \mathcal{K}_{HR}(\dot{\mathbf{u}},\mathbf{v}) - \mathcal{P}(\mathbf{u}) \tag{2.1}$$

where $\mathcal{K}_{HR}$ and $\mathcal{P}$ are kinetic (modified according to the Hellinger-Reisner mixed form) and potential energy defined such that:

$$\begin{aligned}\mathcal{K}_{HR}(\dot{\mathbf{u}},\mathbf{v}) &= \int_\Omega \rho\mathbf{v}\dot{\mathbf{u}} - \frac{1}{2}\rho\mathbf{v}\mathbf{v}d\Omega \\ \mathcal{P}(\mathbf{u}) &= \int_\Omega \frac{1}{2}\boldsymbol{\sigma} : \boldsymbol{\varepsilon}d\Omega - \int_\Omega \mathbf{f}\mathbf{u}d\Omega - \int_{\Gamma_\sigma} \mathbf{T}\mathbf{u}dS\end{aligned} \tag{2.2}$$

Using the stationnarity of the Hamiltonian, $\mathcal{H}(\mathbf{u},\dot{\mathbf{u}},\mathbf{v}) = \int_0^T \mathcal{L}(\mathbf{u},\dot{\mathbf{u}},\mathbf{v})dt$, leads to:

$$-\int_Q \rho(\mathbf{v}-\dot{\mathbf{u}})\delta\mathbf{v}dQ + \int_Q \rho\mathbf{v}\delta\dot{\mathbf{u}}dQ - \int_Q \boldsymbol{\sigma} : \boldsymbol{\varepsilon}(\delta\mathbf{u})dQ + \int_P \mathbf{T}\delta\mathbf{u}dP + \int_Q \mathbf{f}\delta\mathbf{u}dQ = 0 \tag{2.3}$$

By integrating by parts the second integral and choosing $\delta\mathbf{u}$ such that $\delta\mathbf{u}(t=0) = 0$

and $\delta\mathbf{u}(t=T)=0$, we obtain:

$$-\int_Q \rho(\mathbf{v}-\dot{\mathbf{u}})\delta\mathbf{v}dQ-\int_Q \rho\dot{\mathbf{v}}\delta\mathbf{u}dQ-\int_Q \boldsymbol{\sigma}:\boldsymbol{\varepsilon}(\delta\mathbf{u})dQ+\int_P \mathbf{T}\delta\mathbf{u}dP+\int_Q \mathbf{f}\delta\mathbf{u}dQ=0 \tag{2.4}$$

Another alternative is to choose the first order time derivatives as weighting functions (see [48]). Thus, we weight the two first equations of system (2.4) by the time derivatives of the test functions and we integrate over the space-time domain just like we did for the first case, we obtain:

$$\begin{aligned}&\text{Find } (\mathbf{u}(\mathbf{x},t),\mathbf{v}(\mathbf{x},t))\in\mathcal{H}^u\times\mathcal{H}^v,\ \text{such that}\ \ \forall\,(\delta\mathbf{u}(\mathbf{x},t),\delta\mathbf{v}(\mathbf{x},t))\in\mathcal{H}_0^u\times\mathcal{H}_0^v\\&\int_Q\left(\rho\dot{\mathbf{v}}-\mathrm{div}_{\mathbf{x}}\boldsymbol{\sigma}-\mathbf{f}\right)\dot{\delta\mathbf{u}}dQ+\int_Q\rho\left(\mathbf{v}-\dot{\mathbf{u}}\right)\dot{\delta\mathbf{v}}dQ=0\end{aligned} \tag{2.5}$$

where $\mathcal{H}_0^u=\{\mathbf{u}\in(H^{1,1}(Q))^d,\ \mathbf{u}=\mathbf{0}\text{ on }\Gamma_u\}$, $\mathcal{H}_0^v=\{\mathbf{v}\in(H^{0,1}(Q))^d,\ \mathbf{v}=\mathbf{0}\text{ on }\Gamma_u\}$. After integrating by parts the divergence operator and using traction boundary conditions, we can rewrite eqs (2.5) and finally obtain Form 2:

Form 2

$$\begin{aligned}&\text{Find } (\mathbf{u}(\mathbf{x},t),\mathbf{v}(\mathbf{x},t))\in\mathcal{H}^u\times\mathcal{H}^v,\ \text{such that}\ \ \forall\,(\delta\mathbf{u}(\mathbf{x},t),\delta\mathbf{v}(\mathbf{x},t))\in\mathcal{H}_0^u\times\mathcal{H}_0^v\\&\int_Q\rho\dot{\mathbf{v}}\delta\dot{\mathbf{u}}dQ+\int_Q\boldsymbol{\sigma}:\boldsymbol{\varepsilon}(\delta\dot{\mathbf{u}})dQ-\int_P\mathbf{T}\delta\dot{\mathbf{u}}dP-\int_Q\mathbf{f}\delta\dot{\mathbf{u}}dQ\\&\qquad+\int_Q\rho\left(\mathbf{v}-\dot{\mathbf{u}}\right)\delta\dot{\mathbf{v}}dQ=0\end{aligned}$$

Remarks

1. The choice of using the time derivatives of test functions is made here as done previously by other authors (see for e.g. [48, 47, 34] and references therein). The first part of Form 2 can also be obtained from the principle of virtual power if we consider $\dot{\delta\mathbf{u}}$ to be a virtual velocity field.
2. Note that the variational form of Form 2 leads to a non-symmetric bilinear form while the one of From 1 is symmetric as expected. For some specific choices for the approximation space of $\mathbf{u}$ and $\mathbf{v}$ and for structured meshes, classical time integration schemes such as Crank-Nicholson can be recovered in the case of piecewise linear approximation functions. However, the use of continuous B-Spline approximations for test functions and possibly the use of unstructured meshes allow the construction of richer time integration schemes.
3. One advantage of a two field formulation is that it allows to impose velocity conditions (initial or boundaries) as Dirichlet conditions.

2.2.2. Stabilization in presence of discontinuities using Galerkin least squares terms

The variational formulations presented previously give accurate representation of the solution only in the case of smooth problems, whereas these formulations exhibit solutions with spurious oscillations for sharp problems, such as impact problems for example, where time-discontinuities appear. A way to control these oscillations is to add stabilization terms in the variational formulation. In the following, we consider continuous Galerkin forms enriched with least square terms. $(\mathbf{u}_h, \mathbf{v}_h)$ are taken to be the continuous approximation fields of the displacement and the velocity respectively. The space-time cylinder is discretized. We denote by Q_h its discrete form, such that $Q_h = \sum_e Q_e$ where Q_e are elements. Note that the formulation holds for FE and for IGA.

We first define a standard Galerkin Least Square form (GLS) in a similar manner as done in [48, 33]. In these references, the proposed stabilized formulation is shown to be stable. These stabilizing terms are added to Form 1, that becomes:

Form 1 + GLS

$$
\begin{aligned}
&\text{Find } (\mathbf{u}_h(\mathbf{x},t), \mathbf{v}_h(\mathbf{x},t)) \in \mathcal{H}^{u_h} \times \mathcal{H}^{v_h}, \text{ such that } \forall\, (\delta\mathbf{u}_h(\mathbf{x},t), \delta\mathbf{v}_h(\mathbf{x},t)) \\
&\in \mathcal{H}_0^{u_h} \times \mathcal{H}_0^{v_h} \\
&\int_{Q_h} \rho\dot{\mathbf{v}}_h \delta\mathbf{u}_h dQ + \int_{Q_h} \boldsymbol{\sigma} : \boldsymbol{\varepsilon}(\delta\mathbf{u}_h) dQ - \int_{P_h} \mathbf{T}_h \delta\mathbf{u}_h dP - \int_{Q_h} \mathbf{f}_h \delta\mathbf{u}_h dQ \\
&\qquad + \sum_e \int_{Q_e} (\rho\ddot{\mathbf{u}}_h - \mathrm{div}_x\boldsymbol{\sigma} - \mathbf{f}_h)\rho^{-1}\tilde{\tau}(\rho\delta\ddot{\mathbf{u}}_h - \mathrm{div}_x(\mathbf{C} : \boldsymbol{\varepsilon}(\delta\mathbf{u}_h)) dQ \\
&\qquad + \int_{Q_h} \rho\,(\mathbf{v}_h - \dot{\mathbf{u}}_h)\,\delta\mathbf{v}_h dQ = 0
\end{aligned}
$$

where $\tilde{\tau}$ is a stabilization (numerical) parameter (unit s^2) and $\mathbf{C}$ is the 4th order elasticity tensor.

On a second basis, we add the same least square terms to Form 2, that becomes:

Form 2 + GLS

$$
\begin{aligned}
&\text{Find } (\mathbf{u}_h(\mathbf{x},t), \mathbf{v}_h(\mathbf{x},t)) \in \mathcal{H}^{u_h} \times \mathcal{H}^{v_h}, \text{ such that } \forall\, (\delta\mathbf{u}_h(\mathbf{x},t), \delta\mathbf{v}_h(\mathbf{x},t)) \\
&\in \mathcal{H}_0^{u_h} \times \mathcal{H}_0^{v_h} \\
&\int_{Q_h} \rho\dot{\mathbf{v}}_h \delta\dot{\mathbf{u}}_h dQ + \int_{Q_h} \boldsymbol{\sigma} : \boldsymbol{\varepsilon}(\delta\dot{\mathbf{u}}_h) dQ - \int_{P_h} \mathbf{T}_h \delta\dot{\mathbf{u}}_h dP - \int_{Q_h} \mathbf{f}_h \delta\dot{\mathbf{u}}_h dQ \\
&\qquad + \sum_e \int_{Q_e} (\rho\ddot{\mathbf{u}}_h - \mathrm{div}_x\boldsymbol{\sigma} - \mathbf{f}_h)\rho^{-1}\tau(\rho\delta\ddot{\mathbf{u}}_h - \mathrm{div}_x(\mathbf{C} : \boldsymbol{\varepsilon}(\delta\mathbf{u}_h)) dQ \\
&\qquad + \int_{Q_h} \rho\,(\mathbf{v}_h - \dot{\mathbf{u}}_h)\,\delta\dot{\mathbf{v}}_h dQ = 0
\end{aligned}
$$

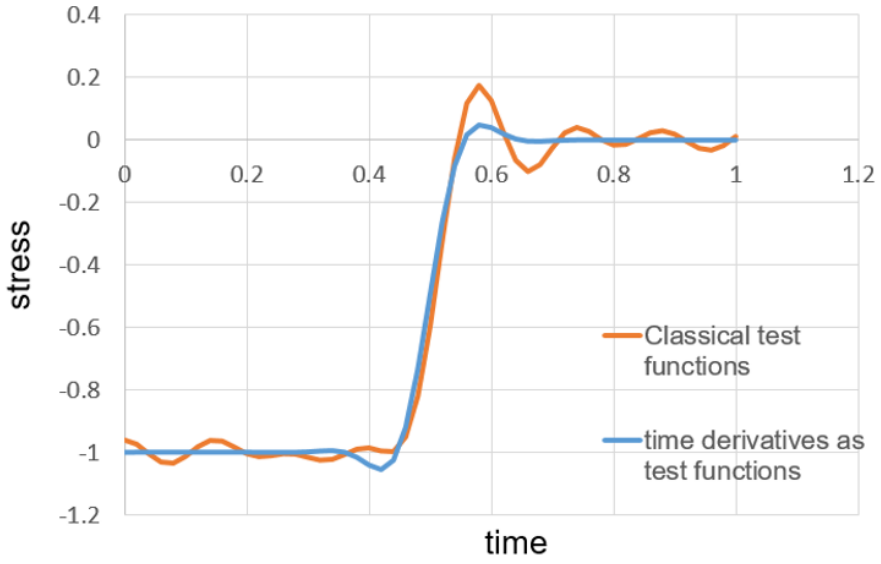

Figure 2.1. – Stress along the bar at $t = 0.5\ s$ using GLS stabilisation for derived and non derived test functions for $\tau = 0.02$ and same mesh size in time and space

where τ is also a stabilization parameter as $\tilde{\tau}$ (unit s).

We compare the two stabilized formulations on the bar impact problem. We investigate this problem on the unit spatial region $\Omega = [0, 1]$ and the temporal interval $[0, 1]$. The parameters of the problem are chosen such that $\rho = 1\ kg.m^{-3}$, $\tau = 0.02\ s$ and $\tilde{\tau} = \tau \Delta t$. We compare the results of the two formulations using for both cases a degree $p = 2$ and 50 elements in space and time for the discretization. Figure 2.1 shows that the oscillations in the solution computed using Form 2 + GLS vanish, whereas spurious oscillations are seen in the solution computed using Form 1 + GLS. This study shows that when dealing with a sharp problem such as bar impact, test functions derived in time must be used in order to obtain a more stable solution. For this reason, time derivative test functions will be adopted for the following.

2.2.3. Stabilization using acceleration consistency

The GLS form can be easily implemented in the linear case but not as easily in the non-linear case because of the term $\mathrm{div}_{\mathbf{x}}\boldsymbol{\sigma}$. We propose an alternative form for which we use the strong form of the first momentum conservation, $\rho\dot{\mathbf{v}} = \mathrm{div}_x\boldsymbol{\sigma} + \mathbf{f}$, as the least square term. We obtain the following form:

Form 2 + GAC

Find $(\mathbf{u}_h(\mathbf{x},t), \mathbf{v}_h(\mathbf{x},t)) \in \mathcal{H}^{u_h} \times \mathcal{H}^{v_h}$, such that $\forall\, (\delta\mathbf{u}_h(\mathbf{x},t), \delta\mathbf{v}_h(\mathbf{x},t)) \in \mathcal{H}_0^{u_h} \times \mathcal{H}_0^{v_h}$

$$\int_{Q_h} \rho\dot{\mathbf{v}}_h\delta\dot{\mathbf{u}}_h dQ + \int_{Q_h} \boldsymbol{\sigma} : \boldsymbol{\varepsilon}(\delta\dot{\mathbf{u}}_h) dQ - \int_{P_h} \mathbf{T}_h\delta\dot{\mathbf{u}}_h dP - \int_{Q_h} \mathbf{f}_h\delta\dot{\mathbf{u}}_h dQ + \sum_e \int_{Q_e} \rho(\ddot{\mathbf{u}}_h - \dot{\mathbf{v}}_h)\tau(\delta\ddot{\mathbf{u}}_h - \delta\dot{\mathbf{v}}_h) dQ + \int_{Q_h} \rho\,(\mathbf{v}_h - \dot{\mathbf{u}}_h)\,\delta\dot{\mathbf{v}}_h dQ = 0$$

This form remains fully consistent even in non-linear cases. The proof of consistency is straightforward and does not pose any difficulties. Its implementation is easier than Form 1 + GLS and Form 2 + GLS. We choose to call it Galerkin with Acceleration Consistency condition (GAC). Both stabilization strategies share the main idea of adding a mesh- dependant perturbation term. In the following, we describe the discretization procedure and the convergence properties of these formulations for both IGA and FE space-time approximations from the numerical point of view.

2.2.4. Space-time discretization

2.2.4.1. B-Spline/NURBS approximation

For the sake of simplicity, we choose to represent a 1D space-time domain, defined by the following parametric surface:

$$\begin{aligned} t(\xi,\eta) &= \sum_{i=1}^{n}\sum_{j=1}^{n} R_{i,p}(\xi)R_{j,p}(\eta)B^t_{i,j} \\ x(\xi,\eta) &= \sum_{i=1}^{n}\sum_{j=1}^{n} R_{i,p}(\xi)R_{j,p}(\eta)B^x_{i,j} \end{aligned} \tag{2.1}$$

where $\mathbf{B}_{i,j} = \{B^t_{i,j}, B^x_{i,j}\}$ are the control points. In Figure 2.2, a synthetic view of the description of a space-time domain within the IGA for a 2D case is given.

For the 1D problem in space, the discretised kinematic and velocity fields are:

$$\begin{aligned} \mathbf{u}_h(\xi,\eta) &= \sum_{i=1}^{n}\sum_{j=1}^{n} R_{i,p}(\xi)R_{j,p}(\eta)\mathbf{d}^u_{i,j} \\ \mathbf{v}_h(\xi,\eta) &= \sum_{i=1}^{m}\sum_{j=1}^{m} R_{i,q}(\xi)R_{j,q}(\eta)\mathbf{d}^v_{i,j} \end{aligned} \tag{2.2}$$

where $\mathbf{d}_{i,j} = \{\mathbf{d}^u_{i,j}, \mathbf{d}^v_{i,j}\}$ are the values that control the approximation of the fields at control points (which are not interpolant in general). Here we illustrate the discretization scheme using same approximations for displacements and velocities.

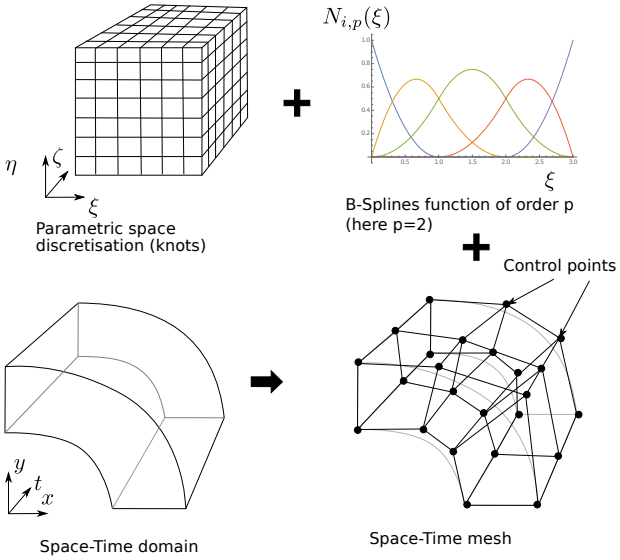

Figure 2.2. – Space-Time cylinder described with B-Spline functions

We use this approximation within this work. Discretisations for 2D and 3D space domains can be derived in the same manner.
Remarks

1. The main concept of space-time IGA (or space-time FE) is not assuming, a priori, any separations of space and time.
2. In this work, we only consider cases where we use the basis functions of same order in all the parametric directions. The tensorial structure of the approximation allows to consider higher polynomial orders in a specific parametric direction. This can be relevant to very specific cases, e.g. when the jacobian operator between the parametric space and the space-time domain is diagonal.
3. We assume in the following that the displacement and the velocity fields are described with the same approximation basis (i.e. $p = q$ and $m = n$). As for the FE method, the IGA in a multifield context allows to control the meshing (subdiscretization technique) and the order of approximation of each field.
4. In the case of IGA, we have additional possibilities: we can control the inter-element order of continuity of each field, which is not the case for FE.

2.2.4.2. Matrix form of space/time problems

The matrix/vector representation of the approximations of eq. (2.2) is given by:

$$\begin{aligned} \mathbf{u}_h(\xi,\eta) &= \mathbf{N_p}\mathbf{d^u} \\ \mathbf{v}_h(\xi,\eta) &= \mathbf{N_p}\mathbf{d^v} \end{aligned} \tag{2.3}$$

where $\mathbf{N_p}$ is a matrix obtained from the approximation functions such that $\mathbf{N_p} = [N_1, ..., N_n]$; n is the number of control points, and $\mathbf{d^u}, \mathbf{d^v}$ are the vectors obtained

from the unknown values at control points. We can define the following differential operators (that operate on real or test fields):

$$\begin{aligned}
\dot{\mathbf{u}}_h(\xi,\eta) &= \mathbf{B_t}\mathbf{d^u} \\
\nabla_{\mathbf{x}}\mathbf{u}_h(\xi,\eta) &= \mathbf{B_x}\mathbf{d^u} \\
\boldsymbol{\varepsilon}(\mathbf{u}_h(\xi,\eta)) &= \mathbf{B_x^{sym}}\mathbf{d^u} \\
\ddot{\mathbf{u}}_h(\xi,\eta) &= \mathbf{B_{tt}}\mathbf{d^u} \\
\nabla_{\mathbf{x}}\dot{\mathbf{u}}_h(\xi,\eta) &= \mathbf{B_{xt}}\mathbf{d^u} \\
\boldsymbol{\varepsilon}(\dot{\mathbf{u}}_h(\xi,\eta)) &= \mathbf{B_{xt}^{sym}}\mathbf{d^u}
\end{aligned} \tag{2.4}$$

such that

$$\begin{aligned}
\mathbf{B_x} &= [\frac{\partial N_1}{\partial x}, ..., \frac{\partial N_n}{\partial x}] \\
\mathbf{B_t} &= [\frac{\partial N_1}{\partial t}, ..., \frac{\partial N_n}{\partial t}] \\
\mathbf{B_{tt}} &= [\frac{\partial^2 N_1}{\partial t^2}, ..., \frac{\partial^2 N_n}{\partial t^2}] \\
\mathbf{B_{xt}} &= [\frac{\partial N_1}{\partial x \partial t}, ..., \frac{\partial N_n}{\partial x \partial t}] \\
\mathbf{B_x^{sym}} &= \frac{1}{2}(\mathbf{B_x} + \mathbf{B_x^T}) \\
\mathbf{B_{xt}^{sym}} &= \frac{1}{2}(\mathbf{B_{xt}} + \mathbf{B_{xt}^T}).
\end{aligned} \tag{2.5}$$

These operators require the computation of the second derivatives of the approximation functions (we therefore need $p \geq 2$). With the operators defined in eq. (2.4) and using the mapping of a space-time element to the parametric space, the previous weak formulations can be rewritten without difficulties into a matrix form. For instance, the formulation of Form 2 + GAC can be written as (linear case):

$$\begin{bmatrix} \mathbf{K_{uu}} & \mathbf{K_{uv}} \\ \mathbf{K_{vu}} & \mathbf{K_{vv}} \end{bmatrix} \begin{Bmatrix} \tilde{\mathbf{d}}^{\mathbf{u}} \\ \tilde{\mathbf{d}}^{\mathbf{v}} \end{Bmatrix} = \begin{Bmatrix} \tilde{\mathbf{f}}_{\mathbf{u}} \\ \tilde{\mathbf{f}}_{\mathbf{v}} \end{Bmatrix} \tag{2.6}$$

The tilde symbol stands for degrees of freedom that are not prescribed by a Dirichlet boundary condition (the right hand side is therefore modified in consequance during the assembly procedure). The matrix and vector introduced in eq. (2.6) are defined

by (again for a 1D space problem for the sake of simplicity):

$$\begin{aligned}
\mathbf{K_{uu}} &= \mathcal{A}_e \int_{Q_e} \left(\mathbf{B}_{xt}^{sym^{\mathrm{T}}} \mathbf{D} \mathbf{B}_{x}^{sym} + \rho \mathbf{B_{tt}}^{\mathrm{T}} \tau \mathbf{B_{tt}} \right) dQ \\
\mathbf{K_{uv}} &= \mathcal{A}_e \int_{Q_e} \left(\rho \mathbf{B_t}^{\mathrm{T}} \mathbf{B_t} - \rho \mathbf{B_{tt}}^{\mathrm{T}} \tau \mathbf{B_t} \right) dQ \\
\mathbf{K_{vu}} &= \mathcal{A}_e \int_{Q_e} \left(-\rho \mathbf{B_t}^{\mathrm{T}} \mathbf{B_t} - \rho \mathbf{B_t}^{\mathrm{T}} \tau \mathbf{B_{tt}} \right) dQ \\
\mathbf{K_{vv}} &= \mathcal{A}_e \int_{Q_e} \left(\rho \mathbf{B_t}^{\mathrm{T}} \mathbf{N_p} + \rho \mathbf{B_t}^{\mathrm{T}} \tau \mathbf{B_t} \right) dQ
\end{aligned} \tag{2.7}$$

and:

$$\begin{aligned}
\mathbf{f_u} &= \mathcal{A}_e \int_{Q_e} \mathbf{B_t}^{\mathrm{T}} \mathbf{f}_h dQ + \mathcal{A}_e \int_{P_e} \mathbf{B_t}^{\mathrm{T}} \mathbf{T}_h dP \\
\mathbf{f_v} &= \mathbf{0}
\end{aligned} \tag{2.8}$$

The assembly operator on elements is denoted by $\mathcal{A}_e$ and P_e are boundary element surfaces of the space domain (i.e. $x = 0$ or $x = L$ for a 1D problem).
Remarks

1. As mentionned previously, the left-hand side of the linear system is unsymmetric.
2. Initial and kinematic/velocity boundary conditions are prescribed directly using the values at control nodes located on the boundary (we have to pay attention to the non interpolant behavior of B-Spline functions on boundaries when $\mathbf{g}(x,t)$ and $\mathbf{T}(x,t)$ are not constant functions).

2.2.5. Numerical applications at small-strain

2.2.5.1. A clamped bar subjected to a body load

We consider a unit bar (1D space problem) with homogeneous boundary conditions in space and time for both the displacement and the velocity, subjected to body load $f(x,t)$ defined such that the exact solution of system (2.4) is:

$$\begin{aligned}
u(x,t) &= \sin(2\pi x) \log\left(\frac{1 + \cos^2(2\pi t)}{2} \right) \\
v(x,t) &= -\frac{4\pi \sin(4\pi t) \sin(2\pi x)}{3 + \cos(4\pi t)}
\end{aligned} \tag{2.9}$$

The space-time domain is a unit square. Figure 2.3 illustrates the test considered. The material parameters are: $E = 2\ Pa$ and $\rho = 1\ kg.m^{-3}$.

This test allows to establish a convergence study while considering both space-time FE and space-time IGA. For the finite elements, we use quadratic quadrangle

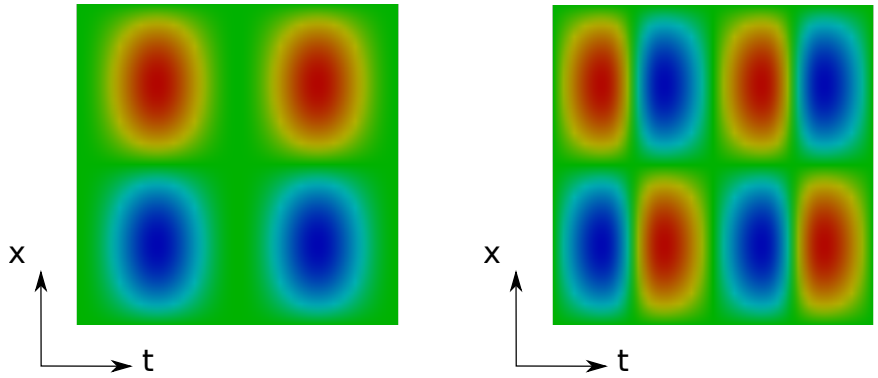

(a) displacement field (b) velocity field

Figure 2.3. – Unit space-time domain with body load and homogeneous dirichlet boundary conditions

with 9 nodes. We compute L_2 errors on the space-time domain Q, such that:

$$\begin{aligned} er_U &= \int_Q \|u_h(x,t) - u(x,t)\|^2 dQ \\ er_V &= \int_Q \|v_h(x,t) - v(x,t)\|^2 dQ \end{aligned} \tag{2.10}$$

where (u_h, v_h) is the approximated solution and (u, v) is the exact solution given by eq. (2.9). We first plot the results without any stabilization ($\tau = 0$). We use a uniform mesh refinement (in space and time) and we plot the L_2 error with respect to the element size. Figure 2.4 shows that we obtain a monotone convergence behavior and by computing the rate of convergence for different polynomial orders (from 2 to 4 for IGA), we obtain an optimal rate of convergence for both ST-FE and ST-IGA. If we consider ST-FE and ST-IGA for the same polynomial order (p=2), we can see that there are no differences between the quadratic finite elements and the quadratic NURBS elements for this test.

Figure 2.5 shows a comparison of the results for different stabilization strategies. It can be noticed that all formulations are convergent. The convergence rate is affected in a similar manner with both stabilization strategies (GAC or GLS) with ST-FE or ST-IGA. For the same value of the stabilization parameter, we obtain a stronger influence on approximations of order 2 while approximations of order 3 do not seem much affected by the additional stabilization terms.

This simple convergence study illustrates the interest of using higher polynomial orders for space-time discretizations. It also confirms that GLS and GAC stabilization strategies behave in a similar manner for both ST-FE and ST-IGA, at least for this simple and smooth test.

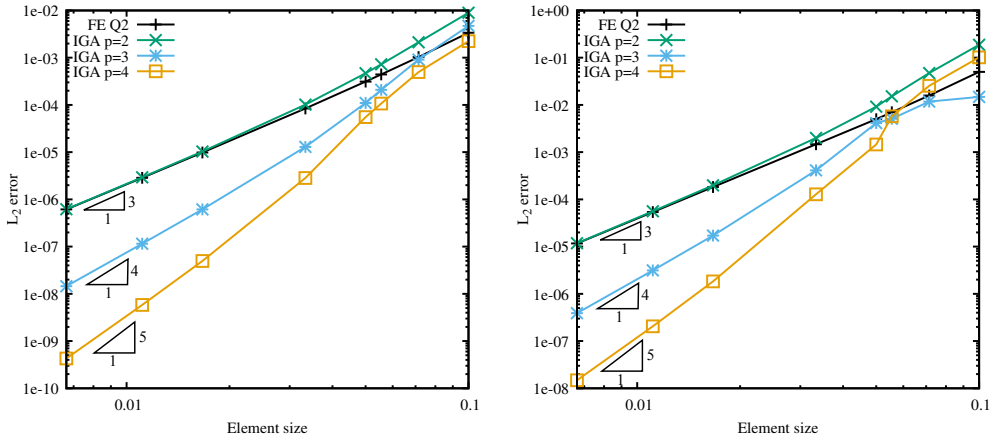

(a) L_2 error on u (b) L_2 error on v

Figure 2.4. – Convergence study for the bar test without stabilization

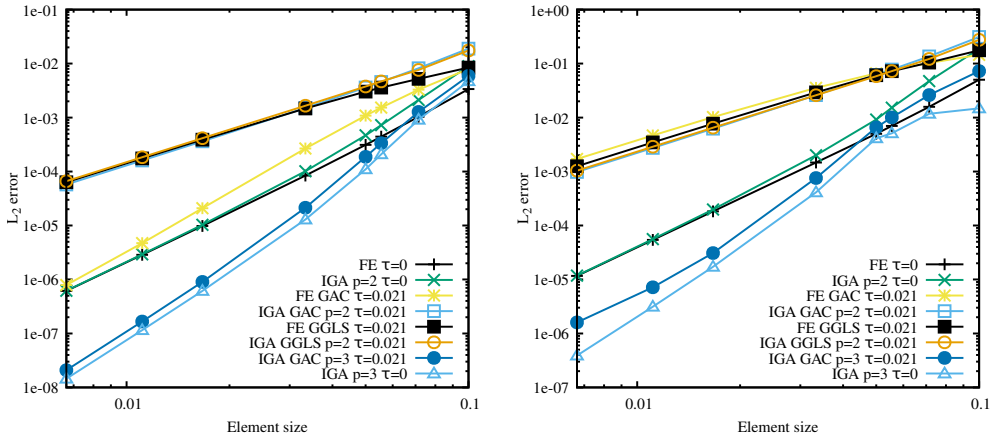

(a) L_2 error on u (b) L_2 error on v

Figure 2.5. – Convergence study for the bar test with stabilization ($p = 2$)

2.2.5.2. Impact of an elastic bar

We consider the test of the impact of a 1D elastic bar on a rigid wall. This test has been investigated with ST-FE in [46] and it is a typical benchmark to investigate the behavior of numerical oscillations for a wave propagation problem. The problem is illustrated in Figure 2.6(a). A 1D bar is submitted to an initial homogeneous velocity v_0. The impact against the rigid wall is taken into account with displacement and velocity conditions at one end of the bar (here $x = 0$) such that: $u(x = 0, t) = 0$ and $v(x = 0, t) = 0$. The other side of the bar is stress free. The material parameters are $E = 1\ Pa$ and $\rho = 1\ kg.m^{-3}$. The bar is of length $L = 1\ m$ and the initial velocity is $v_0 = 1\ m/s$. The analytical stress solution is a compressive wave that propagates with the velocity $c = \sqrt{E/\rho} = 1\ m/s$.

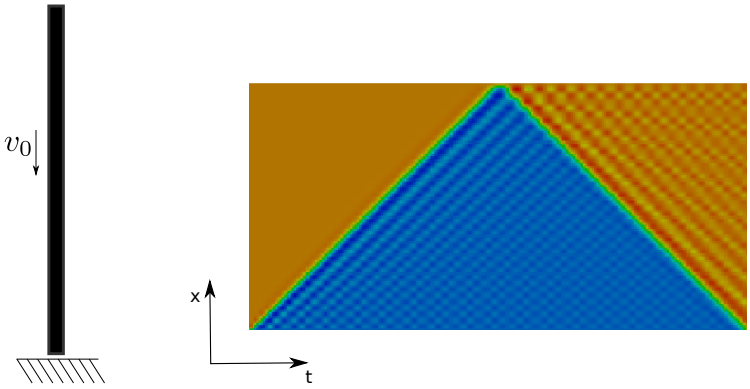

(a) Geometry and boundary conditions

(b) Stress field on the Space-Time domain (ST-IGA without stabilization, $\tau = 0$, $p = 2$)

Figure 2.6. – 1D bar impact problem against a rigid wall

Using ST-IGA or ST-FE without any stabilization, we obtain the typical stress solution in the space-time domain shown at Figure 2.6(b). Spurious numerical oscillations are obtained regardless the mesh size or the polynomial order of the approximations. These oscillations propagate in time and the solution for a longer period of time shows an increasingly noisy solution.

The stress along the bar at $t = 0.5\ s$ and using unstabilized formulations (i.e. for $\tau = 0$) exhibits spurious numerical oscillations. Figure 2.7(a) shows a comparison of the results between ST-FE and ST-IGA using the same mesh size, and we observe the same behavior for both methods. However, as can be seen from the plot of the total energy (see Figure 2.7(b)), non-stabilised space-time methods are conservative.

Numerical oscillations can be controlled by adding stabilization terms as shown in Figures 2.8(a) and 2.8(b). First, we can notice from Figure 2.8(a) that ST-FE and ST-IGA with GLS stabilisation for $p = 2$ behave in the same way. As expected, increasing the order of NURBS while keeping other parameters constant (mesh size and stabilization parameter) leads to a more accurate result in terms of localisation of the compression wavefront. Second, if we compare GAC and GLS stabilizations, we can see from Figure 2.8(b) that the GAC stabilization seems to be less dissipative than GLS for the same order of approximation, both for ST-IGA and ST-FEM. This point is more evident in Figure 2.8(c) where a comparison of the total energy integrated over the bar upon time is plotted: dotted lines (GAC stablization) are always above solid lines (GLS stabilization). It is also important to notice that as shown on the zoom in Figure 2.8(d), small oscillations are still present for ST-FEM but not for ST-IGA.

Another interesting aspect is to investigate the behavior of stabilization strategies

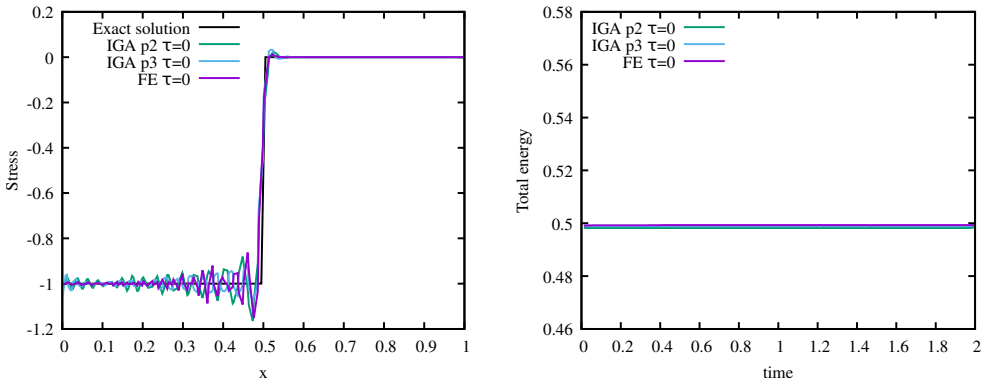

(a) Stress along the bar at $t = 0.5\ s$

(b) Total energy (kinematic + potential energy) integrated over the space domain upon time

Figure 2.7. – Results of the bar impact test without stabilisation with: $\Delta t = 0.0125\ s$ and $\Delta x = 0.0125\ m$

for different values of the stabilization parameter τ. Figure 2.9 shows that as expected, the numerical dissipation is directly related to the value of τ. A good option with ST-IGA of order 2 seems to choose τ approximately in the same order of magnitude of the meshsize of the time because using a larger value leads to a strong numerical dissipation without improving the numerical solution. We can also notice that the GLS stabilization with IGA can produce irregular behavior on the total energy for large values of the stabilization parameter for which the formulation dissipates too much energy.

The mesh size ratio plays an important role in space-time methods. We define $h = \Delta t/\Delta x$ as the ratio of the time increment under the space discretization parameter. Figure 2.10 shows the results obtained with ST-IGA for GLS and GAC stabilization parameters using a constant size of the space discretization and different time increments. We obtain a correct description of the compression wave using GAC and GLS only until $h = 4$. Higher values of the mesh ratio lead to oscillations whatever the value of the stabilization parameter is. Nevertheless, we can obtain satisfactory results for moderate mesh size ratios without being limited by the $CFL \leq 1$ condition where CFL is the Courant-Friedrichs-Lewy number ($CFL = h$ here because $CFL = \frac{\frac{E}{\Delta x}}{\frac{\rho}{\Delta t}}$ with $E = \rho = 1$). Whatever the mesh ratio is, the results seem to be stable. Only the accuracy of the solution seems to be affected.

This example illustrates the behaviour of space-time methods. But these results are obviously not general and should be confirmed by a mathematical study that is beyond the scope of the present work.

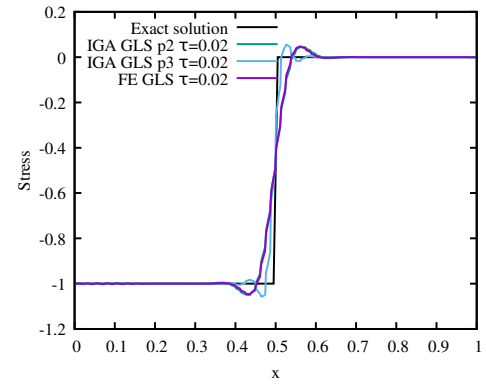

(a) Stress along the bar at $t = 0.5\ s$ using GLS stabilisation

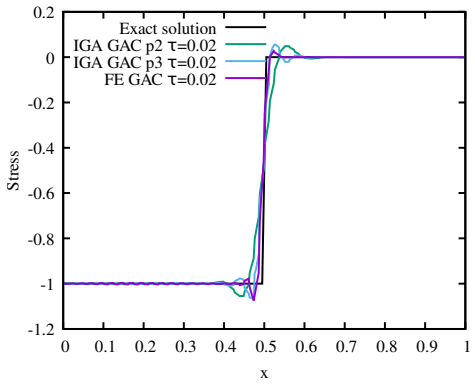

(b) Stress along the bar at $t = 0.5\ s$ using GAC stabilisation

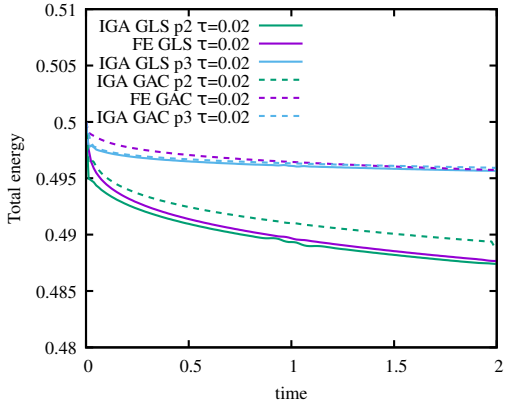

(c) Total energy upon time

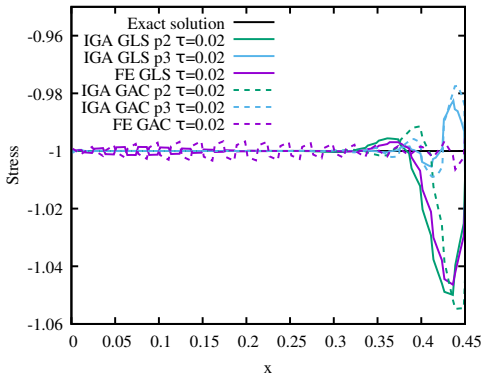

(d) Zoom of the stress along the bar about $t = 0.5\ s$ using stabilisation

Figure 2.8. – Results of the bar impact test with different stabilisation strategies with: $\Delta t = 0.0125\ s$ and $\Delta x = 0.0125\ m$

2.2.5.3. Two bars impact

This test is very similar to the previous one. We consider the case of an elastic bar with an initial velocity $v_0 = 1\ m/s$ that impacts a second elastic bar with different material properties. Boundary conditions and the dimensions of the bars are provided in Figure 2.11. The material properties of the first bar (in blue) are: $\rho = 1\ kg.m^{-3}$, $E = 1\ Pa$, and those of the second bar (in red) are: $\rho = 1\ kg.m^{-3}$, $E = 5.5\ Pa$. The solution just after the impact is the propagation of two compressive waves from the interface (impact zone) with two different velocities. After reflecting on both sides, these waves interact at the interface (with reflexion and transmission) on one hand and with each-other on the other hand. Therefore, we obtain after few interactions several waves that propagate with constant but different velocities (Figure 2.11 shows this typical solution obtained with stabilized ST-IGA with GAC).

For this test, we compare the results obtained with ST-IGA stabilized using

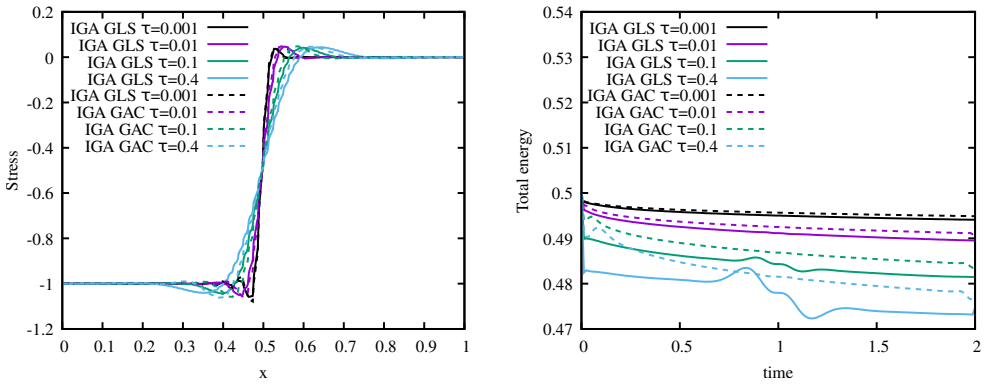

(a) Stress along the bar at $t = 0.5\ s$ (b) Total energy upon time

Figure 2.9. – Comparison of stabilization strategies for the bar impact test with ST-IGA of order 2, $\Delta t = \Delta x = 0.0125$

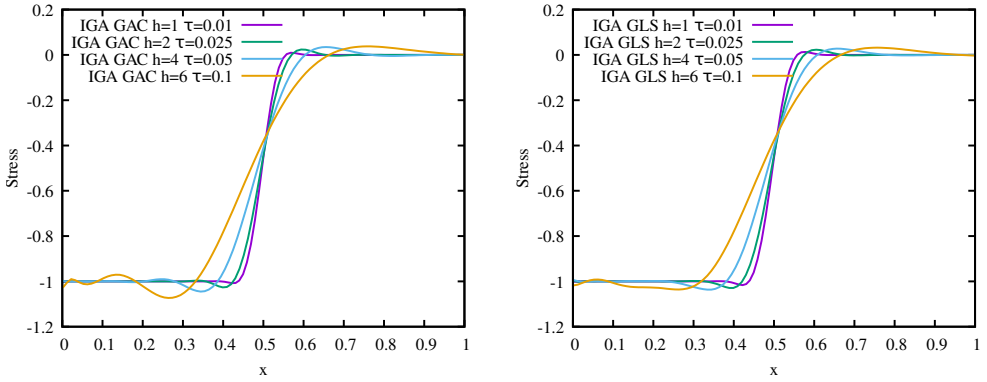

(a) ST-IGA of order 2, stress along the bar at $t = 0.5\ s$ using GAC stabilisation (b) ST-IGA of order 2, stress along the bar at $t = 0.5\ s$ using GLS stabilisation

Figure 2.10. – Results of the bar impact test with ST-IGA and ST-FE for various values of the mesh ratio $h = \Delta t/\Delta x$, with $\Delta x = 0.0125\ m$

the GAC formulation (for this example the stabilization paramater was fixed such that $\tau = (\Delta t)^{1/(p-1)}$ where p is the polynomial order of the approximation) for different polynomial oders from 2 to 4 with a standard finite element model on Abaqus. For this model, we used quadratic truss element with the implicit resolution. The time integration scheme is the Hilber-Hughes-Taylor scheme (see [38]) with the following parameters $\alpha = -0.05$, $\beta = 0.275$, $\gamma = 0.55$ that correspond to a transient fidelity integration. For all models, we used the same space-time discretisation with $\Delta t = 0.033\ s$ and $\Delta x = 0.033\ m$. Figure 2.12 shows the stress along the bar at different times. It can be seen that the finite element models exhibit strong oscillations where the ST-IGA solutions do not. Increasing the order of approximation both in space and time for the ST-IGA allows to obtain better and more conservative numerical solutions. This can be clearly in Figure 2.13,

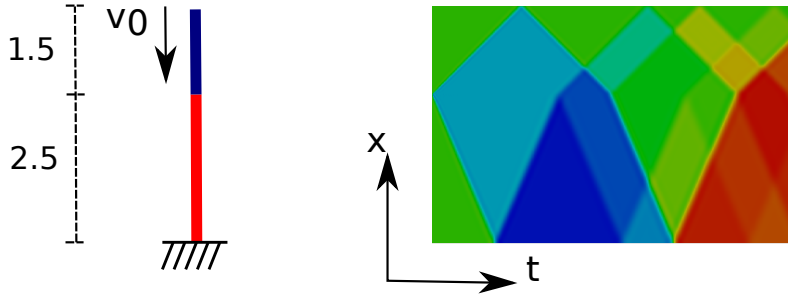

Figure 2.11. – Impact of 2 elastic bars. The blue bar has an initial velocity $v_0 = 1\ m/s$ and it is assumed that the two bars stay perfectly tied after impact. A typical Stress field on the Space-Time domain (ST-IGA with GAC stabilisation) is shown.

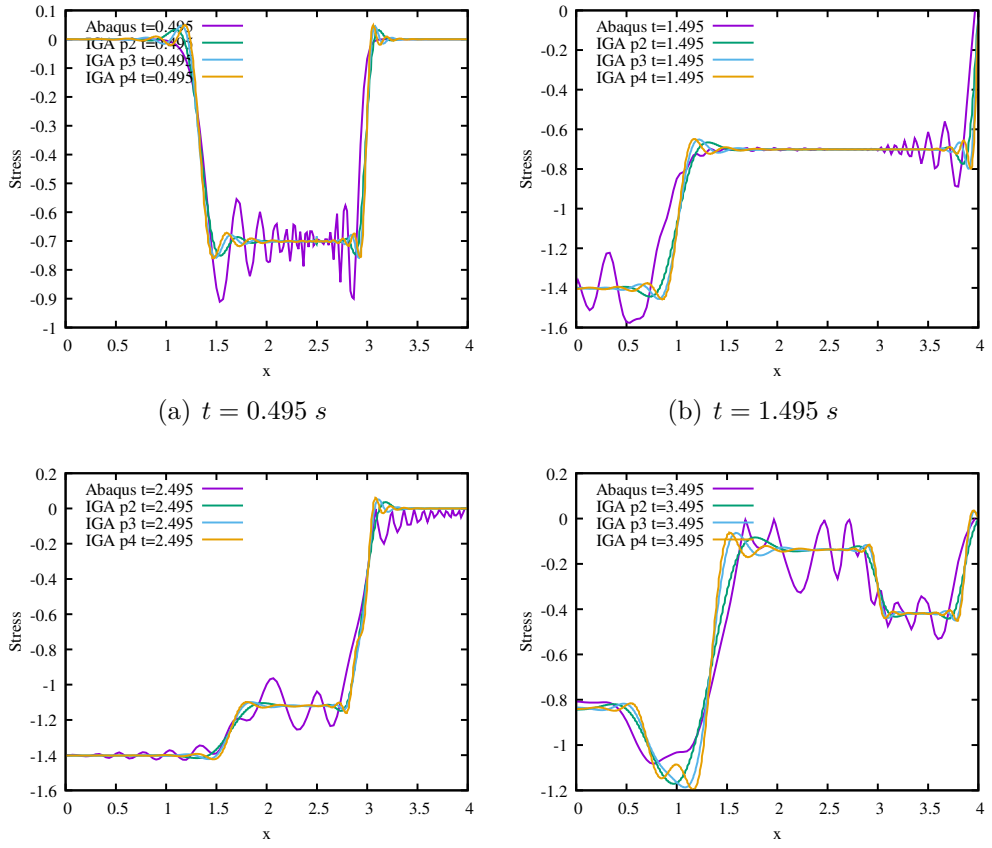

(a) $t = 0.495\ s$ (b) $t = 1.495\ s$

(c) $t = 2.495\ s$ (d) $t = 3.495\ s$

Figure 2.12. – Stress along the two bars for different times after impact. Space and time increments are identical for all models: $\Delta t = \Delta x = 0.033$

ST-IGA schemes of order 3 and 4 are more conservative than the ones obtained with the FE model on Abaqus.

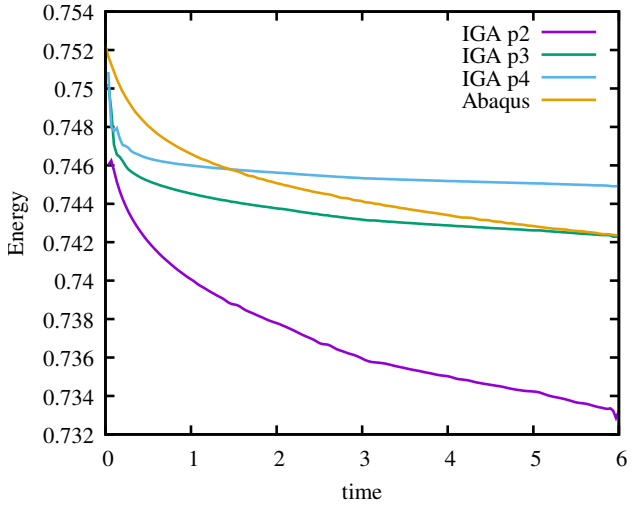

Figure 2.13. – Kinectic energy + strain energy integrated over the two bars upon time

2.2.5.4. Extension of the bar test for truss structures

We show in this section that the previous formulation concerning 1D bar problems can be extended to the case of bar in space for applications to truss structures. We assume that each truss in a structure is described by a space-time patch. Each patch have a local coordinate system with 2 dimensions in space, (e'_x, e'_y), that is related to a global coordinate system (e_x, e_y) with the following rotation matrix:

$$\left\{ \begin{array}{c} e'_x \\ e'_y \end{array} \right\} = \left\{ \begin{array}{c} \mathbf{R}_1 \\ \mathbf{R}_2 \end{array} \right\} = \left[\begin{array}{cc} \cos(\theta) & \sin(\theta) \\ -\sin(\theta) & \cos(\theta) \end{array} \right] \left\{ \begin{array}{c} e_x \\ e_y \end{array} \right\} = \mathbf{R}(\theta) \left\{ \begin{array}{c} e_x \\ e_y \end{array} \right\} \tag{2.11}$$

where $\mathbf{R}_1$ and $\mathbf{R}_2$ correspond respectively to the first and second row of $\mathbf{R}(\theta)$. The axis e'_x corresponds to the direction of the truss and e'_y is normal to the truss. We denote by $(u'_x(\mathbf{x},t), u'_y(\mathbf{x},t))$ and $(v'_x(\mathbf{x},t), v'_y(\mathbf{x},t))$ the displacement and velocity of the truss in a patch. We also assume that the normal velocity is constant and the normal displacement is only a function of time, such that:

$$\begin{cases} v'_y(\mathbf{x},t) = cst \\ u'_y(\mathbf{x},t) = y(t) \end{cases} \tag{2.12}$$

or equivalently:

$$\begin{cases} \dot{v}'_y = 0 \\ \nabla_{x'} u'_y = 0 \end{cases} \tag{2.13}$$

The uniaxial strain and stress in the truss are defined by:

$$\boldsymbol{\varepsilon}(\mathbf{x},t) = \nabla_{x'} u'_x(\mathbf{x},t) \qquad \boldsymbol{\sigma}(\mathbf{x},t) = E\boldsymbol{\varepsilon}(\mathbf{x},t) \tag{2.14}$$

The weak form for this problem on a patch is simply obtained from an extension of eq. Form 2 + GAC. We first assume that the angle θ is constant (no time dependance) and we add two least-square type terms that correspond to the constraints defined in eq. (2.13):

$$\begin{aligned}
&\text{Find } (\mathbf{u}_h(\mathbf{x},t),\mathbf{v}_h(\mathbf{x},t)) \in \mathcal{H}^{u_h} \times \mathcal{H}^{v_h}, \text{ such that } \forall\, (\delta\mathbf{u}_h(\mathbf{x},t),\delta\mathbf{v}_h(\mathbf{x},t)) \in \mathcal{H}_0^{u_h} \times \mathcal{H}_0^{v_h} \\
&\int_{Q_h} \rho(\mathbf{R}_1\dot{\mathbf{v}}_h)(\mathbf{R}_1\delta\dot{\mathbf{u}}_h)dQ + \int_{Q_h} \boldsymbol{\sigma} : \dot{\boldsymbol{\varepsilon}}(\mathbf{R}_1\delta\mathbf{u}_h)dQ - \int_{P_h} (\mathbf{R}_1\mathbf{T}_h)(\mathbf{R}_1\delta\dot{\mathbf{u}}_h)dP \\
&- \int_{Q_h} (\mathbf{R}_1\mathbf{f}_h)(\mathbf{R}_1\delta\dot{\mathbf{u}}_h)dQ + \sum_e \int_{Q_e} \rho(\mathbf{R}_1\ddot{\mathbf{u}}_h - \mathbf{R}_1\dot{\mathbf{v}}_h)\tau(\mathbf{R}_1\delta\ddot{\mathbf{u}}_h - \mathbf{R}_1\delta\dot{\mathbf{v}}_h)dQ \\
&\qquad + \int_{Q_h} \rho\left(\mathbf{R}_1\mathbf{v}_h - \mathbf{R}_1\dot{\mathbf{u}}_h\right)\mathbf{R}_1\delta\dot{\mathbf{v}}_h dQ + \sum_e \int_{Q_e} k_1(\mathbf{R}_2\dot{\mathbf{v}}_h)(\mathbf{R}_2\delta\dot{\mathbf{v}}_h)dQ \\
&\qquad + \sum_e \int_{Q_e} k_2(\nabla_{x'}\mathbf{R}_2\mathbf{u}_h)(\nabla_{x'}\mathbf{R}_2\delta\mathbf{u}_h)dQ = 0
\end{aligned} \tag{2.15}$$

such that $u'_x = \mathbf{R}_1\mathbf{u}_h$ and $u'_y = \mathbf{R}_2\mathbf{u}_h$, k_1, k_2 are penalty parameters. For a multipatch configuration we simply proceed as in the previous example, two connected patches share a common interface with the same refinement and the same controls points.

As an example, we consider the case of an assembly of two trusses that are connected with a given angle θ_0. Each truss is of unit length with the same material such that $E = 1\ Pa, \rho = 1\ kg.m^{-3}$. The trusses have an unit initial velocity and impact a wall on one side (we assume that the trusses stay fixed to the wall after impact), see Figure 2.14.

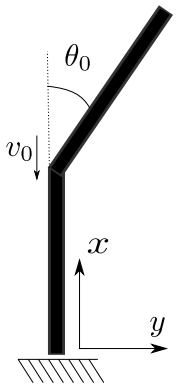

Figure 2.14. – Truss impact: Geometry and boundary conditions

Figure 2.15 shows the results obtained for two configurations: $\theta_0 = 20^o$ and $\theta_0 = 90^o$. The mesh size is chosen such that $\Delta t = 0.02\ s$ and $\Delta x = 0.02\ m$. The parameters of stabilisation and penalty conditions are taken to be $\tau = 0.02, k_1 = 10^9, k_2 = 10^9$. It can be observed that in the situation where $\theta_0 = 90^o$, the upper truss move vertically with a constant velocity but without stress. The impact wave is not transmitted to the upper truss in this case, contrarily to the case where $\theta_0 = 20^o$. This simple example illustrates the potential of space-time methods for

application to wave propagation problems in structures. Furthermore it could be extended to cases where the rotation matrix $\mathbf{R}$ is not constant in time to treat the case of truss structures with pivot connection between truss. Beams, shells and other structural elements can be developed in this framework in a straightforward manner.

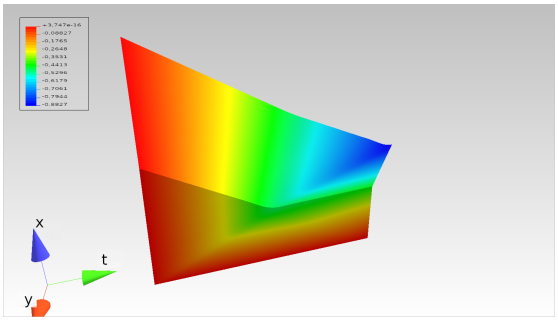

(a) deformed configuration for $\theta_0 = 20^o$ (isocolor correspond to the x component of the displacement field)

(b) stress field for $\theta_0 = 20^o$

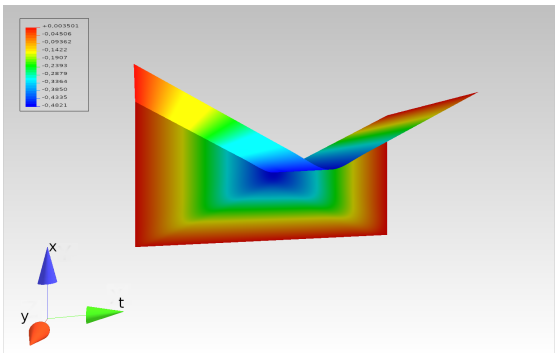

(c) deformed configuration for $\theta_0 = 90^o$ (isocolor correspond to the x component of the displacement field)

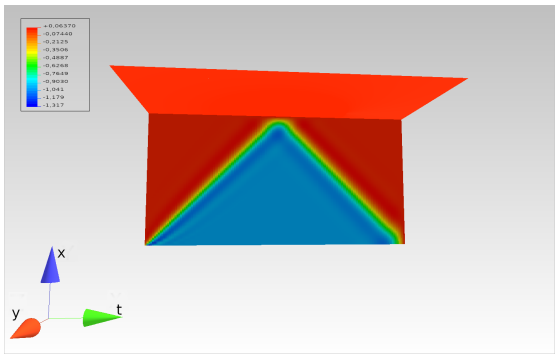

(d) stress field for $\theta_0 = 90^o$

Figure 2.15. – Result of the truss impact test: x direction correspond to time, y to x and z to y (ST-IGA with GAC stabilisation and $p = 2$)

2.3. Finite-strain formulations

2.3.1. Problem statement

In this section, we consider the current domain $\Omega(t)$. The initial one at $t = 0$, Ω_0, is taken as reference. A material point in Ω_0 is denoted by $\mathbf{X}$, and by $\mathbf{x}$ in $\Omega(t)$. The transformation, $\boldsymbol{\phi}(\mathbf{X}, t)$, allows to relate between both configurations, such that $\mathbf{x} = \boldsymbol{\phi}(\mathbf{X}, t)$. We assume that $\boldsymbol{\phi}$ is a bijective function, so we can always switch from a current description to a description in the initial configuration. In the following we adopt a Lagrangian representation of the problem. The space-time

domain is defined such that $Q = \Omega_0 \times [0, T]$. Therefore, time and space integration commute such that $\int_Q dQ = \int_0^T \int_{\Omega_0} dQ = \int_{\Omega_0} \int_0^T dQ$. The conservation of the linear momentum on Q is similar to eq. (2.1):

$$\rho_0 \ddot{\mathbf{u}} - \mathrm{DIV}_{\mathbf{X}} \boldsymbol{\Pi} = \mathbf{f} \tag{2.16}$$

where $\rho_0(\mathbf{X})$ is the initial material density, $\boldsymbol{\Pi}$ is the first Piola-Kirchoff stress, $\mathrm{DIV}_{\mathbf{X}}$ is the Lagrangian divergence operator and $\mathbf{f}$ is the body force defined by unit of initial volume. The dot superscript stands for the so called material time derivative (derivative with respect to time holding $\mathbf{X}$ constant), such that for a Lagrangian field $\dot{\mathbf{u}}(\mathbf{X}, t) = (\partial \mathbf{u}(\mathbf{X}, t)/\partial t)_{\mathbf{X}}$.

For the constitutive behavior, we restrict ourselves to the case of isotropic hyperelastic materials and we consider two cases: compressible and nearly-incompressible materials. For the first case, the stress/strain relation is simply obtained from the derivative of a specific free energy potential $\psi(\mathbf{F})$, such that (Lagrangian form):

$$\boldsymbol{\Pi} = \rho_0 \frac{\partial \psi}{\partial \mathbf{F}} \tag{2.17}$$

where $\mathbf{F}$ is the transformation gradient: $\mathbf{F} = \nabla_{\mathbf{X}} \boldsymbol{\phi} = \nabla_{\mathbf{X}} \mathbf{u} + \mathbf{1}$. For a nearly incompressible behavior, we adopt a formalism based on a hybrid free energy as described in [66]. This formalism is similar to a partial Legendre transformation of the Helmoltz energy formulated with a volumetric part. It allows us to introduce the hydrostatic pressure, p, as a thermodynamic state variable and naturally leads to a displacement/pressure formulation of the conservation equations.

The first Piola-Kirchoff stress is therefore decomposed as:

$$\boldsymbol{\Pi} = \bar{\boldsymbol{\Pi}} : \mathbb{P}_{\mathbf{F}} + J p \mathbf{F}^{-\mathrm{T}} \tag{2.18}$$

where $J = \det(\mathbf{F})$, $\mathbb{P}_{\mathbf{F}}$ is a 4th order tensor that corresponds to the deviatoric operator in the Lagrangian configuration, $\bar{\boldsymbol{\Pi}} = \rho_0 \partial \varphi / \partial \bar{\mathbf{F}}$ where φ is a hybrid free energy potential (a detailed description of the formulation is given in [66]) and $\bar{\mathbf{F}} = J^{-1/3} \mathbf{F}$. The additional field $p(\mathbf{X}, t)$ stands for the hydrostatic pressure and we have to define a supplementary constitutive equation that relates p to the volume variation J. For the sake of simplicity, we consider the simplest form:

$$J - 1 = g(p) \tag{2.19}$$

where g is a compressibility function.

The problem is fully defined by taking into account the same boundary and initial conditions as defined in eqs. (2.3).

2.3.2. Variational formulations for compressible and nearly-incompressible problems

For the compressible problem, the variational formulation is very similar to the one of eq. (2.5):

$$\begin{aligned}&\text{Find } (\mathbf{u}(\mathbf{x},t),\mathbf{v}(\mathbf{x},t)) \in \mathcal{H}^u \times \mathcal{H}^v, \text{ such that } \forall\, (\delta\mathbf{u}(\mathbf{x},t),\delta\mathbf{v}(\mathbf{x},t)) \in \mathcal{H}_0^u \times \mathcal{H}_0^v \\ &\int_Q \left(\rho_0 \dot{\mathbf{v}} - \mathrm{DIV}_{\mathbf{X}}\boldsymbol{\Pi} - \mathbf{f}\right) \delta\dot{\mathbf{u}} dQ + \int_Q \rho_0 \left(\mathbf{v} - \dot{\mathbf{u}}\right) \delta\dot{\mathbf{v}} dQ = 0\end{aligned} \tag{2.20}$$

By integrating by parts the divergence operator and adding a least square term, the stabilized version of the previous equation can be written as:

Form 3 + GAC

$$\begin{aligned}&\text{Find } (\mathbf{u}_h(\mathbf{x},t),\mathbf{v}_h(\mathbf{x},t)) \in \mathcal{H}^{u_h} \times \mathcal{H}^{v_h}, \text{ such that } \forall\, (\delta\mathbf{u}_h(\mathbf{x},t),\delta\mathbf{v}_h(\mathbf{x},t)) \\ &\in \mathcal{H}_0^{u_h} \times \mathcal{H}_0^{v_h} \\ &\int_{Q_h} \rho_0 \dot{\mathbf{v}}_h \delta\dot{\mathbf{u}}_h dQ + \int_{Q_h} \boldsymbol{\Pi} : \nabla_{\mathbf{X}} \delta\dot{\mathbf{u}}_h dQ - \beta \int_{P_h} \mathbf{T}_h \delta\dot{\mathbf{u}}_h dP - \beta \int_{Q_h} \mathbf{f}_h \delta\dot{\mathbf{u}}_h dQ \\ &+ \sum_e \int_{Q_e} \rho_0 (\ddot{\mathbf{u}}_h - \dot{\mathbf{v}}_h) \tau (\delta\ddot{\mathbf{u}}_h - \delta\dot{\mathbf{v}}_h) dQ + \int_{Q_h} \rho_0 \left(\mathbf{v}_h - \dot{\mathbf{u}}_h\right) \delta\dot{\mathbf{v}}_h dQ = 0\end{aligned}$$

Here $\mathbf{T}_h = \boldsymbol{\Pi}\mathbf{N}$ where $\mathbf{N}$ is the normal to the initial contour Γ. A load parameter $\beta \in [0,1]$ is introduced here to control the iterative convergence of the numerical scheme. As for the small strain case, we recover the principle of virtual power in the first part of the system of eqs. (2.3.2).

For the nearly-incompressible formulation, we adopt a 3-field formulation in a similar way as it was previously proposed in [66]:

$$\begin{aligned}&\text{Find } (\mathbf{u}_h(\mathbf{x},t),\mathbf{v}_h(\mathbf{x},t),p_h(\mathbf{x},t)) \in \mathcal{H}^{u_h} \times \mathcal{H}^{v_h} \times L^2(Q) \\ &\qquad \text{such that } \forall\, (\delta\mathbf{u}_h(\mathbf{x},t),\delta\mathbf{v}_h(\mathbf{x},t),\delta p_h(\mathbf{x},t)) \in \mathcal{H}_0^{u_h} \times \mathcal{H}_0^{v_h} \times L^2(Q)\end{aligned}$$

$$\begin{aligned}&\int_{Q_h} \rho_0 \dot{\mathbf{v}}_h \delta\dot{\mathbf{u}}_h dQ + \int_{Q_h} (\bar{\boldsymbol{\Pi}} : \mathbb{P}_{\mathbf{F}} + p_h J \mathbf{F}^{-\mathrm{T}}) : \nabla_{\mathbf{X}} \delta\dot{\mathbf{u}}_h dQ - \beta \int_{P_h} \mathbf{T}_h \delta\dot{\mathbf{u}}_h dP \\ &\quad - \beta \int_{Q_h} \mathbf{f}_h \delta\dot{\mathbf{u}}_h dQ + \sum_e \int_{Q_e} \rho_0 (\ddot{\mathbf{u}}_h - \dot{\mathbf{v}}_h) \tau (\delta\ddot{\mathbf{u}}_h - \delta\dot{\mathbf{v}}_h) dQ \\ &\quad + \int_{Q_h} \rho_0 \left(\mathbf{v}_h - \dot{\mathbf{u}}_h\right) \delta\dot{\mathbf{v}}_h dQ + \int_{Q_h} \left(J(\mathbf{u}_h) - 1 - g(p_h)\right) \delta p_h dQ = 0\end{aligned} \tag{2.1}$$

2.3.3. Space-time discretization

For a non-linear problem, such as the one of eq. Form 3 + GAC, we obtain a non-linear system to be solved in the vector form:

$$\begin{cases} \mathbf{r_u}(\mathbf{d}, \beta) = 0 \\ \mathbf{r_v}(\mathbf{d}, \beta) = 0 \end{cases} \tag{2.2}$$

where $(\mathbf{r_u}, \mathbf{r_v})$ are defined by:

$$\begin{aligned} \mathbf{r_u}(\mathbf{d}, \beta) &= \mathcal{A}_e \int_{Q_e} \left(\rho_0 \mathbf{B_t}^{\mathrm{T}} \dot{\mathbf{v}}_h + \mathbf{B}_{xt}^{\mathrm{T}} \mathbf{\Pi}(\mathbf{u}_h) + \mathbf{B_{tt}}^{\mathrm{T}} \rho_0 \tau (\ddot{\mathbf{u}}_h - \dot{\mathbf{v}}_h) \right) dQ - \beta \mathbf{f_u} \\ \mathbf{r_v}(\mathbf{d}, \beta) &= \mathcal{A}_e \int_{Q_e} \left(\rho_0 \mathbf{B_t}^{\mathrm{T}} \left((\mathbf{v}_h - \dot{\mathbf{u}}_h) + \tau (\ddot{\mathbf{u}}_h - \dot{\mathbf{v}}_h) \right) \right) dQ \end{aligned} \tag{2.3}$$

and $\beta \in [0, 1]$ is a load factor. The procedure used to solve this non-linear system is very standard and completely identical to a predictive/corrective Newton-Raphson procedure for a quasi-static problem. Starting from a known solution, $(\mathbf{d}^k, \beta^k)$, at increment k, we search $\Delta \mathbf{d}^k$ for a given load increment $\Delta \beta^k$ such that $\mathbf{r_u}(\mathbf{d}^k + \Delta \mathbf{d}^k, \beta^k + \Delta \beta^k) = \mathbf{r_v}(\mathbf{d}^k + \Delta \mathbf{d}^k, \beta^k + \Delta \beta^k) = 0$. The linearisation of this non-linear problem leads to:

$$\begin{bmatrix} \mathbf{K_{uu}}(\mathbf{u}_h^k, \mathbf{v}_h^k) & \mathbf{K_{uv}}(\mathbf{u}_h^k, \mathbf{v}_h^k) \\ \mathbf{K_{vu}}(\mathbf{u}_h^k, \mathbf{v}_h^k) & \mathbf{K_{vv}}(\mathbf{u}_h^k, \mathbf{v}_h^k) \end{bmatrix} \begin{Bmatrix} \Delta \mathbf{d^{u^k}} \\ \Delta \mathbf{d^{v^k}} \end{Bmatrix} = \begin{Bmatrix} -\mathbf{r_u}(\mathbf{d^k}, \beta^{\mathbf{k}}) - \mathbf{f}_u \Delta \beta^k \\ -\mathbf{r_v}(\mathbf{d}^k, \beta^k) \end{Bmatrix} \tag{2.4}$$

We distinguish the predictive and the corrective phases. For the predictive phase, the previous solution is convergent and therefore $\mathbf{r_u}(\mathbf{d}^k, \beta^k) = 0$, $\mathbf{r_v}(\mathbf{d}^k, \beta^k) = 0$ and $\Delta \beta^k = l$ where l is a prescribed value. For the corrective phase, the loading is frozen: $\Delta \beta^k = 0$ and $\mathbf{r_u}(\mathbf{d}^k, \beta^k) \neq 0$, $\mathbf{r_v}(\mathbf{d}^k, \beta^k) \neq 0$. We iterate with $(\mathbf{d}^{k+1}, \beta^{k+1}) = (\mathbf{d}^k + \Delta \mathbf{d}^k, \beta^k + \Delta \beta^k)$ until convergence to a given tolerance. The matrix terms $\mathbf{K_{vu}}, \mathbf{K_{vv}}, \mathbf{K_{uv}}$ are identical to the one defined previously in eq. (2.7), the term $\mathbf{K_{uu}}$ is slightly different and is defined as follow:

$$\mathbf{K_{uu}} = \mathcal{A}_e \int_{Q_e} \left(\mathbf{B}_{xt}^{\mathrm{T}} \mathbf{D}_{nl} \mathbf{B}_x + \rho \mathbf{B_{tt}}^{\mathrm{T}} \tau \mathbf{B_{tt}} \right) dQ \tag{2.5}$$

where $\mathbf{D}_{nl} = \partial \mathbf{\Pi} / \partial \mathbf{F}$.

2.3.4. The specific case of nearly-incompressible problems

The three field formulation presented in eq. (2.3.2) is well adapted for nearly-incompressible situations but we have to pay attention to numerical instabilities or oscillations that occur if we don't carefully choose the approximation spaces for the pressure and displacement. For isogeometric analysis, different propositions can be found in the literature. We chose here the one proposed in [58]. It consists of using the same order of approximations for the pressure and the displacement fields but with a grid subdivision for the pressure field (*i.e.* a coarser mesh for pressure than

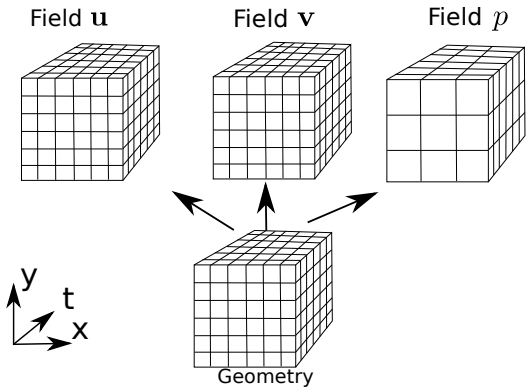

Figure 2.16. – Mesh subdivision technique for the pressure field (3-field formulation for nearly-incompressible problems)

the one used for velocity/displacement). Using the same interpolation order for the displacement and pressure fields mostly leads to unstable formulations with Lagrange finite elements. But due to the subdivision properties of B-Splines, this is not the case for IGA. It was shown in [**kadapa2016**] that this formulation satisfies the inf-sup or Ladyzhenskaya-Babuska-Brezzi (LBB) condition for small strain formulations. This property seems conserved for finite strain formulations, at least for simple problems. In any case, no typical pressure instabilities or volumetric locking were observed with this formulation.

For the space-time formulation, we chose to use a coarser mesh size for the pressure only for space discretization. Figure 2.3.4 presents a synthetic view for a 2D space problem. The numerical integration is done on the finest mesh for all fields using a standard Gauss-Legendre scheme.

2.3.5. Numerical applications at finite-strain

2.3.5.1. Nearly-incompressible plane-strain structure subjected to a harmonic loading

We consider the case of a non-linear beam like structure (2D plane-strain case) that is of 5 length unit height and 1 length width (see Figure 2.17(a)). The beam is clamped at one side and subjected to a harmonic homogeneous body load $f(t) = f_0 \cos(2\pi F t)$ in direction x. The constitutive material is chosen to be hyperelastic and we adopt a Mooney-Rivlin potential:

$$\rho_0 \varphi = c_{10}(I_1(\bar{\mathbf{C}}) - 3) + c_{01}(I_2(\bar{\mathbf{C}}) - 3)$$

For the compressible part, we consider the following compressibility function:

$$g(p) = \exp\left(\frac{p}{k}\right) - 1$$

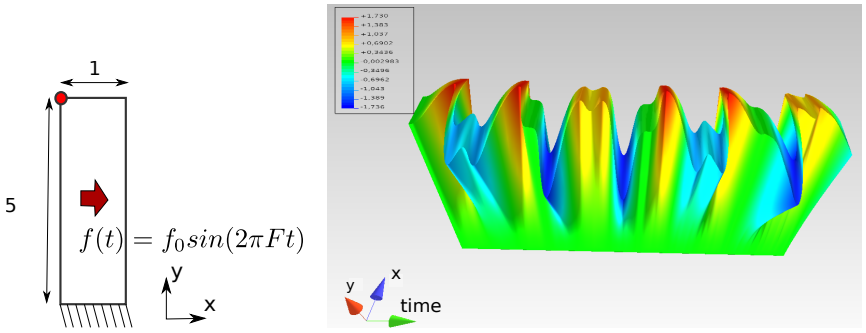

(a) Geometry of the structure (plane strain case)

(b) ST-IGA solution on a time slab (isocolor correspond to the horizontal displacement)

Figure 2.17. – Harmonic oscillations of a nearly-incompressible beam-like structure

The material parameters are: $c_{10} = 0.9, c_{01} = 0.1, k = 1000\ N/sK$, $\rho_0 = 0.001\ Ns^2/m^4$. From a linear vibration analysis, we determine the three first linear modes of this structure. The frequencies of these modes are: $F_1 = 0.56\ Hz, F_2 = 2.92\ Hz, F_3 = 4.5\ Hz$. In the following we consider a harmonic body load and choose the frequency between the first and the second modes of the structure: $F = 1.3\ Hz$ with an amplitude of $f_0 = 0.0184$. As for the previous example, we compare the results of ST-IGA with the one obtained on Abaqus using implict and explicit solvers. For the space discretization, we used the following mesh size: $\Delta x = \Delta y = 0.25\ m$. For the implicit solver, we considered quadratic hybrid elements (CPE8H) that are adapted to the case of near-incompressible behavior. For the explicit solver, we are restricted to use linear element with reduced integration (CPE4R). For ST-IGA model, we use the GAC stabilized form with the stabilisation parameter taken at $\tau = \Delta t/(\sqrt{E/\rho})$, where $E = 6(c_{10} + c_{0.1})$ is the infinitesimal Young modulus and $\Delta t = 0.14\ s$ is the time mesh size.

A typical response of the ST-IGA model for the time interval, $[0, 10]$, is given in Figure 2.17(b). Figure 2.18 shows a comparison between the different numerical methods for the displacement and the velocity at a node located at the top of the structure (the red point of figure 2.17(a)). As expected, the solutions obtained using ST-IGA and FE with implicit resolution are almost identical, while the explicit resolution exhibits some differences that are certainly due to the fact that only linear elements are used.

Figure 2.19 illustrates the best numerical performances of ST-IGA methods for non-linear problems: we can obtain more conservative solutions than with standard implicit integration schemes such as the HHT scheme. Table 2.1 allows us to compare the numerical behaviour of the different methods. For ST-IGA, we obtain the solution on the time slab with only 6 Newton iterations (for only one increment for this test) while the implicit resolution requires 250 increments with 1 or 2 Newton iterations per increments. Obviously, the difference between space-time continuous formulations and other methods in terms of the size of the linear system to be solved at each iteration is much larger. The advantage of the ST formulation

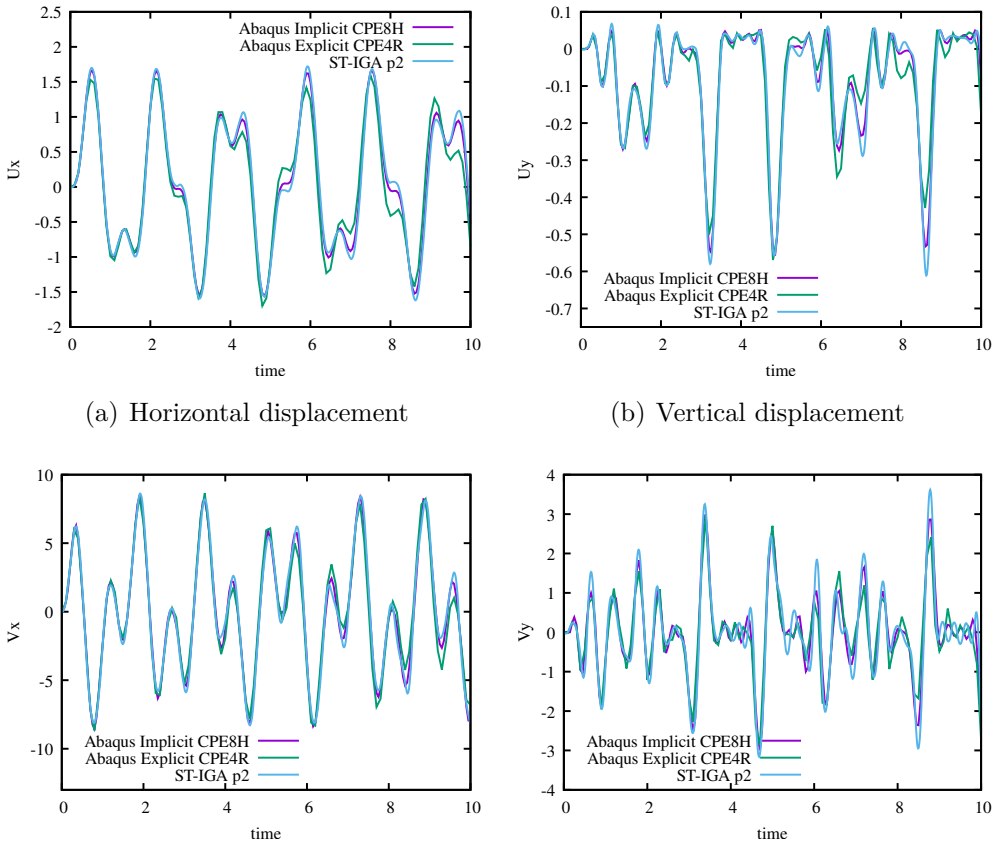

(a) Horizontal displacement

(b) Vertical displacement

(c) Horizontal velocity

(d) Vertical velocity

Figure 2.18. – Displacement and velocity of at the top left corner of the structure upon time

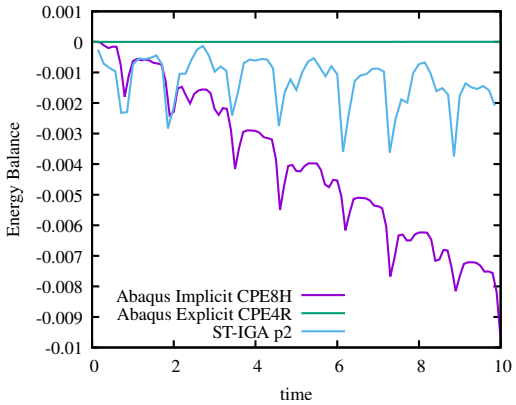

Figure 2.19. – Energy balance (kinetic energy + strain energy - external power integrated over time) integrated over the space domain

depends drastically on it.

	Δt	Number of load increments	Newton Iterations
ST-IGA	0.14	1	6
FE implicit (HHT)	0.05	250	1 or 2 per increments
FE explicit	0.00016	62500	-

Table 2.1. – Comparison between classical and space-time time integration

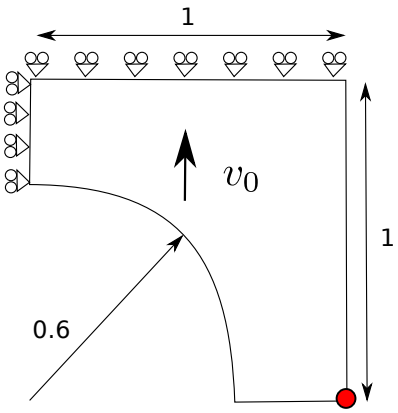

(a) Geometry and boundary conditions of a plane strain structure impact

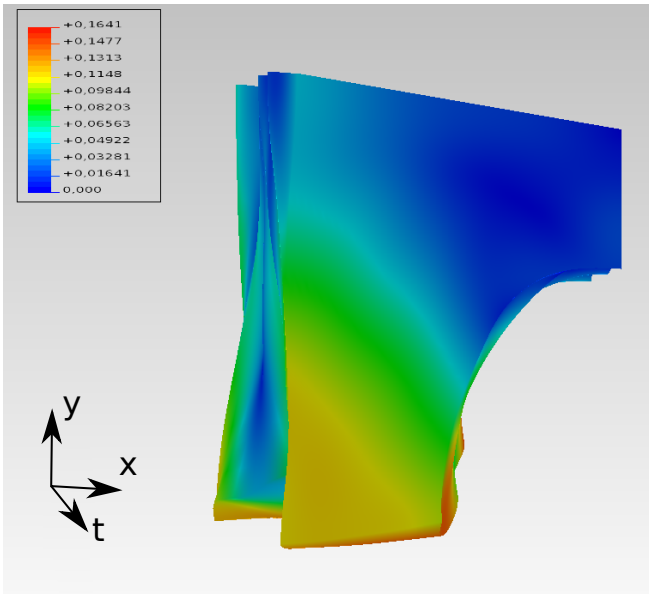

(b) ST-IGA solution on a time slab (isocolor corresponds to the norm of the displacement)

Figure 2.20. – Impact of a plane strain structure on a wall at finite strain

2.3.5.2. Plane strain structure subjected to an impact

The purpose of this test is to qualitatively evaluate the numerical behavior of the ST-IGA method in a context where we have a complexity due to both the dynamics (impact situation and non-linear behavior) and the geometry. The boundary conditions and the geometry of the structure are given in Figure 2.20. This plane strain structure has an initial vertical velocity $v_0 = 5\ m/s$. At $t = 0\ s$, it impacts a wall on the top of the structure. The material is assumed to be elastic and isotropic and we adopt the following potential of energy:

$$\rho_0 \psi = \frac{\mu}{2}(I_1(\mathbf{C}) - 3) + \frac{\lambda}{2}\ln(J)^2 - \mu \ln(J) \tag{2.6}$$

where $\lambda = 0.52$, $\mu = 0.34$ and $\rho_0 = 0.001\ Ns^2/m^4$. As in the previous example, we compare the results obtained with standard implicit and explicit finite elements on Abaqus with the results of space-time methods (FE or IGA based) stabilized with GAC. On Abaqus, the constitutive law is defined using the subroutine UHYPER.

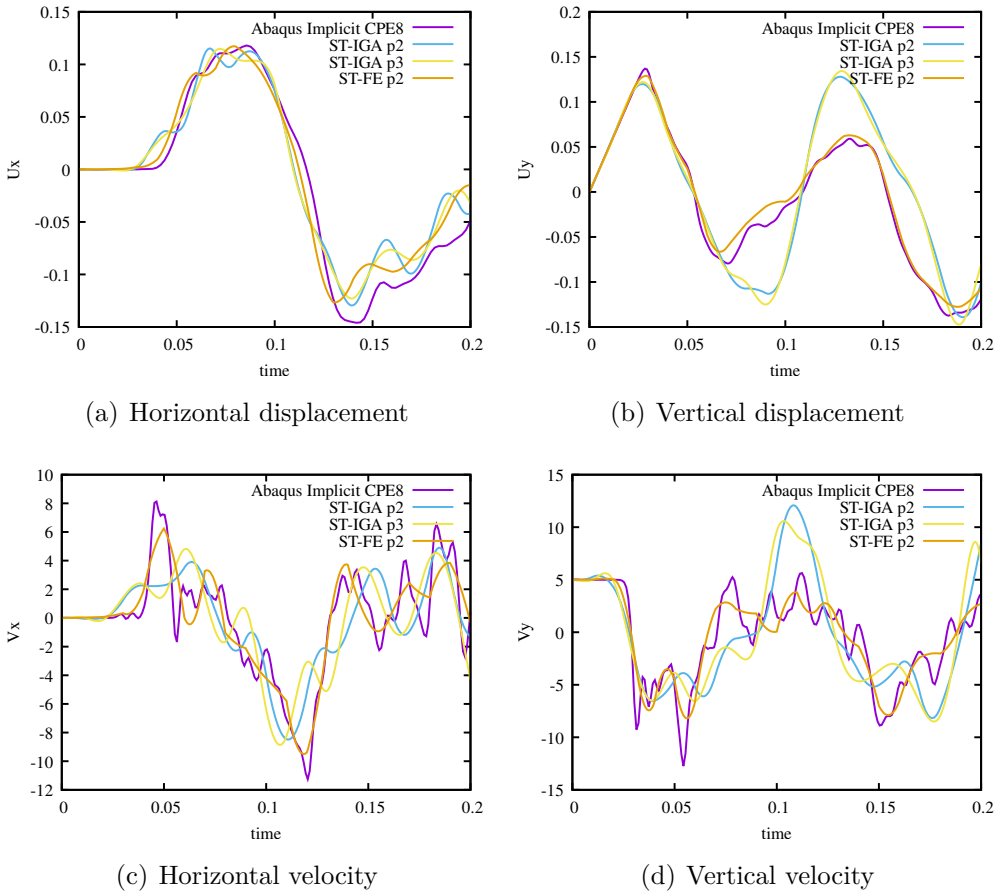

(a) Horizontal displacement

(b) Vertical displacement

(c) Horizontal velocity

(d) Vertical velocity

Figure 2.21. – Displacement and velocity at the bottom right corner of the structure upon time

Therefore we only use the implicit version of Abaqus with transient-fidelity resolution (HHT scheme with $\alpha = -0.05$, $\beta = 0.275$, $\gamma = 0.55$). We use the same mesh size for the discretisation of the space domain: $\Delta x = \Delta y = 0.036\ m$ for all models.

Figure 2.21 shows a comparison of the methods for solutions concerning the displacement and velocity components of a point located at the bottom of the structure (red point in figure 2.20(a)). First, it can be seen that the response obtained with Abaqus exhibits a lot of oscillations for the velocity field. The solution obtained using ST-FE is globally in accordance with the one obtained with Abaqus implicit. ST-IGA exhibits a similar response just after the impact but deviates from FE responses especially on the vertical componant (both for displacement and velocity). Obviously, all these models are questionable and we cannot define a reference solution for this problem as each model has its own bias.

We also plot the evolution of the total energy (kinetic energy+strain energy integrated over the space domain) upon time. Figure 2.22 shows that the evolution of this energy with the implicit solver of Abaqus exhibits a non monotonic behavior (increase and decrease of the total energy). This non-monotonic behavior is

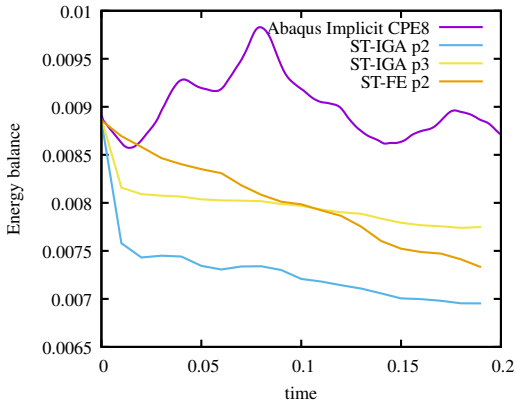

Figure 2.22. – Energy balance (kinetic energy + strain energy - external power integrated over time) integrated over the space domain

obviously completely inconsistent: we can expect a loss of energy due to numerical dissipation which is intrinsic to the HHT scheme but we do not expect an energy increase. Space-time methods have a more expected behavior with a monotonic decrease in energy due to the contribution of stabilization terms. It can also be noted that ST-FE have a higher rate of decrease than ST-IGA. Therefore, from an energy point of view, space-time methods behave better than Abaqus Implicit for this test.

Table 2.2 allows to compare the numerical behaviour of each model.

	Δt	Nbr of load increments	Newton Iterations
ST-IGA (p=2,3)	0.01	2	5 for 1^{st} inc. & 1 for 2^{nd}
ST-FE (p=2)	0.01	2	5 for 1^{st} inc. & 1 for 2^{nd}
FE Implicit (HHT)	0.001	212	3 to 6 per inc.

Table 2.2. – Comparison of characteristics between incremental and space-time resolutions

We can see from Table 2.2 that for a fixed mesh in space, the HHT scheme uses a time step that is 10 times smaller compared to the time step used for space-time metods in order to converge. Moreover, for space-time methods, 2 load increments per time step are enough to solve this non-linear problem with a small number of Newton iterations per increment, whereas for the implicit case, 212 load increments are needed, with 3 to 6 Newton iterations per increment, which shows that the number of Newton iterations needed in the case of the implicit method for this problem to converge is huge. These results show that the ST methods represent a very interesting alternative for solving nonlinear dynamics problems.

2.4. Conclusion

In this chapter, stabilized ST IGA methods are used for solving elastodynamics problems in both linear and non-linear cases. We introduced a new form of stabilization which is the so-called GAC based on classical GLS techniques. A qualitative study of the GAC formulation on 1D impact problems shows the stability of the formulation compared to classical forms. Moreover, comparisons between our ST-IGA formulation and ST-FEM methods and semi-discrete FEM simulations (HHT scheme) were made for transient dynamic problems showing the efficiency of the method. The ST IGA was also employed for the first time for solving finite strains elastodynamics including compressible and nearly-incompressible cases, and accurate results were obtained showing the interest and potential of the method. The formulation is general enough to be applied to different kinds of problems: small-strain elasticity, compressible and quasi-incompressible hyperelasticity with displacement/velocity/pressure formulations. It is also is easily extendable to multi-field and multi-physics problems such as thermo-elasticity. Space-time methods were shown to be more conservative than traditional semi-discrete methods on the examples chosen here. They seem to have better stability properties than the classical methods such as the explicit ones when employed in simple test problems. However, in the case of problems with discontinuous solutions, dissipative terms of type GLS or GAC should be added in order to control the oscillations. Obviously the numerical cost of such methods is high, especially for multi-field formulations, but employing high-order space-time schemes allows to obtain accurate numerical solutions with coarser mesh in time compared to implicit semi-discrete methods (in space and time). Furthermore, the numerical cost must be carefully considered as it strongly depends on the problem. Space-time formulations are also well adapted for the development of parallel resolution in space and time, references on this topic can be found in the literature (e.g. [37, 64]). Time-stepping strategies based on Galerkin discontinuous formulation in time should lead to have solvers with large time steps, allowing computations for long-term simulations.

3. Space-Time for Multiphysics Problems

Chapter Contents

3.1. Introduction

In this chapter, we are interested in the resolution of thermo-mechanical problems. The thermodynamics leads to strong or weak coupling depending on the problem considered and/or on the material parameters dependency. In literature, one can find various strategies to tackle these problems: fully coupled resolutions mainly based on backward Euler scheme for the time discretization or alternate resolution

of each physics with staggered schemes. The temperature plays a crucial role in engineering problems. During a mechanical solicitation, the deformation of an elastomer is frequently accompanied by thermal changes. When an isotropic, linearly elastic material is subjected to a temperature field θ, this may imply expansions and contractions in the material. In the literature, only few references can be found where the thermoelasticity problems are treated using a space-time numerical method, e.g. [59, 65]. To the author's knowledge, the IGA space-time method has not yet been used for the resolution of such problems, and it could be a good alternative of the usual semi-discrete methods. Notice that space-time methods allow the use of different interpolation degrees for space and time approximations for each field in the case of a multifield problem such as multiphysics. Different grids could be chosen for each field of the equation, especially in time. Space-time methods allow us to have heterogeneous and asynchronous schemes. In this chapter, a space-time B-spline/NURBS based isogeometric analysis is investigated for a 3-field formulation (displacement, velocity and temperature). Such as for elastodynamics, both linear and non-linear cases are investigated.

3.2. Small-strain thermoelasticity: linear case

3.2.1. Problem statement

We consider a thermo-elastodynamic problem. The basic equations of linear thermoelasticity are as follows:

$$\begin{aligned} \rho\ddot{\mathbf{u}} - \mathrm{div}_{\mathbf{x}}\boldsymbol{\sigma} &= \mathbf{f} \quad \forall(\mathbf{x},\mathbf{t}) \in Q \\ \rho C\dot{\theta} + div\mathbf{q} &= \mathbf{r} \quad \forall(\mathbf{x},\mathbf{t}) \in Q \end{aligned} \tag{3.1}$$

where $\mathbf{u}(\mathbf{x},t)$ is the displacement field, $\boldsymbol{\sigma}(\mathbf{x},t)$ is the Cauchy stress tensor, $\mathbf{f}(\mathbf{x},t)$ is the applied body load, $\theta(\mathbf{x},t)$ is the temperature field. The vector field $\mathbf{q}(\mathbf{x},t)$ denotes the heat flux, $\mathbf{r}(\mathbf{x},t)$ is the external heat supply, $\rho(\mathbf{x})$ is the initial material density, C is the specific heat, $\mathbf{q} = -K_\theta\nabla\theta$ is the heat flux density linearly dependent to the gradient of the temperature (isotropic Fourier's law); K_θ is the thermal conductivity (isotropic conduction for the sake of simplicity). The definition of the thermoelastic stress is given by:

$$\boldsymbol{\sigma} = 2\mu\boldsymbol{\varepsilon} + \lambda tr\boldsymbol{\varepsilon}\boldsymbol{I} - \alpha K_B\boldsymbol{\Delta}\theta I \tag{3.2}$$

where μ and λ are the Lamé parameters, K_B is the bulk modulus and $\boldsymbol{\Delta}\theta = \theta - \theta_0$; θ_0 is the initial temperature value .

The problem's boundary and initial conditions are the following:

$$\begin{aligned}
&\mathbf{u} = \mathbf{g}(\mathbf{x}, t) \text{ for } \mathbf{x} \in \Gamma_u, t \in [0, T] \\
&\boldsymbol{\sigma}.\mathbf{n} = \mathbf{T}(\mathbf{x}, t) \text{ for } \mathbf{x} \in \Gamma_\sigma, t \in [0, T] \\
&\mathbf{u}(\mathbf{x}, t = 0) = \mathbf{u}_0(\mathbf{x}) \text{ for } \mathbf{x} \in \Omega \\
&\dot{\mathbf{u}}(\mathbf{x}, t = 0) = \mathbf{v}_0(\mathbf{x}) \text{ for } \mathbf{x} \in \Omega \\
&\theta = \mathbf{h}(\mathbf{x}, t) \text{ for } \mathbf{x} \in \Gamma_\theta, t \in [0, T] \\
&\mathbf{q}.\mathbf{n} = \bar{\mathbf{q}}(\mathbf{x}, t) \text{ for } \mathbf{x} \in \Gamma_q, t \in [0, T] \\
&\theta(\mathbf{x}, t = 0) = \theta_{\mathbf{0}}(\mathbf{x})
\end{aligned} \tag{3.3}$$

where $\mathbf{n}(\mathbf{x})$ is the normal to the boundary Γ_σ, $\mathbf{u}_0(\mathbf{x})$ and $\mathbf{v}_0(\mathbf{x})$ are respectively the initial displacement and velocity fields, $\mathbf{h}$ is the prescribed boundary temperature and $\bar{\mathbf{q}}$ is the prescribed boundary heat flux.

3.2.2. A 3-field weak form

As done in the previous chapter, we introduce the velocity field, thereby tranforming the problem into a 3-field form:

$$\begin{aligned}
&\begin{cases}
\rho\mathbf{v} - \mathrm{div}_{\mathbf{x}}\boldsymbol{\sigma} - \mathbf{f} = 0 \\
\rho(\mathbf{v} - \dot{\mathbf{u}}) = 0 \qquad\qquad \forall(\mathbf{x}, \mathbf{t}) \in Q \\
\rho C\dot{\theta} + div\mathbf{q} = \mathbf{r}
\end{cases} \\
&\mathbf{u} = \mathbf{g}(\mathbf{x}, t) \text{ for } \mathbf{x} \in \Gamma_u, t \in [0, T] \\
&\boldsymbol{\sigma}.\mathbf{n} = \mathbf{T}(\mathbf{x}, t) \text{ for } \mathbf{x} \in \Gamma_\sigma, t \in [0, T] \\
&\mathbf{u}(\mathbf{x}, t = 0) = \mathbf{u}_0(\mathbf{x}) \text{ for } \mathbf{x} \in \Omega \\
&\mathbf{v}(\mathbf{x}, t = 0) = \mathbf{v}_0(\mathbf{x}) \text{ for } \mathbf{x} \in \Omega \\
&\theta = \mathbf{h}(\mathbf{x}, t) \text{ for } \mathbf{x} \in \Gamma_\theta, t \in [0, T] \\
&\mathbf{q}.\mathbf{n} = \bar{\mathbf{q}}(\mathbf{x}, t) \text{ for } \mathbf{x} \in \Gamma_q, t \in [0, T] \\
&\theta(\mathbf{x}, t = 0) = \theta_{\mathbf{0}}(\mathbf{x})
\end{aligned} \tag{3.4}$$

Concerning the choice of test functions, we would like to study the results using both variational formulations consisting first of classical test functions for the elastodynamics equation, and second of test functions derived in time, for the elastodynamics equation as well. To begin, we propose a variational formulation consisting of the classical test functions for both the parabolic (heat conduction) and hyperbolic (elastodynamics) equations, that is:

Form 1 + GAC

Find $(\mathbf{u}(\mathbf{x},t),\mathbf{v}(\mathbf{x},t),\theta(\mathbf{x},t)) \in \mathcal{H}^u \times \mathcal{H}^v \times \mathcal{H}^\theta$, such that $\forall\, (\delta\mathbf{u}(\mathbf{x},t),\delta\mathbf{v}(\mathbf{x},t),\delta\theta(\mathbf{x},t)) \in \mathcal{H}_0^u \times \mathcal{H}_0^v \times \mathcal{H}_0^\theta$

$$\int_Q \rho\dot{\mathbf{v}}\delta\mathbf{u}dQ + \int_Q \varepsilon(\delta\mathbf{u}) : C : \varepsilon(\mathbf{u})dQ - \int_Q \alpha K_B \Delta\theta I : \boldsymbol{\varepsilon}(\delta\mathbf{u})dQ - \int_P \mathbf{T}\delta\mathbf{u}dP$$
$$+ \int_Q \mathbf{f}\delta\mathbf{u}dQ + \sum_e \int_{Q_e} \rho(\ddot{\mathbf{u}}_h - \dot{\mathbf{v}}_h)\tau(\delta\ddot{\mathbf{u}}_h - \delta\dot{\mathbf{v}}_h)dQ + \int_Q \rho\left(\mathbf{v} - \dot{\mathbf{u}}\right)\delta\mathbf{v}dQ +$$
$$\int_Q \rho C\dot{\theta}\delta\theta dQ + \int_Q K_\theta \nabla\theta\nabla\delta\theta dQ - \int_{P_\theta} \mathbf{q}.\mathbf{n}\delta\theta dP_\theta - \int_Q \mathbf{r}\delta\theta dQ = 0$$

where $P_\theta = \Gamma_\theta \times [0,T]$. The variational formulation consisting of derived test functions in time for the elastodynamics equation is:

Form 2 + GAC

Find $(\mathbf{u}(\mathbf{x},t),\mathbf{v}(\mathbf{x},t),\theta(\mathbf{x},t)) \in \mathcal{H}^u \times \mathcal{H}^v \times \mathcal{H}^\theta$, such that $\forall\, (\delta\mathbf{u}(\mathbf{x},t),\delta\mathbf{v}(\mathbf{x},t),\delta\theta(\mathbf{x},t)) \in \mathcal{H}_0^u \times \mathcal{H}_0^v \times \mathcal{H}_0^\theta$

$$\int_Q \rho\dot{\mathbf{v}}\delta\dot{\mathbf{u}}dQ + \int_Q \boldsymbol{\varepsilon}(\delta\dot{\mathbf{u}}) : C : \boldsymbol{\varepsilon}(\mathbf{u})dQ - \int_Q \alpha K_B \Delta\theta I : \boldsymbol{\varepsilon}(\delta\dot{\mathbf{u}})dQ - \int_P \mathbf{T}\delta\dot{\mathbf{u}}dP$$
$$+ \int_Q \mathbf{f}\delta\dot{\mathbf{u}}dQ + \sum_e \int_{Q_e} \rho(\ddot{\mathbf{u}}_h - \dot{\mathbf{v}}_h)\tau(\delta\ddot{\mathbf{u}}_h - \delta\dot{\mathbf{v}}_h)dQ + \int_Q \rho\left(\mathbf{v} - \dot{\mathbf{u}}\right)\delta\dot{\mathbf{v}}dQ +$$
$$\int_Q \rho C\dot{\theta}\delta\theta dQ + \int_Q K_\theta \nabla\theta\nabla\delta\theta dQ - \int_{P_\theta} \mathbf{q}.\mathbf{n}\delta\theta dP_\theta - \int_Q \mathbf{r}\delta\theta dQ = 0$$

3.2.3. Space-time matrix form

In this section, the matrix form is derived. The representations of the displacement, velocity and temperature are:

$$\begin{aligned} \mathbf{u}_h(\xi,\eta) &= \mathbf{N}^{\mathbf{u}}\mathbf{d}^{\mathbf{u}} \\ \mathbf{v}_h(\xi,\eta) &= \mathbf{N}^{\mathbf{v}}\mathbf{d}^{\mathbf{v}} \\ \theta_h(\xi,\eta) &= \mathbf{N}^{\theta}\mathbf{d}^{\theta} \end{aligned} \tag{3.1}$$

We define the following differential operators:

$$\begin{aligned}
&\dot{\mathbf{u}}_h(\xi,\eta) = \mathbf{B}_{\mathbf{t}}^{\mathbf{u}}\mathbf{d}^{\mathbf{u}}\\
&\mathrm{GRAD}_{\mathbf{x}}u_h(\xi,\eta) = \mathbf{B}_{\mathbf{x}}^{\mathbf{u}}\mathbf{d}^{\mathbf{u}}\\
&\boldsymbol{\varepsilon}(\mathbf{u}_h(\xi,\eta)) = (\mathbf{B}_{\mathbf{x}}^{\mathbf{u}})^{sym}\mathbf{d}^{\mathbf{u}}\\
&\ddot{\mathbf{u}}_h(\xi,\eta) = \mathbf{B}_{\mathbf{tt}}^{\mathbf{u}}\mathbf{d}^{\mathbf{u}}\\
&\mathrm{GRAD}_{\mathbf{x}}\dot{u}_h(\xi,\eta) = \mathbf{B}_{\mathbf{xt}}^{\mathbf{u}}\mathbf{d}^{\mathbf{u}}\\
&\boldsymbol{\varepsilon}(\dot{\mathbf{u}}_h(\xi,\eta)) = (\mathbf{B}_{\mathbf{xt}}^{\mathbf{u}})^{sym}\mathbf{d}^{\mathbf{u}}\\
&tr\boldsymbol{\varepsilon}(\dot{\mathbf{u}}_h(\xi,\eta)) = (\mathbf{B}_{\mathbf{xt}}^{\mathbf{u}})^{sym^{\mathrm{Tr}}}\mathbf{d}^{\mathbf{u}}\\
&\dot{\theta}_h(\xi,\eta) = \mathbf{B}_{\mathbf{t}}^{\theta}\mathbf{d}^{\theta}\\
&\mathrm{GRAD}_{\mathbf{x}}\theta_h(\xi,\eta) = \mathbf{B}_{\mathbf{x}}^{\theta}\mathbf{d}^{\theta}
\end{aligned} \tag{3.2}$$

Then, the matrix form of the thermoelasticity problem (in 1D) holds:

$$\begin{bmatrix} \mathbf{K}_{\mathbf{uu}} & \mathbf{K}_{\mathbf{uv}} & \mathbf{K}_{\mathbf{u}\theta} \\ \mathbf{K}_{\mathbf{vu}} & \mathbf{K}_{\mathbf{vv}} & \mathbf{K}_{\mathbf{v}\theta} \\ \mathbf{K}_{\theta\mathbf{u}} & \mathbf{K}_{\theta\mathbf{v}} & \mathbf{K}_{\theta\theta} \end{bmatrix} \left\{ \begin{array}{c} \tilde{\mathbf{d}}^{\mathbf{u}} \\ \tilde{\mathbf{d}}^{\mathbf{v}} \\ \tilde{\mathbf{d}}^{\theta} \end{array} \right\} = \left\{ \begin{array}{c} \tilde{\mathbf{f}}_{\mathbf{u}} \\ \tilde{\mathbf{f}}_{\mathbf{v}} \\ \tilde{\mathbf{f}}_{\theta} \end{array} \right\}$$

where for Form 2 + GAC, one has:

$$\begin{aligned}
\mathbf{K}_{\mathbf{uu}} &= \mathcal{A}_e \int_{Q_e} \left((\mathbf{B}_{\mathbf{xt}}^{\mathbf{u}})^{sym^{\mathrm{T}}} \mathbf{D} \mathbf{B}_{\mathbf{x}}^{\mathbf{u}sym} + \rho {\mathbf{B}_{\mathbf{tt}}}^{\mathrm{T}} \tau \mathbf{B}_{\mathbf{tt}} \right) dQ \\
\mathbf{K}_{\mathbf{uv}} &= \mathcal{A}_e \int_{Q_e} \left(\rho \mathbf{B}_{\mathbf{t}}^{\mathbf{u}\mathrm{T}} \mathbf{B}_{\mathbf{t}}^{\mathbf{v}} - \rho {\mathbf{B}_{\mathbf{tt}}}^{\mathrm{T}} \tau \mathbf{B}_{\mathbf{t}} \right) dQ \\
\mathbf{K}_{\mathbf{u}\theta} &= \mathcal{A}_e \int_{Q_e} -\mathbf{N}^{\theta\mathrm{T}} \alpha K_B \mathbf{B}_{\mathbf{xt}}^{\mathbf{u}} dQ \\
\\
\mathbf{K}_{\mathbf{vu}} &= \mathcal{A}_e \int_{Q_e} \left(-\rho \mathbf{B}_{\mathbf{t}}^{\mathbf{v}\mathrm{T}} \mathbf{B}_{\mathbf{t}}^{\mathbf{u}} - \rho {\mathbf{B}_{\mathbf{t}}}^{\mathrm{T}} \tau \mathbf{B}_{\mathbf{tt}} \right) dQ \\
\mathbf{K}_{\mathbf{vv}} &= \mathcal{A}_e \int_{Q_e} \left(\rho \mathbf{B}_{\mathbf{t}}^{\mathbf{v}\mathrm{T}} \mathbf{N}^{\mathbf{v}} + \rho {\mathbf{B}_{\mathbf{t}}}^{\mathrm{T}} \tau \mathbf{B}_{\mathbf{t}} \right) dQ \\
\mathbf{K}_{\mathbf{v}\theta} &= 0 \\
\\
\mathbf{K}_{\theta\theta} &= \mathcal{A}_e \int_{Q_e} \left(\rho C {\mathbf{N}^{\theta}}^{\mathrm{T}} \mathbf{B}_{\mathbf{t}}^{\theta} + K_\theta {\mathbf{B}_{\mathbf{x}}^{\theta}}^{\mathrm{T}} \mathbf{B}_{\mathbf{x}}^{\theta} \right) dQ \\
\mathbf{K}_{\theta\mathbf{u}} &= 0 \\
\mathbf{K}_{\theta\mathbf{v}} &= 0
\end{aligned} \tag{3.3}$$

and:

$$\begin{aligned}
\mathbf{f_u} &= \mathcal{A}_e \int_{Q_e} \mathbf{B_t}^{\mathrm{T}} \mathbf{f}_h dQ + \mathcal{A}_e \int_{Q_e} \alpha (\mathbf{B^u_{xt}})^{sym^{\mathrm{Tr}}} K_B \theta_0 dQ \\
&+ \mathcal{A}_e \int_{P_e} \mathbf{B_t}^{\mathrm{T}} \mathbf{T}_h dP \\
\mathbf{f_v} &= \mathbf{0} \\
\mathbf{f}_\theta &= \mathcal{A}_e \int_{Q_e} \mathbf{N_p}^{\mathrm{T}} \mathbf{r}_h dQ + \mathcal{A}_e \int_{P_e} \mathbf{N_p}^{\mathrm{T}} \bar{\mathbf{q}} dP
\end{aligned} \tag{3.4}$$

In the case of Form 1 + GAC, the matrix form is obtained in a similar way but all the terms $\mathbf{B}_{xt}^{sym^{\mathrm{T}}}$ should be replaced by $\mathbf{B}_{x}^{sym^{\mathrm{T}}}$ in $\mathbf{K_{uu}}$ and the terms $\mathbf{B_t}^{\mathrm{T}}$ should be replaced by $\mathbf{N_u}^{\mathrm{T}}$ in the other components of the tangent matrix.

3.2.4. Numerical applications at small-strain

3.2.4.1. Space-Time domain submitted to a body load

We solve the thermoelastodynamics problem applied on an elastic bar. The space-time domain with boundary and initial conditions is shown in Figure 3.1. The length of the bar is $L = 1\ m$, and so is the final time, $T = 1\ s$. Elasticity modulus is chosen such that $E = 2\ Pa$, heat capacity is $C = 0.1\ J$, density ρ and thermal conductivity K_θ are taken to be unity. The coupling coefficient α is taken to be $\alpha = 0.01\ K^{-1}$.

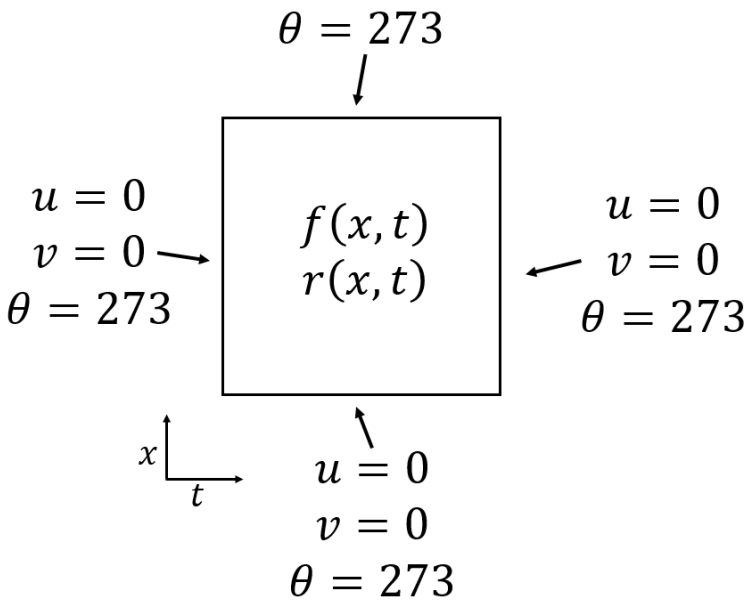

Figure 3.1. – Space-time domain with boundary and initial conditions for a trial thermoelastic problem

No GAC terms were added to the formulation here, the stabilizing parameter is chosen such that $\tau = 0$. B-Splines are used as basis functions. The space-time

solution was compared to the exact solution of the problem. The exact solution is given by : $u_{exact} = t^2(t-T)^2 sin(2\pi x)$ and $\theta_{exact} = \frac{1}{4} sin(2\pi x) sin(2\pi t) + \theta_0$ where $\theta_0 = 273\ K$. The corresponding body load is $\mathbf{f} = \rho[2(t-T)^2 sin(2\pi x) + 8t(t-T) sin(2\pi x) + 2t^2 sin(2\pi x)] + 4E\pi^2 t^2 (t-T)^2 sin(2\pi x) + \frac{\pi}{2}\alpha K_B cos(2\pi x) sin(2\pi t)$ and the heat source is $\mathbf{r} = \rho C \frac{\pi}{2} sin(2\pi x) cos(2\pi t) + K_\theta \pi^2 sin(2\pi x) sin(2\pi t)$. Optimal convergence rates for this problem are obtained for the displacement, the velocity and the temperature, showing the convergence of the space-time method, for both of the variational formulations proposed in the last section, as Figures 3.2 and 3.3 show, on this simple problem.

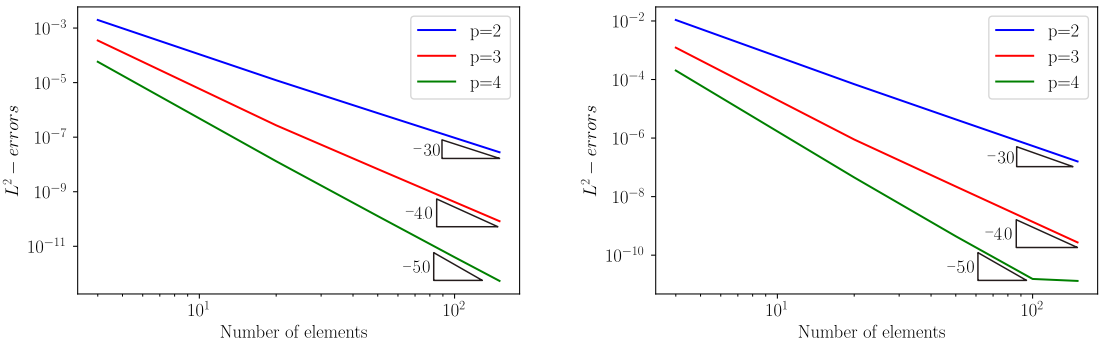

(a) Displacement field

(b) Velocity field

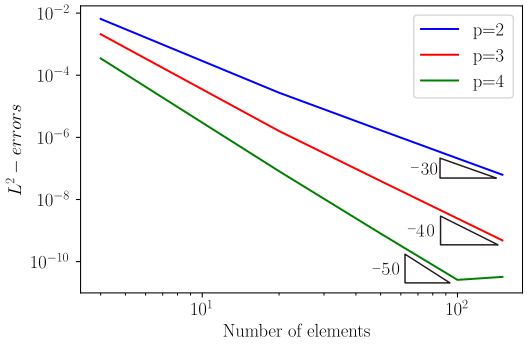

(c) Temperature field

Figure 3.2. – Convergence curves for displacement, velocity and temperature for degrees $p = 2, 3$, and 4 for the thermoelasticity equation applied on a 1D elastic bar using the variational formulation Form 1 + GAC

These results show that both of these formulations give similar results with the optimal rates of convergence for this simple test. Next, we would like to study the consequence of using subgrid techniques in time for some fields (asynchroneous scheme in time). For that, the same test case is done while taking a coarser mesh in time for the temperature field. The number of elements in space is the same for all fields. We then plot the convergence curves obtained.

Figure 3.4 shows that similar convergence rates are observed for displacement and velocity for the asynchroneous scheme and for the scheme where all 3 fields have

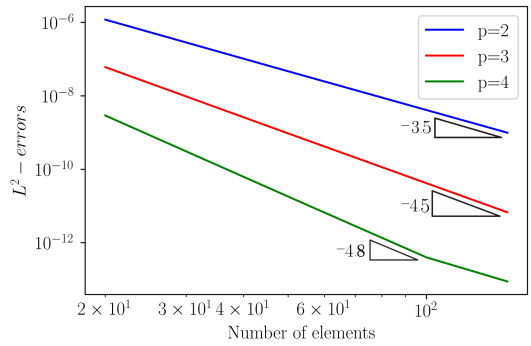

(a) Displacement field

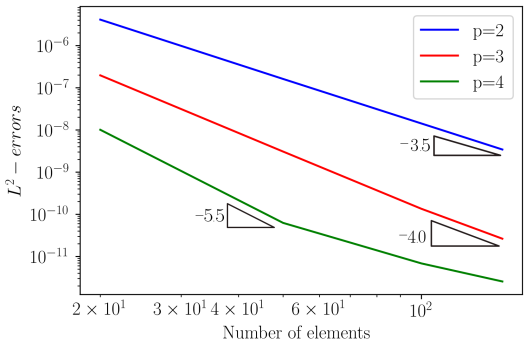

(b) Velocity field

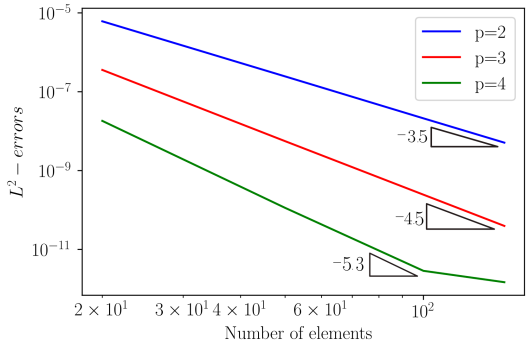

(c) Temperature field

Figure 3.3. – Convergence curves for displacement, velocity and temperature for degrees $p = 2, 3$, and 4 for the thermoelasticity equation applied on a 1D elastic bar using the variational formulation Form 2 + GAC

the same time grid: taking a coarser subgrid for the temperature field and a finer subgrid for the displacement and the velocity fields also gives optimal convergence rates. In the case of the temperature field, we can notice that the convergence curves concerning the subdivision test are always above the convergence curves concerning the test where the same number of elements was taken in space and in time. This result is normal because in the case of the subdivision, half the number of elements in time was used for the temperature field, making the mesh of the temperture looser than the mesh of the 2 other fields.

3.2.4.2. Impact of a thermoelastic bar on a wall

In this case, we investigate the bar impact problem as done in Chapter 2. We adopt first the formulation Form 1 + GAC proposed previously in section 3.2.2 where classical test functions are used for both of the equations. The stabilizing parameter is chosen such that $\tau = 0.02$ and $\tilde{\tau} = \tau \Delta t$. As Figure 3.5 shows, the 1D thermoelastic bar is submitted to an initial velocity v_0. For $t \geq 0$, we impose conditions for displacement, velocity and temperature on the rigid wall: $u(x = 0, t) = 0$, $v(x = 0, t) = 0$ and $\theta(x = 0, t) = 293\ K$. The free end is stress

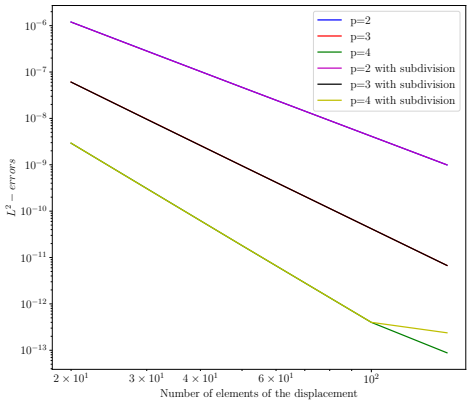

(a) Displacement field

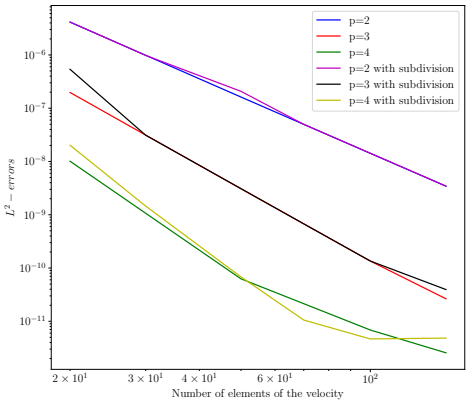

(b) Velocity field

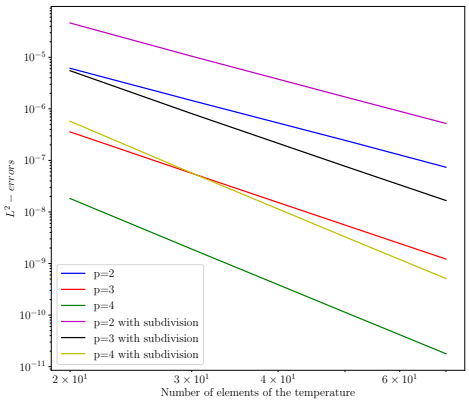

(c) Temperature field

Figure 3.4. – Comparison of convergence curves for displacement, velocity and temperature for the thermoelasticity equation applied on a 1D elastic bar using a regular and a coarser mesh in time for the temperature field

free and the temperature is imposed such that $\theta(x = 1, t) = 293\ K$. The material parameters are $E = 1\ Pa$, $\rho = 1\ kg.m^{-3}$, the bar is of length $L = 1\ m$, the initial velocity is $v_0 = 1\ m/s$, $\alpha = 0.01\ K^{-1}, C = 0.1\ J$.

The number of elements in space and time are chosen such that $\Delta x = 0.02\ m$ and $\Delta t = 0.02\ s$. The degree of approximation is $p = 2$.

The isovalues of displacement, velocity and temperature are given in Figure 3.6. The oscillations are clearly numerous for all 3 fields. This result is coherent with the one already obtained in Chapter 2 where a comparison on the test functions was done for elastodynamics. For a better visualization, the solution of the problem for the displacement, velocity and temperature along the time interval $[0, 1]$ at the

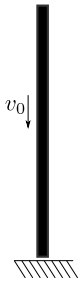

Figure 3.5. – 1D bar impact problem against a rigid wall

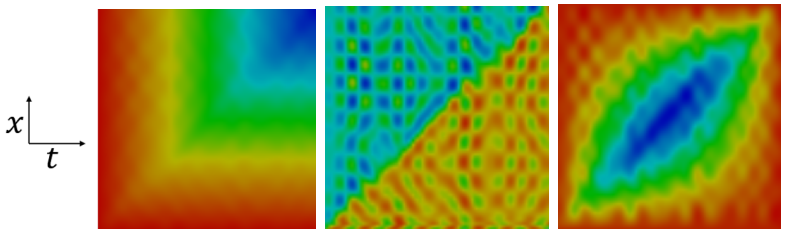

(a) Displacement field (b) Velocity field (c) Temperature field

Figure 3.6. – Space-time isovalues of displacement, velocity and temperature for the thermoelastic impact problem with formulation Form 1 + GAC

center of the bar is given in Figure 3.7 using Form 1 + GAC. The plot confirms the presence of multiple oscillations on all of the 3 fields, making the solution computed not accurate at all.

The same test problem is solved with the formulation Form 2 + GAC. The results are plotted in Figure 3.8. Compared to formulation Form 1 + GAC, the oscillations on the displacement, temperature and velocity fields are vanished.

Once again, the plot of the solution of the problem for the displacement, velocity and temperature along the time interval $[0, 1]$ at the center of the bar is given in Figure 3.9, now for Form 2 + GAC.

These results confirm the fact that the choice of test functions used highly affects the computational results, and using test functions derived in time gives much better results. In the following, we will definitely adopt Form 2 + GAC.

The same test case is held with a coarser mesh in time for the temperature field compared to the displacement and velocity fields. The isovalues in space-time for displacement, velocity and temperature are plotted in Figure 3.10.

The results are similar to the ones obtained with the same grid for the 3 fields. To confirm the results, we plot the solution for the displacement, velocity and temperature fields along the time interval $[0, 1]$ at the center of the bar.

Figure 3.11 shows that accurate solutions are obtained with respect to time, proving the efficiency of the method when using smaller subgrids for a specific field.

At last, the same test case is used to evaluate mixed order interpolation for displacement, velocity and temperature: we take one order lower for the temperature

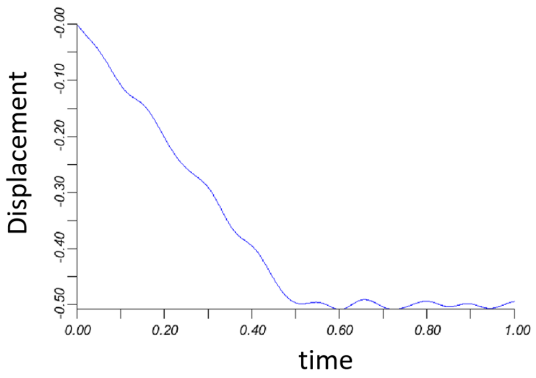

(a) Displacement field

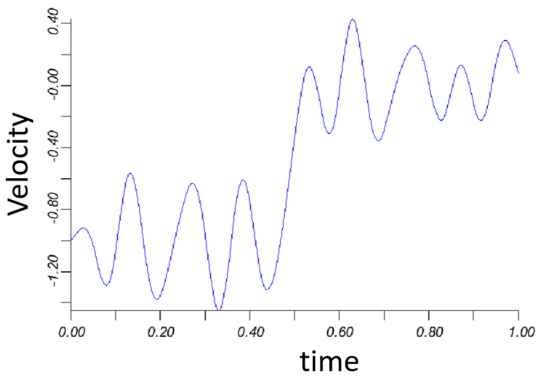

(b) Velocity field

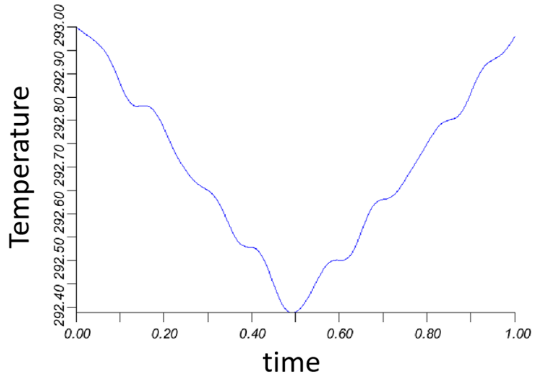

(c) Temperature field

Figure 3.7. – Time evolution of the solution for the thermoelastic impact problem at the center of the bar with formulation Form 1 + GAC

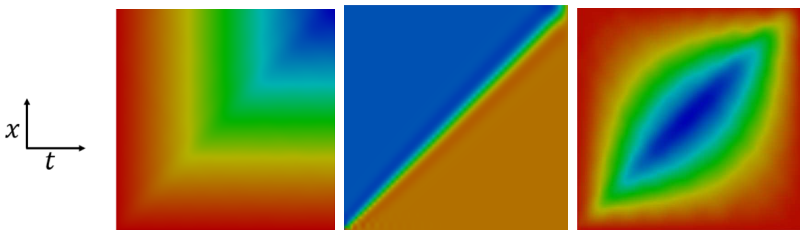

(a) Displacement field (b) Velocity field (c) Temperature field

Figure 3.8. – Space-time isovalues of displacement, velocity and temperature for the thermoelastic impact problem with formulation Form 2 + GAC

field. The idea is to test the use of consistent approximation scheme for displacement and temperature with respect to the formulation (see [102] and references therein). The number of elements in space and time is similar for all fields (50 elements in space and 50 elements in time). We choose a degree $p = 2$ for the displacement and velocity fields, and a degree $p = 1$ for the temperature field.

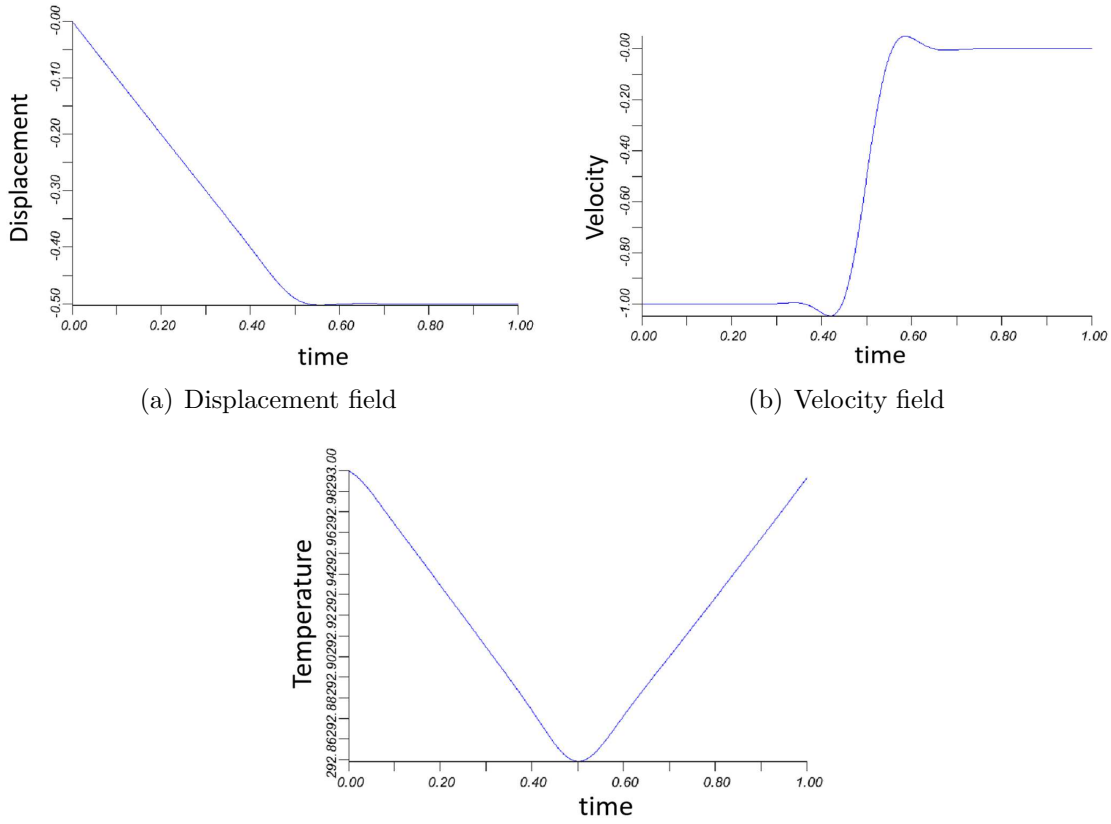

(a) Displacement field (b) Velocity field

(c) Temperature field

Figure 3.9. – Time evolution of the solution for the thermoelastic impact problem at the center of the bar with formulation Form 2 + GAC

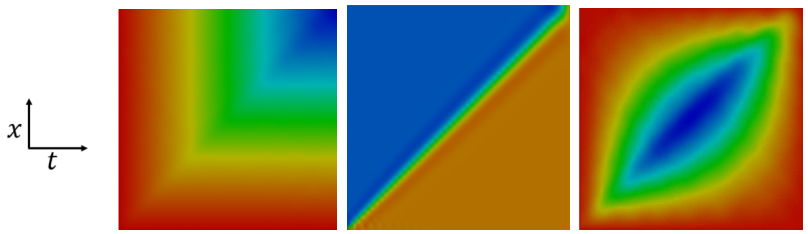

(a) Displacement field (b) Velocity field (c) Temperature field

Figure 3.10. – Space-time isovalues of displacement, velocity and temperature for the thermoelastic impact problem with formulation Form 2 + GAC and coarse mesh in time for temperature

Results shown in Figure 3.12 and Figure 3.13 are similar to the ones of the previous test. We can observe that no oscillations appear with this mixed order of approximation which is consistent.

In Figure 3.14, we plot on the same graph the temperature solutions. No difference is observed when taking a different grid and different approximation

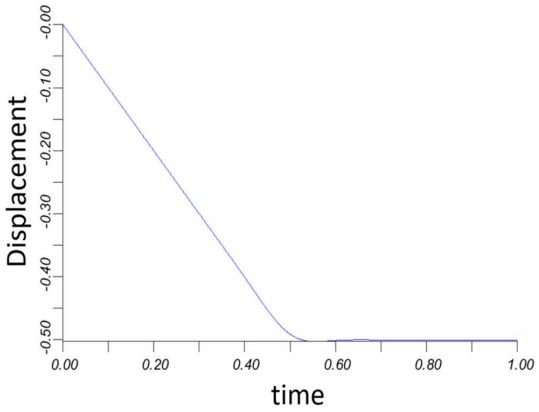

(a) Displacement field

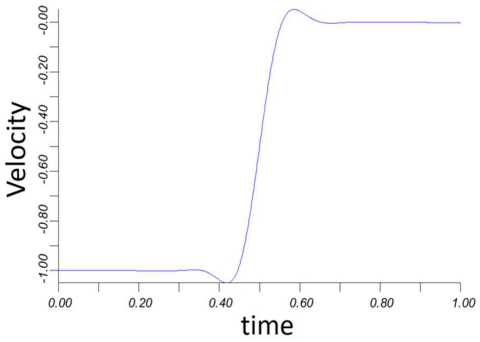

(b) Velocity field

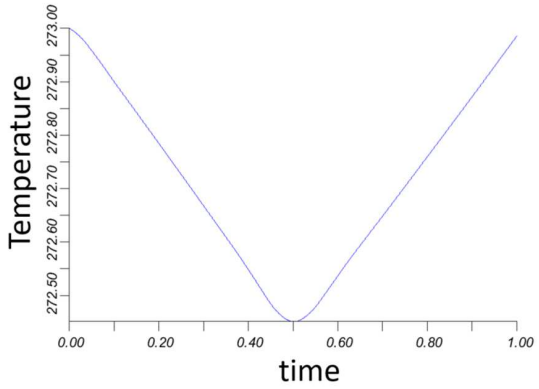

(c) Temperature field

Figure 3.11. – Time evolution of displacement, velocity and temperature solution at the center of the bar with formulation Form 2 + GAC and a coarse mesh in time for temperature

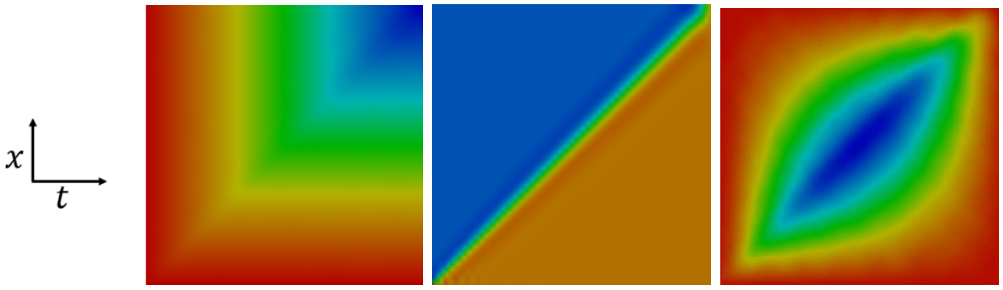

(a) Displacement field (b) Velocity field (c) Temperature field

Figure 3.12. – Space-time isovalues of displacement, velocity and temperature for the thermoelastic impact problem with $p = 2$ for the displacement and velocity and $p = 1$ for the temperature with formulation Form 2 + GAC

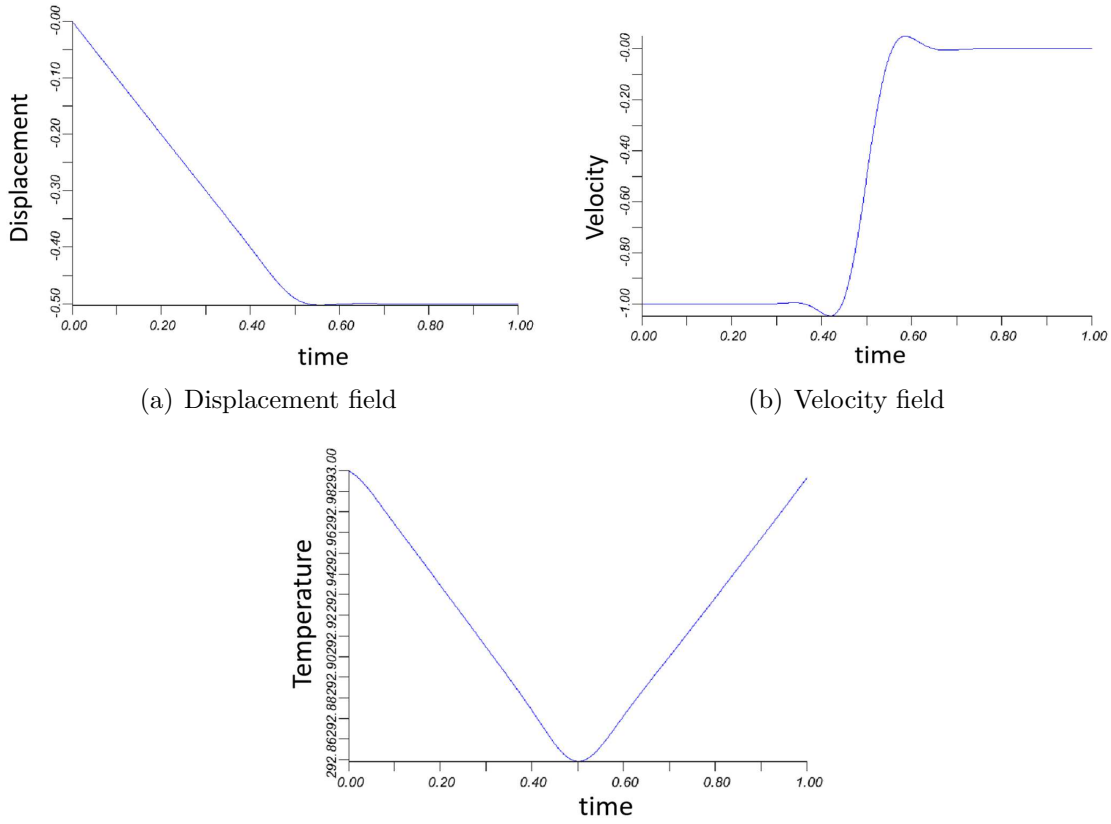

(a) Displacement field

(b) Velocity field

(c) Temperature field

Figure 3.13. – Time evolution of displacement, velocity and temperature solution with $p = 2$ for the displacement and velocity and $p = 1$ for the temperature at the center of the bar with formulation Form 2 + GAC

order for the temperature field. As shown, the solutions obtained are very similar. A close zoom is made on the solution, confirming that the 3 solutions are indeed very close to one another. The ST method allowed to obtain the same quality of the solution with less numerical cost.

3.3. Small-strain thermoelasticity: non-linear case

3.3.1. Problem statement

In this section, we consider a non-linear thermoelastic problem. A term is added into the model problem. It is the term in red in eq. (3.5), it is the latent heat term, the coupling effect applied on the equation of heat, making the problem to be solved non-linear.

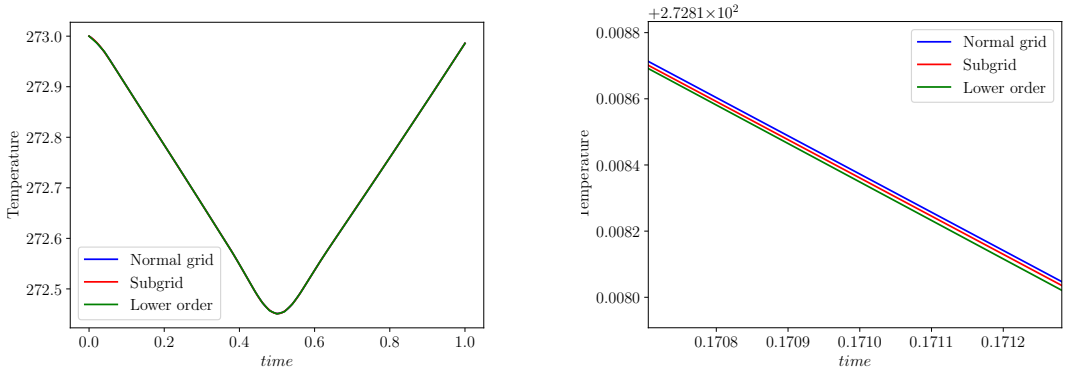

(a) Space-time solution

(b) Zoom in on the solution

Figure 3.14. – Space-time temperature solution of the thermoelastic impact problem with the standard case, the case of one order lower, and the case of a coarser subgrid

$$\begin{cases} \rho\dot{\mathbf{v}} - \mathrm{div}_{\mathbf{x}}\boldsymbol{\sigma} - \mathbf{f} = 0 \\ \rho(\mathbf{v} - \dot{\mathbf{u}}) = 0 \\ \rho C\dot{\theta} - \theta(\dfrac{\partial\sigma}{\partial\theta} : \dot{\boldsymbol{\varepsilon}}) + div\mathbf{q} = \mathbf{r} \end{cases} \qquad \forall(\mathbf{x},\mathbf{t}) \in Q \tag{3.5}$$

3.3.2. Variational formulation

The variational formulation is directly inspired from Form 2 + GAC, and the difference between the two formulations is only one term. The variational formulation helds :

$$\begin{aligned} &\text{Find } (\mathbf{u}(\mathbf{x},t),\mathbf{v}(\mathbf{x},t),\theta(\mathbf{x},t)) \in \mathcal{H}^u \times \mathcal{H}^v \times \mathcal{H}^\theta, \text{ such that } \forall\, (\delta\mathbf{u}(\mathbf{x},t),\delta\mathbf{v}(\mathbf{x},t), \\ &\delta\theta(\mathbf{x},t)) \in \mathcal{H}_0^u \times \mathcal{H}_0^v \times \mathcal{H}_0^\theta \\ &\int_Q \rho\dot{\mathbf{v}}\delta\dot{\mathbf{u}}dQ + \int_Q \boldsymbol{\varepsilon}(\delta\dot{\mathbf{u}}) : C : \boldsymbol{\varepsilon}(\mathbf{u})dQ - \int_Q \alpha K_B \Delta\theta I : \boldsymbol{\varepsilon}(\delta\dot{\mathbf{u}})dQ - \int_P \mathbf{T}\delta\dot{\mathbf{u}}dP \\ &\quad + \int_Q \mathbf{f}\delta\dot{\mathbf{u}}dQ + \sum_e \int_{Q_e} \rho_0(\ddot{\mathbf{u}}_h - \dot{\mathbf{v}}_h)\tau(\delta\ddot{\mathbf{u}}_h - \delta\dot{\mathbf{v}}_h)dQ + \int_Q \rho\,(\mathbf{v} - \dot{\mathbf{u}})\,\delta\dot{\mathbf{v}}dQ \\ &\quad + \int_Q \rho C\dot{\theta}\delta\theta dQ - \int_Q \theta(\frac{\partial\sigma}{\partial\theta} : \dot{\boldsymbol{\varepsilon}})\delta\theta dQ + \int_Q K_\theta\nabla\theta\nabla\delta\theta dQ - \int_{P_\theta} \mathbf{q}.\mathbf{n}\delta\theta dP_\theta \\ &\quad - \int_Q \mathbf{r}\delta\theta dQ = 0 \end{aligned} \tag{3.6}$$

Note that for this non-linear case, and as discussed in Chapter 2, the addition of stabilization terms of type GAC is possible, easy and straightforward.

3.3.3. Space-time matrix form

The matrix form of the non-linear thermoelastic system is:

$$\begin{cases} \mathbf{r_u}(\mathbf{d},\beta) = 0 \\ \mathbf{r_v}(\mathbf{d},\beta) = 0 \\ \mathbf{r}_\theta(\mathbf{d},\beta) = 0 \end{cases} \tag{3.7}$$

such that $\mathbf{d} = (\mathbf{d^u}, \mathbf{d^v}, \mathbf{d}^\theta)$. $\mathbf{r_u}, \mathbf{r_v}$ and $\mathbf{r}_\theta$ are defined by:

$$\begin{aligned} \mathbf{r_u}(\mathbf{d},\beta) &= \mathcal{A}_e \int_{Q_e} \left(\rho_0 \mathbf{B_t}^{\mathrm{T}} \dot{\mathbf{v}}_h + \mathbf{B}_{xt}^{\mathrm{T}} \sigma(\mathbf{u}_h) + \mathbf{B_{tt}}^{\mathrm{T}} \rho_0 \tau(\ddot{\mathbf{u}}_h - \dot{\mathbf{v}}_h) \right) dQ - \beta \mathbf{f_u} \\ \mathbf{r_v}(\mathbf{d},\beta) &= \mathcal{A}_e \int_{Q_e} \left(\rho_0 \mathbf{B_t}^{\mathrm{T}} (\mathbf{v}_h - \dot{\mathbf{u}}_h) + \tau(\ddot{\mathbf{u}}_h - \dot{\mathbf{v}}_h) \right) dQ \\ \mathbf{r}_\theta(\mathbf{d},\beta) &= \mathcal{A}_e \int_{Q_e} \left(\rho C \mathbf{N}_\theta^{\mathrm{T}} \dot{\theta}_h - \mathbf{N}_\theta^{\mathrm{T}} \theta_h [\frac{\partial \sigma_h}{\partial \theta} : \dot{\boldsymbol{\varepsilon}}_h] + K_\theta \mathbf{B}_{\mathbf{x}}^{\mathrm{T}} \mathrm{GRAD}_{\mathbf{x}} \theta_h \right) dQ - \beta \mathbf{f}_\theta \end{aligned} \tag{3.8}$$

As was done in the precedent chapter, we employ the Newton-Raphson procedure for a quasi-static problem to solve this non-linear system. So starting from a known solution, $(\mathbf{d}^k, \beta^k)$, at increment k, we search $\Delta\mathbf{d}^k$ for a given load increment $\Delta\beta^k$ such that $\mathbf{r_u}(\mathbf{d}^k + \Delta\mathbf{d}^k, \beta^k + \Delta\beta^k) = \mathbf{r_v}(\mathbf{d}^k + \Delta\mathbf{d}^k, \beta^k + \Delta\beta^k) = \mathbf{r}_\theta(\mathbf{d}^k + \Delta\mathbf{d}^k, \beta^k + \Delta\beta^k) = 0$. The linerization of this problem leads to the following linear system:

$$\begin{bmatrix} \mathbf{K_{uu}}(\mathbf{u}_h^k, \mathbf{v}_h^k, \theta_h^k) & \mathbf{K_{uv}}(\mathbf{u}_h^k, \mathbf{v}_h^k, \theta_h^k) & \mathbf{K_{u}}\theta(\mathbf{u}_h^k, \mathbf{v}_h^k, \theta_h^k) \\ \mathbf{K_{vu}}(\mathbf{u}_h^k, \mathbf{v}_h^k, \theta_h^k) & \mathbf{K_{vv}}(\mathbf{u}_h^k, \mathbf{v}_h^k, \theta_h^k) & \mathbf{K_{v}}\theta(\mathbf{u}_h^k, \mathbf{v}_h^k, \theta_h^k) \\ \mathbf{K}_{\theta\mathbf{u}}(\mathbf{u}_h^k, \mathbf{v}_h^k, \theta_h^k) & \mathbf{K}_{\theta\mathbf{v}}(\mathbf{u}_h^k, \mathbf{v}_h^k, \theta_h^k) & \mathbf{K}_{\theta\theta}(\mathbf{u}_h^k, \mathbf{v}_h^k, \theta_h^k) \end{bmatrix} \begin{Bmatrix} \Delta\mathbf{d^{u^k}} \\ \Delta\mathbf{d^{v^k}} \\ \Delta\mathbf{d}^{\theta^k} \end{Bmatrix} \tag{3.9}$$

$$= \begin{Bmatrix} -\mathbf{r_u}(\mathbf{u}_h^k, \mathbf{v}_h^k, \theta_h^k) - \mathbf{f}_u \Delta\beta^k \\ -\mathbf{r_v}(\mathbf{u}_h^k, \mathbf{v}_h^k, \theta_h^k) \\ -\mathbf{r}_\theta(\mathbf{u}_h^k, \mathbf{v}_h^k, \theta_h^k) - \mathbf{f}_\theta \Delta\beta^k \end{Bmatrix}$$

$\mathbf{K_{uu}}, \mathbf{K_{uv}}, \mathbf{K_{vu}}$ and $\mathbf{K_{vv}}$ are exactly similar to the ones defined in eqs. (3.3). The extra term which is the coupling term in the thermal equation gives:

$$\begin{aligned} \mathbf{K}_{\theta\mathbf{u}} &= \mathcal{A}_e \int_{Q_e} \mathbf{N}^{\theta\mathrm{T}} \mathbf{B_{xt}^u} \left(-\mathcal{G}_\theta^h \mathbf{B_{xt}^u} \mathbf{N}^\theta + \mathcal{G}_{\varepsilon\theta}^h \mathbf{B_x^u} \right) dQ \\ \mathbf{K}_{\theta\theta} &= \mathcal{A}_e \int_{Q_e} \mathbf{N}^{\theta\mathrm{T}} \left(\rho C \mathbf{B_t^\theta} - \mathbf{N}^\theta \mathcal{G}_\theta^h \mathbf{B_{xt}^u} - \mathbf{N}^\theta \mathcal{G}_{\theta\theta}^h \mathbf{B_{xt}^u} \right) + K_\theta \mathbf{B_x^\theta}^{\mathrm{T}} \mathbf{B_x^\theta} dQ \\ \mathbf{K}_{\theta\mathbf{v}} &= 0 \end{aligned}$$

The matrix terms $\mathcal{G}_\theta^h$, $\mathcal{G}_{\theta\theta}^h$ and $\mathcal{G}_{\varepsilon\theta}^h$ are issued from the matrix/vector representa-

tion of the constitutive tangent operator $\mathcal{G}_\theta$, $\mathcal{G}_{\theta\theta}$ and $\mathcal{G}_{\varepsilon\theta}$ defined by:

$$\begin{aligned}\mathcal{G}_\theta &= \frac{\partial \boldsymbol{\sigma}}{\partial \theta}\\ \mathcal{G}_{\theta\theta} &= \frac{\partial^2 \boldsymbol{\sigma}}{\partial \theta^2}\\ \mathcal{G}_{\varepsilon\theta} &= \frac{\partial^2 \boldsymbol{\sigma}}{\partial \boldsymbol{\varepsilon}\partial \theta}\end{aligned}$$

3.3.4. Numerical applications at small-strain

3.3.4.1. Non-linear space-time domain submitted to a body load

In this section, we use the variational formulation defined in eq. (3.6). The domain, the boundary and initial conditions are defined in Figure 3.1. In this case, we choose $\rho = 0.1\ kg.m^{-3}$, $\alpha = 0.1\ K^{-1}$, and the parameters of the problem are chosen to be the same as the one of the linear case. In this case, the source term of the heat equation is defined by $r = \rho C\frac{\pi}{2}sin(2\pi x)cos(2\pi t)+K_\theta\pi^2 sin(2\pi x)sin(2\pi t)+\alpha K_B[\frac{1}{4}sin(2\pi x)sin(2\pi t)+\theta_0][4\pi t(t-T)^2cos(2\pi x)+4\pi t^2(t-T)cos(2\pi x)]$.

Optimal convergence rates are obtained for this test case for the case of the displacement field, the velocity field and the temperature field, as shown in Figure 3.15. On this non-linear thermomechanical problem, the ST formulation exhibits good convergence properties.

3.3.4.2. Lamé parameters θ-dependent

We consider the case of non constant material parameters. Lamé parameters λ and μ depend on θ here. The body loads and heat source are defined as:

$$\begin{aligned}f = {}& \rho[2(t-T)^2sin(2\pi x)+8t(t-T)sin(2\pi x)+2t^2sin(2\pi x)]\\ &+4E\pi^2t^2(t-T)^2sin(2\pi x)+\frac{\pi}{2}\alpha K_B cos(2\pi x)sin(2\pi t)-E'\frac{\pi}{2}cos(2\pi x)sin(2\pi t)\\ &+\alpha K'_B\frac{\pi}{2}cos(2\pi x)sin(2\pi t)(\theta-\theta_0)\\ r = {}& \rho C\frac{\pi}{2}sin(2\pi x)cos(2\pi t)+K_\theta\pi^2sin(2\pi x)sin(2\pi t)+\alpha K_B[\frac{1}{4}sin(2\pi x)sin(2\pi t)\\ &+\theta_0][4\pi t(t-T)^2cos(2\pi x)+4\pi t^2(t-T)cos(2\pi x)]\\ &+\alpha K'_B[\frac{1}{4}sin(2\pi x)sin(2\pi t)+\theta_0][4\pi t(t-T)^2cos(2\pi x)\\ &+4\pi t^2(t-T)cos(2\pi x)](\theta-\theta_0)-\theta E'[4\pi t(t-T)^2cos(2\pi x)\\ &+4\pi t^2(t-T)cos(2\pi x)][2\pi t^2(t-T)^2cos(2\pi x)\end{aligned} \tag{3.10}$$

The boundary conditions of this test are as the ones defined in Figure 3.1. Optimal convergence rates are obtained for the degrees $p = 2, 3$ and 4. The results

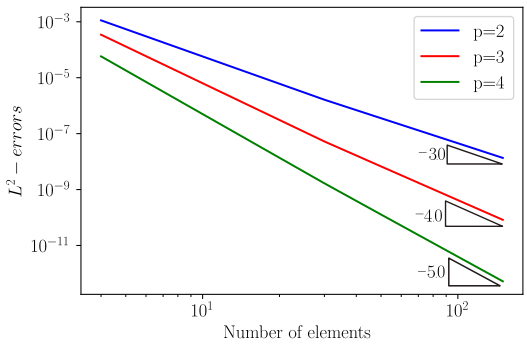

(a) Displacement field

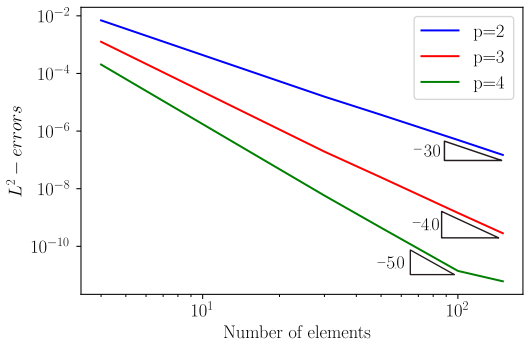

(b) Velocity field

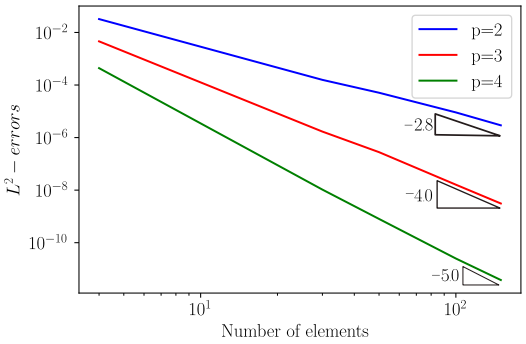

(c) Temperature field

Figure 3.15. – Convergence curves for displacement, velocity and temperature for degrees $p = 2, 3$, and 4 for the non-linear thermoelasticity equation of the variational formulation of eq. (3.6) for a 1D elastic bar

confirm that the space-time IGA is effective for the linear and non-linear problems defined here.

3.4. Finite-strain thermoelasticity

3.4.1. Thermomechanical coupling at finite strain for nearly-incompressible media

3.4.1.1. Free energy and thermodynamics principles

In this section, we use the results obtained in [66] to develop the process of construction of the equations of the problem at finite strains. We assume first that the transformation can be split into a pure thermal expansion and a pure mechanical deformation. The intermediate thermal state free of mechanical deformation is assumed to be stress free and we adopt the following multiplicative decomposition:

$$\mathbf{F} = \mathbf{F}_\Theta \mathbf{F}_m \tag{3.11}$$

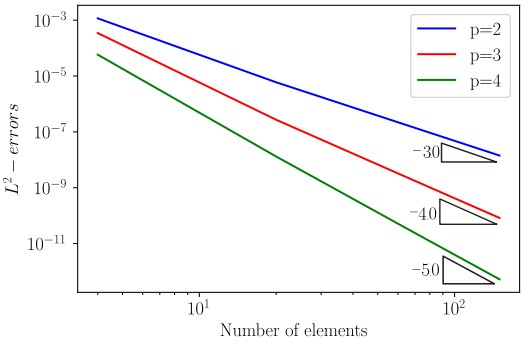

(a) Displacement field

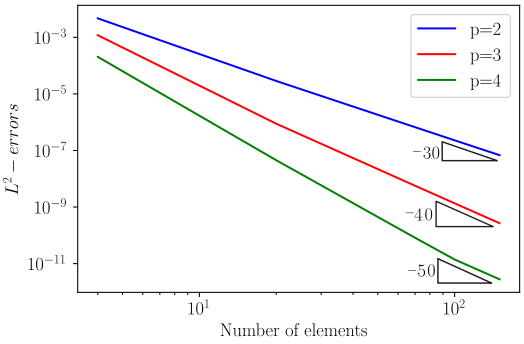

(b) Velocity field

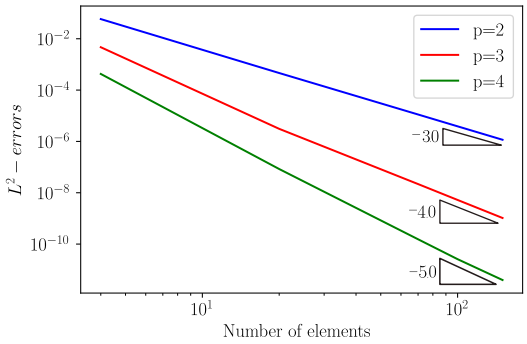

(c) Temperature field

Figure 3.16. – Convergence curves for displacement, velocity and temperature for the non-linear thermoelasticity problem of a 1D elastic bar

where $\mathbf{F}_\Theta = J_\Theta^{1/3}\mathbf{1}$ is a pure thermal expansion and $\mathbf{F}_m$ is the mechanical deformation gradient (this is a classical approach, see e.g. [40]). Splitting the isochoric-volumetric of the total deformation gradient $\mathbf{F} = (J^{1/3}\mathbf{1})\bar{\mathbf{F}}$, one has:

$$J = J_\Theta J_m \quad \text{and} \quad \mathbf{F}_m = \bar{\mathbf{F}} \tag{3.12}$$

We adopt here the hybrid free energy concept that can be viewed as a generalization of a partial Legendre transform of the Helmoltz free energy to take into account the nearly-incompressible behavior (see [66]). We assume that the state variables are the isochoric deformation $\bar{\mathbf{F}}$, the temperature Θ and a stress like variable q that is dual to the mechanical volume variation J_m . The first thermodynamics principle (conservation of energy) can be written in the reference configuration as:

$$\rho_0 \dot{e} = \mathbf{\Pi} : \dot{\mathbf{F}} + \rho_0 r - \mathrm{div}_X \mathbf{Q}_\Theta \tag{3.13}$$

where e is the internal energy, $\mathbf{\Pi}$ is the first Piola-Kirchoff stress, r is an external heat source, div_X is the Lagrangian divergence, $\mathbf{Q}_\Theta$ is the Lagrangian heat flux. The entropy production (second principle of thermodynamics) in the reference

configuration can be written under the following local form:

$$\rho_0 \Theta \dot{s} - \rho_0 r + \mathrm{div}_X \mathbf{Q}_\Theta - \frac{\mathrm{grad}_\mathbf{X} \Theta}{\Theta} \cdot \mathbf{Q}_\Theta \geq 0 \tag{3.14}$$

where $\mathrm{grad}_\mathbf{X}$ is the gradient in the reference configuration. Introducing the time derivative of the hybrid free energy φ, one has:

$$\dot{\varphi} = \dot{e} - \dot{s}\Theta - s\dot{\Theta} + \dot{\beta} \tag{3.15}$$

where β here is an additional volumetric potential. Combining eq. (3.15) and eq. (3.13) in eq. (3.14), the so-called Clausius-Duhem inequality is obtained:

$$\phi = \mathbf{\Pi} : \dot{\mathbf{F}} - \rho_0 \dot{\varphi} + \rho_0 \dot{\beta} - \rho_0 s \dot{\Theta} - \frac{\mathrm{grad}_\mathbf{X} \Theta}{\Theta} \cdot \mathbf{Q}_\Theta \geq 0 \quad \forall \dot{\mathbf{F}}, \dot{\Theta}, \mathbf{Q}_\Theta \tag{3.16}$$

where ϕ is the dissipation. The time derivative of the hybrid free energy and the volumic energy can also be computed taking into account their dependency on the state variables $(\bar{\mathbf{F}}, q, \Theta)$ such that:

$$\dot{\varphi} = \frac{\partial \varphi}{\partial \bar{\mathbf{F}}} : \dot{\bar{\mathbf{F}}} + \frac{\partial \varphi}{\partial q}\dot{q} + \frac{\partial \varphi}{\partial \Theta}\dot{\Theta} \tag{3.17}$$

$$\dot{\beta} = \frac{\partial \beta}{\partial J}\dot{J} + \frac{\partial \beta}{\partial q}\dot{q} + \frac{\partial \beta}{\partial \Theta}\dot{\Theta} \tag{3.18}$$

The time derivative of strain quantities leads to the following expressions:

$$\dot{J} = J\mathbf{F}^{-T} : \dot{\mathbf{F}} \tag{3.19}$$

$$\dot{\bar{\mathbf{F}}} = J^{-1/3}\left[\mathbb{I} - \frac{1}{3}\mathbf{F} \otimes \mathbf{F}^{-T}\right] : \dot{\mathbf{F}} = \mathbb{P}_\mathbf{F} : \dot{\mathbf{F}} \tag{3.20}$$

where $\mathbb{I}$ is the fourth order identity tensor. Inserting eqs. (3.19), (3.20) in eqs. (3.17) and (3.18) and combining with eq. (3.16), the Clausius-Duhem inequality can be rewritten as follows:

$$\boxed{\begin{aligned}\phi = &\left(\mathbf{\Pi} - \rho_0 \frac{\partial \varphi}{\partial \bar{\mathbf{F}}} : \mathbb{P}_\mathbf{F} + \rho_0 J \frac{\partial \beta}{\partial J}\mathbf{F}^{-T}\right) : \dot{\mathbf{F}} - \rho_0 \left(s + \frac{\partial \varphi}{\partial \Theta} - \frac{\partial \beta}{\partial \Theta}\right)\dot{\Theta} \\ &- \rho_0 \left(\frac{\partial \varphi}{\partial q} - \frac{\partial \beta}{\partial q}\right)\dot{q} - \frac{\mathrm{grad}_X \Theta}{\Theta} \cdot \mathbf{Q}_\Theta \geq 0 \qquad \forall \mathbf{D}, \dot{\alpha}_i, \dot{\Theta}, \dot{q}, \mathbf{Q}_\Theta\end{aligned}} \tag{3.21}$$

We can therefore obtain a relation between entropy and hybrid energy:

$$s = -\frac{\partial \varphi}{\partial \Theta} + \frac{\partial \beta}{\partial \Theta} \tag{3.22}$$

and the following expressions for the dissipation terms:

$$\begin{aligned}\phi^{int} &= \left(\mathbf{\Pi} - \rho_0 \frac{\partial \varphi}{\partial \bar{\mathbf{F}}} : \mathbb{P}_{\mathbf{F}} + \rho_0 J \frac{\partial \beta}{\partial J} \mathbf{F}^{-T}\right) : \dot{\mathbf{F}} \\ &\quad -\rho_0 \left(\frac{\partial \varphi}{\partial q} - \frac{\partial \beta}{\partial q}\right) \dot{q} \geq 0 \qquad (3.23)\\ \phi^{therm} &= -\frac{\mathrm{grad}_X \Theta}{\Theta} \cdot \mathbf{Q}_\Theta \geq 0 \qquad (3.24)\end{aligned}$$

We also assume that the behavior is perfectly elastic ($\phi^{int} = 0$), therefore we have:

$$\begin{aligned}\mathbf{\Pi} &= \rho_0 \frac{\partial \varphi}{\partial \bar{\mathbf{F}}} : \mathbb{P}_{\mathbf{F}} + \rho_0 J \frac{\partial \beta}{\partial J} \mathbf{F}^{-T} \qquad (3.25)\\ \frac{\partial \varphi}{\partial q} &= \frac{\partial \beta}{\partial q} \qquad (3.26)\end{aligned}$$

To proceed further, the hybrid energy is assumed to be decomposed additively as follows:

$$\varphi(\bar{\mathbf{F}}, q, \Theta) = \varphi_{iso}(\bar{\mathbf{F}}, \Theta) - \frac{g(q)}{\rho_0} + \varphi_{ther}(\Theta) \qquad (3.27)$$

where $g(q) = q^2/2k$ with k the bulk modulus. For the potential β, we choose:

$$\beta(J, q, \Theta) = q \frac{(1 - J_m)}{\rho_0} \qquad (3.28)$$

We therefore obtain the following expression for the entropy:

$$\boxed{s = -\frac{\partial \varphi_{iso}}{\partial \Theta} - \frac{\partial \varphi_{ther}}{\partial \Theta} + \frac{Jq}{J_\Theta^2 \rho_0} \frac{\partial J_\Theta}{\partial \Theta}} \qquad (3.29)$$

We can also notice that the hydrostatic pressure p is related to q through: $p = q/J_\Theta$.

Combining eq. (3.15) and eq. (3.13), we obtain:

$$\rho_0 \dot{s}\Theta = \mathbf{\Pi} : \dot{\mathbf{F}} + \rho_0 r - \mathrm{div}_X \mathbf{Q}_\Theta - \rho_0 \dot{\varphi} + \rho_0 \dot{\beta} - \rho_0 s \dot{\Theta} \qquad (3.30)$$

Using equations (3.17) and (3.18) and regrouping terms, we have:

$$\rho_0 \dot{s}\Theta = \phi^{int} + \rho_0 r - \mathrm{div}_X \mathbf{Q}_\Theta \qquad (3.31)$$

The variation of the entropy can be computed from (3.29):

$$\begin{aligned}\dot{s} = &-\left(\frac{\partial^2 \varphi_{ther}}{\partial \Theta^2} + \frac{\partial^2 \varphi_{iso}}{\partial \Theta^2} + \frac{2Jq}{J_\Theta^3 \rho_0} \left(\frac{\partial J_\Theta}{\partial \Theta}\right)^2 - \frac{Jq}{J_\Theta^2 \rho_0} \frac{\partial^2 J_\Theta}{\partial \Theta^2}\right) \dot{\Theta} \\ &- \left(\frac{\partial^2 \varphi_{iso}}{\partial \Theta \partial \bar{\mathbf{F}}} : \mathbb{P}_{\mathbf{F}} - \frac{Jq\mathbf{F}^{-\mathrm{T}}}{J_\Theta^2 \rho_0} \frac{\partial J_\Theta}{\partial \Theta}\right) : \dot{\mathbf{F}} + \frac{1}{\rho_0} \left(\frac{J}{J_\Theta^2} \frac{\partial J_\Theta}{\partial \Theta}\right) \dot{q}\end{aligned} \qquad (3.32)$$

Inserting (3.32) in (3.31) and recalling that $\phi^{int} = 0$ in the thermoelastic case, we obtain the heat transfer equation:

$$\boxed{\rho_0 C_p \dot{\Theta} = l_m + l_q + \rho_0 r - \mathrm{div}_X \mathbf{Q}_\Theta} \tag{3.33}$$

where C_p is the isobaric heat capacity

$$C_p = -\Theta \left(\frac{\partial^2 \varphi_{ther}}{\partial \Theta^2} + \frac{\partial^2 \varphi_{iso}}{\partial \Theta^2} + \frac{2Jq}{J_\Theta^3 \rho_0} \left(\frac{\partial J_\Theta}{\partial \Theta} \right)^2 - \frac{Jq}{J_\Theta^2 \rho_0} \frac{\partial^2 J_\Theta}{\partial \Theta^2} \right) \tag{3.34}$$

and l_m, l_q are mechanical coupling terms

$$\begin{aligned} l_m &= \Theta \left(\rho_0 \frac{\partial^2 \varphi_{iso}}{\partial \Theta \partial \bar{\mathbf{F}}} : \mathbb{P}_{\mathbf{F}} - \frac{Jq\mathbf{F}^{-\mathrm{T}}}{J_\Theta^2} \frac{\partial J_\Theta}{\partial \Theta} \right) : \dot{\mathbf{F}} = \Theta \frac{\partial \mathbf{\Pi}}{\partial \Theta} : \dot{\mathbf{F}} \\ l_q &= -\Theta \left(\frac{J}{J_\Theta^2} \frac{\partial J_\Theta}{\partial \Theta} \right) \dot{q} \end{aligned} \tag{3.35}$$

3.4.2. Variational formulation for nearly-incompressible materials

We restrict our study to quasi-static loading. The mechanical equilibrium of the continuum body at time t is expressed in the initial configuration:

$$\mathrm{DIV}_{\mathbf{X}} \mathbf{\Pi} + \rho_0 \mathbf{f} = \mathbf{0} \quad \text{in } Q, \quad \mathbf{\Pi} \cdot \mathbf{N} = \mathbf{t} \quad \text{on } \Gamma_\sigma, \quad \mathbf{u} = \mathbf{u}_0 \quad \text{on } \Gamma_u \tag{3.36}$$

where $\mathbf{\Pi} = J\boldsymbol{\sigma} \cdot \mathbf{F}^{-\mathrm{T}}$ is the first Piola-Kirchoff stress, $\mathbf{f}$ are body loads, $\mathbf{t}$ are surface loads applied on Γ_σ, $\mathbf{N}$ is the outward normal on Γ_σ, $\mathbf{u}_0$ are the prescribed displacements on the reference surface Γ_u. Thermal equilibrium is expressed in the initial configuration:

$$\begin{aligned} \rho_0 C_p \dot{\Theta} = l_m + l_q + \rho_0 \mathbf{r} - J\mathrm{DIV}_{\mathbf{X}} \mathbf{Q} \quad \text{in } Q, \quad \Theta(t=0) = \Theta_0, \\ \mathbf{Q} = \mathbf{Q}_h \quad \text{on } \Gamma_0, \quad \Theta = \Theta_d \quad \text{on } \Gamma_\Theta \end{aligned} \tag{3.37}$$

where $\mathbf{Q} = J\mathbf{q} \cdot \mathbf{F}^{-\mathrm{T}}$ is the Lagrangian heat flux. We propose the following weak form of the equilibrium equations [1]:

1. The functional space of variations is defined by the spaces $\mathcal{H}^u = \{\delta\mathbf{u} \in (H^1(\Omega_0))^n, \delta\mathbf{u} = 0 \text{ on } \partial\Omega_{u_d}\}$, $\mathcal{H}^\Theta = \{\delta\Theta \in (H^1(\Omega_0))^n, \delta\Theta = 0 \text{ on } \partial\Omega_{\Theta_0}\}$, with n the physical dimension of the space, $H^1(\Omega_0)$ a one order Hilbert space.

$$
\begin{aligned}
&\text{Find } (\mathbf{u},\Theta,p)\in\mathcal{H}^u\times\mathcal{H}^\Theta\times\mathcal{H}^p \text{ such that } \forall(\delta\mathbf{u},\delta\Theta,\delta p)\in\mathcal{H}_0^u\times\mathcal{H}_0^\Theta\times\mathcal{H}_0^p, \text{ one has:}\\
&\int_Q(\mathbf{\Pi}+p\frac{J}{J_\Theta}\mathbf{F}^{-\mathrm{T}}):\mathbf{F}(\delta\mathbf{u})dQ-\int_Q\rho_0\mathbf{f}\cdot\delta\mathbf{u}dQ-\int_S\mathbf{t}\cdot\delta\mathbf{u}dS+\int_Q\rho_0C_p\dot{\Theta}\delta\Theta dQ\\
&-\int_Q\left(l_m+l_q+\rho_0 r\right)\delta\Theta dQ-\int_Q J\mathbf{Q}\cdot\mathrm{GRAD}_{\mathbf{X}}\delta\Theta dQ+\int_S\mathbf{Q}_h\cdot\mathbf{N}\delta\Theta dS=0\\
&\int_Q\left((J_m-1)+\frac{pJ_\Theta}{K_v}\right)\delta p dQ=0
\end{aligned}
\tag{3.38}
$$

Note that the previous variational system is obtained without the use of Lagrange multipliers as done in general. The variable p naturally comes from the thermodynamical framework.

3.4.3. Space-time discretization

Our aim is to check the capacities of the numerical schemes we usually use to accurately solve the proposed model. In the following, we give the main issues of both models, the finite element model and the isogeometric analysis one. A similar formalism can be used to derive the matrix equation for both the finite element model and the isogeometric analysis one. Once again, the Newton-Raphson procedure is employed to solve this non-linear system. We start from a known solution, $(\mathbf{d}^k,\beta^k)$, at increment k, we search $\Delta\mathbf{d}^k$ for a given load increment $\Delta\beta^k$ such that $\mathbf{r_u}(\mathbf{d}^k+\Delta\mathbf{d}^k,\beta^k+\Delta\beta^k)=\mathbf{r_\Theta}(\mathbf{d}^k+\Delta\mathbf{d}^k,\beta^k+\Delta\beta^k)=\mathbf{r_p}(\mathbf{d}^k+\Delta\mathbf{d}^k,\beta^k+\Delta\beta^k)$. The linerization of this problem leads to the following linear system:

$$
\begin{bmatrix}
\mathbf{K_{uu}}(\mathbf{u}_h^k,\Theta_h^k,p_h^k) & \mathbf{K_{u\Theta}}(\mathbf{u}_h^k,\Theta_h^k,p_h^k) & \mathbf{K_{up}}(\mathbf{u}_h^k,\Theta_h^k,p_h^k)\\
\mathbf{K_{\Theta u}}(\mathbf{u}_h^k,\Theta_h^k,p_h^k) & \mathbf{K_{\Theta\Theta}}(\mathbf{u}_h^k,\Theta_h^k,p_h^k) & \mathbf{K_{\Theta p}}(\mathbf{u}_h^k,\Theta_h^k,p_h^k)\\
\mathbf{K_{pu}}(\mathbf{u}_h^k,\Theta_h^k,p_h^k) & \mathbf{K_{p\Theta}}(\mathbf{u}_h^k,\Theta_h^k,p_h^k) & \mathbf{K_{pp}}(\mathbf{u}_h^k,\Theta_h^k,p_h^k)
\end{bmatrix}
\left\{\begin{array}{c}\Delta\mathbf{d^{u^k}}\\ \Delta\mathbf{d^{\Theta^k}}\\ \Delta\mathbf{d^{p^k}}\end{array}\right\}
\tag{3.39}
$$

$$
=\left\{\begin{array}{c}
-\mathbf{r_u}(\mathbf{u}_h^k,\Theta_h^k,p_h^k)-\mathbf{f}_u\Delta\beta^k\\
-\mathbf{r_\Theta}(\mathbf{u}_h^k,\Theta_h^k,p_h^k)-\mathbf{f}_\Theta\Delta\beta^k\\
-\mathbf{r_p}(\mathbf{u}_h^k,\Theta_h^k,p_h^k)
\end{array}\right\}
$$

The components of the tangent matrix are given by:

$$
\begin{aligned}
\mathbf{K}^e_{t_{pp}} &= \mathcal{A}_e\int_{Q_e}\mathbf{N}^{p\mathrm{T}}\frac{J_\Theta}{K_v}\mathbf{N}^p dQ\\
\mathbf{K}^e_{t_{p\mathbf{u}}} &= \mathcal{A}_e\int_{Q_e}\mathbf{N}^{p\mathrm{T}}\mathbf{F}^{-\mathrm{T}}\frac{J}{J_\Theta}\mathbf{B}_{\mathbf{F}}dQ\\
\mathbf{K}^e_{t_{p\Theta}} &= \mathcal{A}_e\int_{Q_e}\mathbf{N}^{p\mathrm{T}}\left(\frac{\alpha J}{J_\Theta}+\frac{\alpha p}{K_v}\right)\mathbf{N}^\Theta dQ
\end{aligned}
$$

$$\mathbf{K}^e_{t_{\Theta u}} = -\mathcal{A}_e \int_{Q_e} \mathbf{N}^{\mathbf{\Theta}\mathrm{T}} \mathcal{C}^h_\Theta \dot{\mathbf{F}} \mathbf{N}^{\mathbf{\Theta}} dQ$$

$$\mathbf{K}^e_{t_{\Theta p}} = -\mathcal{A}_e \int_{Q_e} \mathbf{N}^{\mathbf{\Theta}\mathrm{T}} \mathbf{B}^p_t \left(\mathcal{G}^h_\Theta + \Theta^h \frac{\partial \mathcal{G}^h_\Theta}{\partial \Theta} \right) dQ$$

$$\mathbf{K}^e_{t_{\Theta\Theta}} = \mathcal{A}_e \int_{Q_e} \mathbf{N}^{\mathbf{\Theta}\mathrm{T}} \left[\rho_0 C_p \mathbf{B}^\Theta_t - \left(\mathcal{C}^h_\Theta + \mathcal{C}^h_{\Theta\Theta} \Theta^h \right) [J\dot{\mathbf{F}}] \right]$$

$$+ K_\Theta \mathbf{B}^{\mathbf{\Theta}\mathrm{T}}_x \mathbf{B}^\Theta_x dQ$$

$$\begin{aligned}
\mathbf{K}^e_{t_{uu}} &= \mathcal{A}_e \int_{Q_e} \mathbf{B_F}^T \mathcal{C}^h_u \mathbf{B_F} dQ \\
\mathbf{K}^e_{t_{up}} &= \mathcal{A}_e \int_{Q_e} \mathbf{B_F}^T \mathbf{F} \frac{J}{J_\Theta} \mathbf{N}^p dQ \\
\mathbf{K}^e_{t_{u\Theta}} &= \mathcal{A}_e \int_{Q_e} \mathbf{B_F}^T \mathcal{C}^h_\Theta \mathbf{N}^{\mathbf{\Theta}} dQ
\end{aligned}$$

such that the differential operator $\mathbf{B_F}$ is defined by:

$$\frac{\partial \mathbf{u}}{\partial \mathbf{X}} = \mathbf{B_F} \mathbf{d}^{\mathbf{u}} \tag{3.40}$$

The matrix terms $\mathcal{C}^h_u$, $\mathcal{C}^h_\Theta$, $\mathcal{C}^h_{\Theta\Theta}$ and $\mathcal{G}^h_\Theta$ are derived from the matrix/vector representation of the constitutive tangent operator $\mathcal{C}_u$, $\mathcal{C}_\Theta$, $\mathcal{C}_{\Theta\Theta}$ and $\mathcal{G}_\Theta$ defined from:

$$\begin{aligned}
\mathcal{C}_u &= \frac{\partial \mathbf{\Pi}}{\partial \mathbf{F}} \\
\mathcal{C}_\Theta &= \frac{\partial \mathbf{\Pi}}{\partial \Theta} \\
\mathcal{C}_{\Theta\Theta} &= \frac{\partial^2 \mathbf{\Pi}}{\partial \Theta^2} \\
\mathcal{G}_\Theta &= \frac{\partial}{\partial \Theta} \left(\frac{J}{J^2_\Theta} \frac{\partial J_\Theta}{\partial \Theta} \right)
\end{aligned}$$

Moreover, we have:

$$\begin{aligned}
\mathbf{r}_u &= \mathcal{A}_e \int_{Q_e} \mathbf{B_F}^T \mathbf{\Pi} dQ - \beta \mathbf{f_u} \\
\mathbf{r}_\Theta &= \mathcal{A}_e \int_{Q_e} \rho_0 C_p \mathbf{N}^{\Theta \mathrm{T}} \left(\mathbf{B}_t^\Theta + \dot{\mathbf{F}} \mathcal{C}_\Theta^h \mathbf{N}^\Theta - \mathbf{N}^\Theta \mathbf{B}_t^p \alpha \frac{J}{J_\Theta^2} \right) dQ - \beta \mathbf{f_\Theta} \\
\mathbf{r}_p &= -\mathcal{A}_e \int_{Q_e} \mathbf{N^p}^{\mathrm{T}} \left(J_h - 1 - g(p_h) \right) dQ
\end{aligned}$$

such that:

$$\begin{aligned}
\mathbf{f}_u &= \mathcal{A}_e \int_{Q_e} \mathbf{N}^{u\mathrm{T}} \mathbf{f}_h dQ + \mathcal{A}_e \int_{P_u} \mathbf{N}^{u\mathrm{T}} \mathbf{T}_h dP \\
\mathbf{f}_\Theta &= \mathcal{A}_e \int_{Q_e} \mathbf{N}^{\Theta\mathrm{T}} \mathbf{r}_h dQ - \mathcal{A}_e \int_{P_q} \mathbf{N}^{\Theta\mathrm{T}} \mathbf{Q} \mathbf{N} dP
\end{aligned}$$

3.4.4. Numerical applications at finite-strain

We consider the following isochoric and thermal potentials:

$$\rho_0 \varphi_{iso} = c_{10} \frac{\Theta}{\Theta_0} (\bar{I}_1 - 3), \quad \rho_0 \varphi_{ther} = C_0 \left(\Theta - \Theta_0 - \Theta \log \left(\frac{\Theta}{\Theta_0} \right) \right) - C_1 \frac{(\Theta - \Theta_0)^2}{2\Theta_0} \tag{3.41}$$

where c_{10}, C_0 and C_1 are material coefficients. For the thermal volume variation, we consider a very simple linear expansion relation:

$$J_\Theta = 1 + \alpha(\Theta - \Theta_0) \tag{3.42}$$

where α is the volumetric expansion coefficient and Θ_0 is the initial temperature. The isobaric heat capacity takes the following form:

$$C_p = \frac{1}{\rho_0} \left(C_0 + C_1 \frac{\Theta}{\Theta_0} - \frac{2\alpha^2 J q \Theta}{J_\Theta^3} \right) = \frac{1}{\rho_0} \left(C_0 + C_1 \frac{\Theta}{\Theta_0} - \frac{2\alpha^2 J p \Theta}{J_\Theta^2} \right) \tag{3.43}$$

The problem chosen here is taken from Erbts and Düster [30]. It concerns an incompressible beam submitted to a thermomechanical loading. The length of the beam is taken such that $L = 10\ m$, and the final time is $T = 1\ s$.

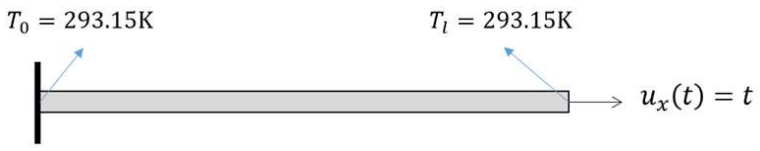

Figure 3.17. – 2D clamped beam for the thermoelastic problem

The domain of the problem is plotted in Figure 3.17. The boundary conditions

are considered such that the left end of the beam is clamped and the temperature at both ends is imposed for it to be equal to the reference temperature $\theta_0 = 293.15\ K$. Adiabatic conditions are considered on the other faces. On the right end, a time-dependent displacement is imposed. Due to the thermoelastic coupling, the temperature of the beam will evolve due to the deformation of the beam. The parameters of the problem are chosen such that $c_{10} = 0.22 \times 10^6, K_v = 1500 \times 10^6$, $\rho = 1\ kg.m^{-3}$, $\alpha = 6.0 \times 10^{-4}\ K^{-1}$, $C_0 = 1.6 \times 10^6$, $C_1 = 3.6 \times 10^3$.

This problem is solved with the space-time isogeometric method on one side, and with the finite element method for the space discretization equipped with the Euler implicit scheme for the time discretization on the other side. A comparison of the results is given in Figure 3.18.

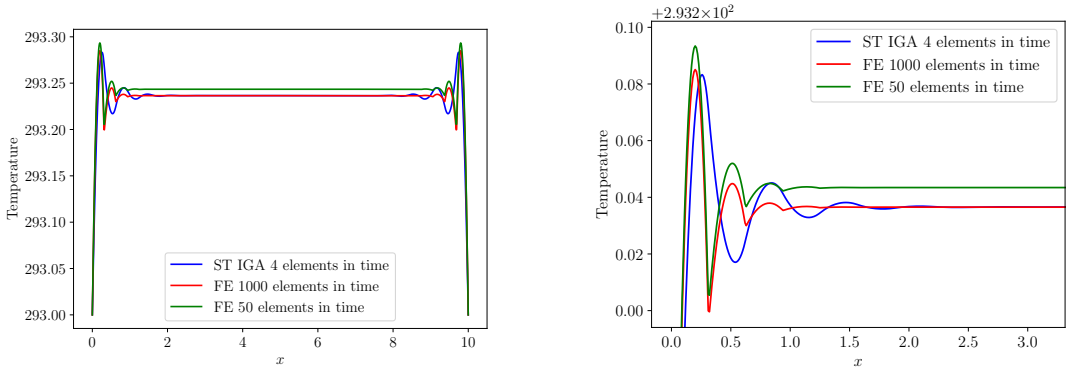

(a) Space-time solution

(b) Zoom on the space-time solution

Figure 3.18. – Space-time solution of the thermoelastic problem at finite strains computed with the IGA and FE method

The results show that only 4 elements in time are needed in the case of the space-time isogeometric method, versus 1000 elements in time for the classical finite element method (with backward Euler scheme for time advancing) to obtain a similar solution. This huge difference between the number of time elements in both cases underlines the interest of using space-time methods compared to classical methods. Note that the number of space elements is fixed for both cases at 32 space elements. Figure 3.18 also represents a zoom of the solution. It can be seen that on the boundaries of the solutions, there are some oscillations. In the middle of the solution, the blue line, referring to the ST IGA solution obtained using only 4 elements in time, meets perfectly the red line, which is the FE element solution obtained using 1000 elements in time.

We would like to test the heterogeneous and asynchronous aspects of the space-time method on this test as well, as done for the small strain case. For this reason, the same test is repeated taking, for the first case, one order of approximation that is lower for the temperature field compared to the displacement, the velocity and the pressure fields: we choose $p = 1$ for the temperature field and $p = 2$ for the other fields. For the second case, we take a coarser grid in time for the temperature

field compared to the time grid of all the other fields: the number of elements in time is 4 time steps for the temperature field and 8 time steps for the other fields. Note that the number of elements in space is fixed to 32 elements for all fields. The plot of the 2 solutions computed for these 2 test cases, along with the solution computed where no heterogeneous nor asynchroneous scheme was taken, are plotted in Figure 3.19. This figure shows that the 3 solutions are very close to eachother, meaning that an accurate solution could be obtained for a lower cost, and a close zoom in on the space-time solution confirms this result. This is a strong aspect for the space-time methods and it indeed opens up a valuable track of research: a similar and accurate response could be obtained for a given problem by using a cost that is lower, whether it is in terms of the approximation order or the mesh size of time.

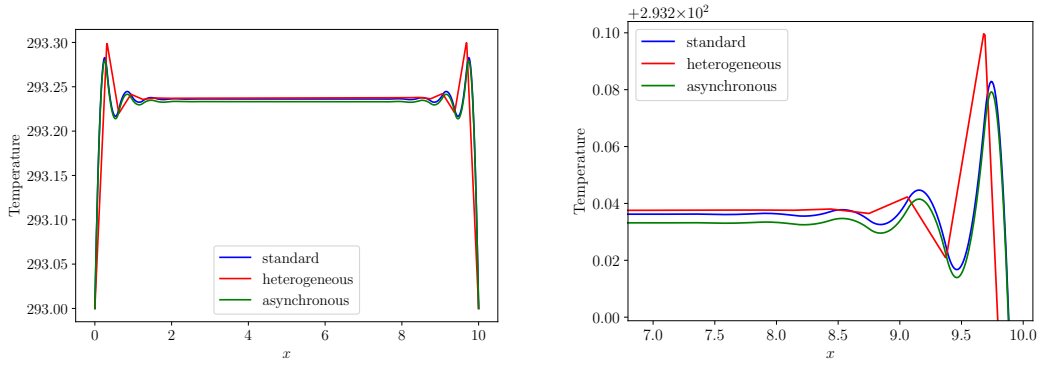

(a) Space-time solution

(b) Zoom on the space-time solution

Figure 3.19. – Space-time solution of the thermoelastic problem at finite strains computed with a standard scheme, heterogeneous scheme and asynchroneous scheme

3.5. Conclusion

In this chapter, the space-time isogeometric method was applied for the resolution of thermomechanical problems at small-strain in a linear and non-linear context and at finite strains. Optimal rates of convergence were obtained on simple problems, and accurate solutions were observed for impact problems. Subdivision techniques were tested and proved to be effective for space-time methods. These techniques consist of taking a subgrid in time that is finer for certain fields and looser for others. In our case, we chose to take a finer grid for the displacement and velocity fields, and a looser one for the temperature field, and accurate results were achieved. Another technique was to take a higher order approximation for some fields and a lower one for other fields: a lower order was taken for the temperature field generating accurate results as well. All these qualitative results confirm the efficiency of space-time methods when dealing with thermomechanical problems at small strains

for linear and non-linear cases and at finite strains. They also show that it is possible to have heterogeneous and asynchroneous schemes using the space-time methods. We can therefore adapt in a very simple way the parameters of the model (mesh size, approximation order, sub-discretization, etc) without changing the formulation while having a very effective model whatever the level of coupling (strong or weak) is.

4. Space-time Formulations and Internal Variables

Chapter Contents

4.1. Introduction

As discussed in Chapter 1, the viscoelastic problem was treated in a space-time context in the literature, e.g. [83, 17], but only in linear cases. The viscosity in these references is treated by considering an additional viscous part of the displacement. Here, we adopt another strategy, where its novelty consists of considering the problem's unknown to be an internal variable. Hence, we would not consider any additional contribution on the displacement field, but we will consider a deformation field. The idea is to approximate internal variables such as the unknowns of the problem. This has an obvious advantage for non-local problem but may be interesting for local constitutive law in order to have better convergence rate of non-linear problems. To the author's knowledge, the space-time method has not yet been applied for the resolution of non-linear viscoelastic problems. In this chapter, viscoelastic problems of Zener's viscoelastic model are investigated for linear and non-linear cases using the space-time isogeometric method: both small

and finite strain cases are treated. We use a 3-field formulation (displacement, velocity and viscous deformation). Stabilizing terms of type GAC were adopted in responses where numerous oscillations are found in order to vanish these oscillations. Accurate results are obtained for all cases: the linear case and the non-linear case at finite strains.

4.2. Small-strain formulation

4.2.1. Problem Statement

In this section, the problem of Chapter 3 is considered with a slightly different form. Here, the strain $\boldsymbol{\varepsilon}$ is divided into two parts : an elastic strain $\boldsymbol{\varepsilon}_e$ and a viscous strain $\boldsymbol{\varepsilon}_v$. The basic equations of viscoelasticity are the following:

$$\begin{aligned}
&\rho\ddot{\mathbf{u}} - div_x\boldsymbol{\sigma} = \mathbf{f} \text{ equilibrium equation}\\
&\boldsymbol{\sigma} = \left(2\mu\boldsymbol{\varepsilon}^D + Ktr\boldsymbol{\varepsilon}I\right) + 2\mu_V\boldsymbol{\varepsilon}_e^D = \boldsymbol{\sigma}_1 + \boldsymbol{\sigma}_2 \text{ constitutive law}\\
&\boldsymbol{\varepsilon}^D = DEV(\boldsymbol{\varepsilon}) = \boldsymbol{\varepsilon} - \frac{1}{3}tr\boldsymbol{\varepsilon}I \text{ Deviatoric operator}\\
&\boldsymbol{\varepsilon} = \boldsymbol{\varepsilon}_e + \boldsymbol{\varepsilon}_v \text{ strain decomposition}\\
&\dot{\boldsymbol{\varepsilon}}_v = \frac{1}{\eta}\boldsymbol{\sigma}_2 = \frac{2\mu_v}{\eta}\left(\boldsymbol{\varepsilon} - \boldsymbol{\varepsilon}_v\right)^D = \frac{1}{\tau_v}\left(\boldsymbol{\varepsilon} - \boldsymbol{\varepsilon}_v\right)^D \text{ evolution law of viscosity}
\end{aligned} \tag{4.1}$$

where $\mathbf{u}(\mathbf{x},t)$ is the displacement field, $\mathbf{v}(\mathbf{x},t)$ is the velocity field, $\boldsymbol{\varepsilon}_v(\mathbf{x},t)$ is the viscous deformation, τ_v is the characteristic time of viscosity and $K = 3\lambda + 2\mu$. The constitutive model corresponds to Zener's linear viscoelasticity model, see Figure 4.1 for the equivalent rhelogical model.

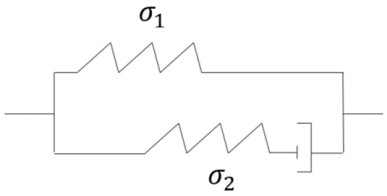

Figure 4.1. – Zener's equivalent rheological model

The problem's boundary and initial conditions are defined as:

$$\begin{aligned}
&\mathbf{u} = \mathbf{g}(\mathbf{x},t) \text{ for } \mathbf{x} \in \Gamma_u, t \in [0,T]\\
&\boldsymbol{\sigma}.\mathbf{n} = \mathbf{T}(\mathbf{x},t) \text{ for } \mathbf{x} \in \Gamma_{\boldsymbol{\sigma}}, t \in [0,T]\\
&\mathbf{u}(\mathbf{x},t=0) = \mathbf{u}_0(\mathbf{x}) \text{ for } \mathbf{x} \in \Omega\\
&\dot{\mathbf{u}}(\mathbf{x},t=0) = \mathbf{v}_0(\mathbf{x}) \text{ for } \mathbf{x} \in \Omega\\
&\boldsymbol{\varepsilon_v}(\mathbf{x},t=0) = \mathbf{0} \text{ for } \mathbf{x} \in \Omega
\end{aligned}$$

As done in the previous chapter, we introduce the velocity field $\mathbf{v}$ as unknown:

$$\begin{aligned} \dot{\boldsymbol{\varepsilon}}_v &= \frac{1}{\tau_v}\left(\boldsymbol{\varepsilon} - \boldsymbol{\varepsilon}_v\right)^D \\ \rho\dot{\mathbf{v}} - div\boldsymbol{\sigma} &= \mathbf{f} \\ \rho(\mathbf{v} - \dot{\mathbf{u}}) &= 0 \end{aligned} \tag{4.2}$$

where

$$\boldsymbol{\sigma} = \left(2\mu\boldsymbol{\varepsilon}^D + Ktr\boldsymbol{\varepsilon}I\right) + 2\mu_V\left(\boldsymbol{\varepsilon} - \boldsymbol{\varepsilon}_v\right)^D$$

The initial and boundary conditions of the system (4.2) are:

$$\begin{aligned} &\mathbf{u} = \mathbf{g}(\mathbf{x}, t) \text{ for } \mathbf{x} \in \Gamma_u, t \in [0, T] \\ &\boldsymbol{\sigma}.\mathbf{n} = \mathbf{T}(\mathbf{x}, t) \text{ for } \mathbf{x} \in \Gamma_{\boldsymbol{\sigma}}, t \in [0, T] \\ &\mathbf{u}(\mathbf{x}, t = 0) = \mathbf{u}_0(\mathbf{x}) \text{ for } \mathbf{x} \in \Omega \\ &\mathbf{v}(\mathbf{x}, t = 0) = \mathbf{v}_0(\mathbf{x}) \text{ for } \mathbf{x} \in \Omega \\ &\boldsymbol{\varepsilon_v}(\mathbf{x}, t = 0) = \mathbf{0} \text{ for } \mathbf{x} \in \Omega \end{aligned}$$

4.2.2. Space-time variational formulation for viscoelasticity

Multiplying the equations of system (4.2) by test functions defined on appropriate spaces and integrating over the space-time cylinder Q, the following 3-field variational formulation is obtained:

Find $(\mathbf{u}(\mathbf{x}, t), \mathbf{v}(\mathbf{x}, t), \boldsymbol{\varepsilon}_v(\mathbf{x}, t)) \in \mathcal{H}^u \times \mathcal{H}^v \times \mathcal{H}^{\boldsymbol{\varepsilon}}$ such that $\forall\ (\delta\mathbf{u}(\mathbf{x}, t), \delta\mathbf{v}(\mathbf{x}, t), \delta\boldsymbol{\varepsilon}_v(\mathbf{x}, t)) \in \mathcal{H}_0^u \times \mathcal{H}_0^v \times \mathcal{H}_0^{\boldsymbol{\varepsilon}}$

$$\begin{aligned} &\int_Q \dot{\boldsymbol{\varepsilon}}_v \delta\dot{\boldsymbol{\varepsilon}}_v dQ - \int_Q \frac{1}{\tau_v}\left(\boldsymbol{\varepsilon} - \boldsymbol{\varepsilon}_v\right)^D \delta\dot{\boldsymbol{\varepsilon}}_v dQ + \\ &\int_Q \rho\dot{v}\delta\dot{\mathbf{u}} dQ + \int_Q \boldsymbol{\sigma}\boldsymbol{\varepsilon}\left(\delta\dot{\mathbf{u}}\right) dQ - \int_Q \mathbf{f}\delta\dot{\mathbf{u}} dQ + \sum_e \int_{Q_e} \rho_0(\ddot{\mathbf{u}}_h - \dot{\mathbf{v}}_h)\tau(\delta\ddot{\mathbf{u}}_h - \delta\dot{\mathbf{v}}_h) dQ \\ &+ \int_Q \rho\left(\mathbf{v} - \dot{\mathbf{u}}\right)\delta\dot{\mathbf{v}} dQ = 0 \end{aligned} \tag{4.3}$$

Note that the variational formulation here is obtained in the same manner as the formulations of the precedent chapter. $\mathcal{H}^u$ and $\mathcal{H}^v$ are defined in Chapter 2, and $\mathcal{H}^{\boldsymbol{\varepsilon}} = \{\boldsymbol{\varepsilon} \in (H^{0,1}(Q))^d,\ \boldsymbol{\varepsilon}(x, t = 0) = 0\}$

4.2.3. Numerical examples

We propose a test case of a viscoelastic bar submitted to a body load as shown in Figure 4.2. The representation of the body load chosen for this test case is also

sketched in Figure 4.2.

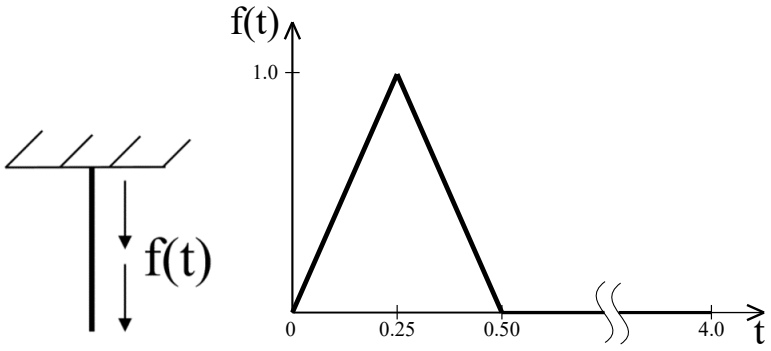

(a) Space-time domain (b) Body load

Figure 4.2. – Space-time domain of the viscoelastic problem and body load **f** applied to the bar

The parameters of the problem are chosen such that $L = 1\ m$ and $T = 4\ s$. The discretization is 90 elements in the time direction and 20 elements in the space direction and the interpolation is of degree $p = 2$. The evolution with respect to time at the center of the bar of the displacement field and the velocity field for different values of ρ is computed. For ρ small, stabilizing terms are needed in the variational formulations in order to reduce the oscillations, and we choose $\tau = 0.02\ s$. The results were obtained using different values of μ_V : $\mu_V = 0$ (no viscosity is considered), $\mu_V = 0.1\ Pa$ and $\mu_V = 0.9\ Pa$. Figures 4.3, 4.4 and 4.5 show the evolution of the displacement, velocity and stress fields for $\rho = 0.001\ kg.m^{-3}$ using the different values of μ_V. It is clear that the GAC terms play a crucial role in the stabilization of the oscillations present in the numerical response for the 3 fields.

The same test case was done using a higher value $\rho = 1\ kg.m^{-3}$, see Figure 4.6. No stabilization terms are needed in this case. Figure 4.6 illustrates the displacement, velocity and stress fields obtained for different viscosity degrees (i.e for different values of μ_V). The effect of the viscosity is obvious in the representation of this numerical solution, that seems to be quite accurate. This shows that the space-time isogeometric method is well-suited for solving linear viscoelastic problems.

4.3. Finite-strain formulation

4.3.1. Nearly incompressible viscoelasticity with internal variables

4.3.1.1. Local constitutive behavior: the non-linear generalized maxwell model

To take into account the nearly incompressibility constraint, we proceed as done in Chapter 3. First, the deformation gradient is decomposed into an isochoric part

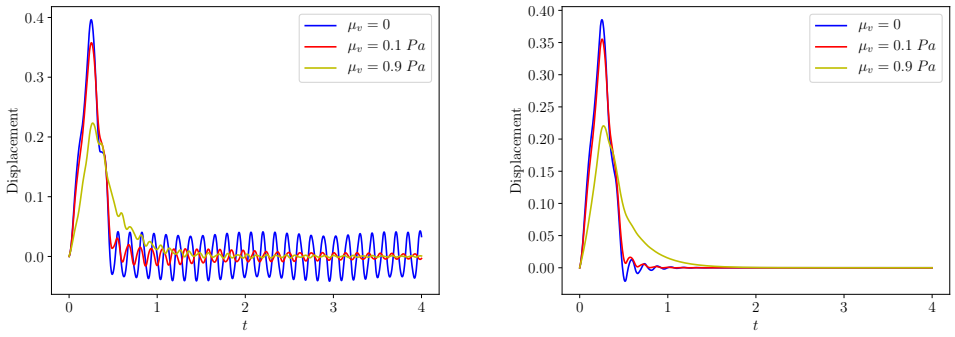

(a) Displacement field without stabilization (b) Displacement field with stabilization

Figure 4.3. – Displacement field for the viscoelastic test with and without GAC stabilizing terms for $\rho = 0.001\ kg.m^{-3}$

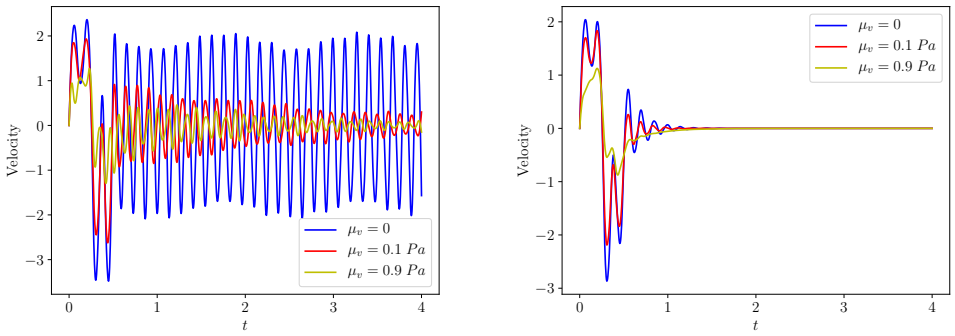

(a) Velocity field without stabilization (b) Velocity field with stabilization

Figure 4.4. – Velocity field for the viscoelastic test with and without GAC stabilizing terms for $\rho = 0.001\ kg.m^{-3}$

and a volumetric part:

$$\mathbf{F} = \bar{\mathbf{F}}(J^{1/3}\mathbf{1}) \tag{4.4}$$

where $J = det\mathbf{F}$ is the volume variation. As seen in Chapter 3, the hybrid energy concept can be viewed as a generalization of a partial Legendre transform of a Helmoltz free energy by replacing the volume variation, J, by a pressure like variable that is noted q. The viscosity is modelled here with internal variables by a decomposition of the isochoric deformation gradient, $\bar{\mathbf{F}}$, in n elastic and viscous intermediates deformation gradients with the so-called multiplicative split (following the concept of intermediate configurations, e.g. [88, 89]):

$$\bar{\mathbf{F}} = \bar{\mathbf{F}}_{\mathbf{e}}^{i}\bar{\mathbf{F}}_{\mathbf{v}}^{\ i} \qquad i = 1..n \tag{4.5}$$

where the indice i denotes the i^{th} viscous mechanism. It is important to note that the intermediate configurations are not uniquely defined (there is an arbitrary

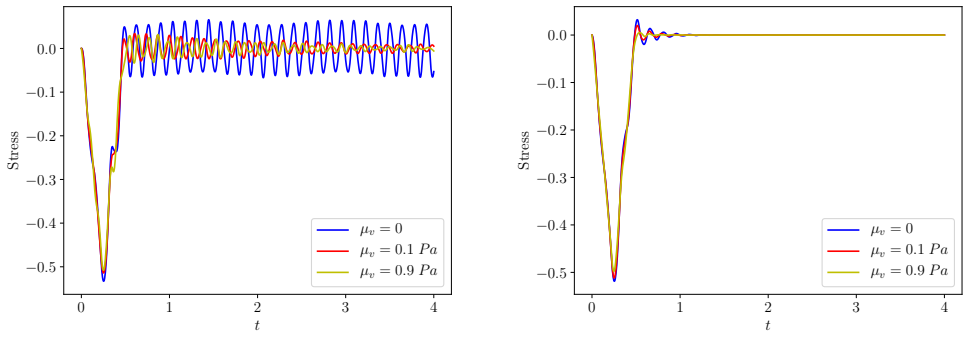

(a) Stress field without stabilization (b) Stress field with stabilization

Figure 4.5. – Stress field for the viscoelastic test with and without GAC stabilizing terms for $\rho = 0.001\ kg.m^{-3}$

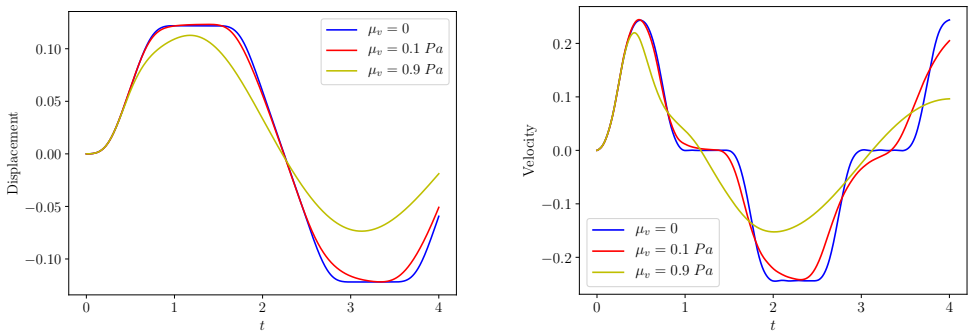

(a) Displacement field (b) Velocity field

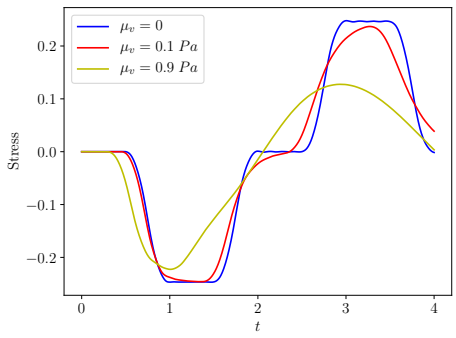

(c) Stress field

Figure 4.6. – Displacement and velocity fields for the viscoelastic test without stabilization terms for $\rho = 1.0\ kg.m^{-3}$

rotation). Furthermore, we assume in the following that the viscous flow is purely incompressible, therefore $\det(\overline{\mathbf{F}}^i_{\mathbf{e}}) = \det(\overline{\mathbf{F}}_{\mathbf{v}}{}^i) = 1$. Neglecting the effect of the

temperature (isothermal and adiabatic conditions), the state variables that define the local behavior are $\bar{\mathbf{F}}, q, \overline{\mathbf{F}}_{\mathbf{v}}^{\,i}$. Restricting the model to an isotropic behavior, the hybrid free energy φ can be considered as a function of $\bar{\mathbf{C}}, \bar{\mathbf{C}}_{\mathbf{e}}^{i}, q$ due to representation theorem of isotropic functions where $\bar{\mathbf{C}} = \bar{\mathbf{F}}^{\mathrm{T}}\bar{\mathbf{F}}$ and $\bar{\mathbf{C}}_{\mathbf{e}}^{i} = \bar{\mathbf{F}}_{\mathbf{e}}^{i^{\mathrm{T}}}\bar{\mathbf{F}}_{\mathbf{e}}^{i}$ are right Cauchy green tensors. The hybrid free energy can be related to the internal energy e and the entropy s through the relation:

$$\varphi(\bar{\mathbf{C}}, q, \bar{\mathbf{C}}_{\mathbf{e}}^{i}) = e - s\Theta + \beta(J, q) \tag{4.6}$$

where the function β allows to relate J and q from a thermodynamical point of view (duality principle). Combining the first and second thermodynamics principles, we can obtain the so-called Claussius-Duhem (or Coleman-Noll) inequality in adiabatic and isothermal conditions:

$$\Phi = \boldsymbol{\Pi} : \dot{\mathbf{F}} - \rho_0\dot{\varphi} + \rho_0\dot{\beta} \geq 0 \quad \forall\, \dot{\mathbf{F}} \tag{4.7}$$

where Φ is the dissipation, $\rho_0(\mathbf{X})$ is the initial local density and the dot superscript denotes the so-called material time derivative. The material time derivatives of the hybrid free energy and volumic energy can be computed such that:

$$\dot{\varphi} = \left(2\bar{\mathbf{F}}\frac{\partial\varphi}{\partial\bar{\mathbf{C}}}\right) : \dot{\bar{\mathbf{F}}} + \frac{\partial\varphi}{\partial q} : \dot{q} + \sum_{i=1}^{n}\left(2\bar{\mathbf{F}}_{\mathbf{e}}^{i}\frac{\partial\varphi}{\partial\bar{\mathbf{C}}_{\mathbf{e}}^{i}}\right) : \dot{\bar{\mathbf{F}}}_{\mathbf{e}}^{\,i} \tag{4.8}$$

$$\dot{\beta} = \frac{\partial\beta}{\partial J}\dot{J} + \frac{\partial\beta}{\partial q}\dot{q} \tag{4.9}$$

Computing the material time derivative of eqs (4.4) and (4.5), one can show that:

$$\dot{\bar{\mathbf{F}}} = J^{-1/3}\left(\mathbb{I} - \frac{1}{3}\mathbf{F}\otimes\mathbf{F}^{-\mathrm{T}}\right) : \dot{\mathbf{F}} = \mathbb{P} : \dot{\mathbf{F}} \tag{4.10}$$

$$\dot{\bar{\mathbf{F}}}_{\mathbf{e}}^{\,i} = \dot{\bar{\mathbf{F}}}\overline{\mathbf{F}}_{\mathbf{v}}^{\,i^{-1}} - \bar{\mathbf{F}}_{\mathbf{e}}^{i}\dot{\bar{\mathbf{F}}}_{\mathbf{v}}^{\,i}\overline{\mathbf{F}}_{\mathbf{v}}^{\,i^{-1}} \tag{4.11}$$

Inserting eqs. (4.8-4.11) in eq. (4.7), we obtain the following expression for the dissipation:

$$\begin{aligned}\Phi = &\left(\boldsymbol{\Pi} - \rho_0\left(2\bar{\mathbf{F}}\frac{\partial\varphi}{\partial\bar{\mathbf{C}}}\right) : \mathbb{P} - \rho_0\sum_{i=1}^{n}(2\bar{\mathbf{F}}_{\mathbf{e}}^{i}\frac{\partial\varphi}{\partial\bar{\mathbf{C}}_{\mathbf{e}}^{i}}\overline{\mathbf{F}}_{\mathbf{v}}^{\,i^{-\mathrm{T}}}) : \mathbb{P} + \rho_0\frac{\partial\beta}{\partial J}J\mathbf{F}^{-\mathrm{T}}\right) : \dot{\mathbf{F}}\\ &- \rho_0\left(\frac{\partial\varphi}{\partial q} - \frac{\partial\beta}{\partial q}\right)\dot{q}\\ &+ \rho_0\sum_{i=1}^{n}(2\bar{\mathbf{F}}_{\mathbf{e}}^{i}\frac{\partial\varphi}{\partial\bar{\mathbf{C}}_{\mathbf{e}}^{i}}\overline{\mathbf{F}}_{\mathbf{v}}^{\,i^{-\mathrm{T}}}) : (\bar{\mathbf{F}}_{\mathbf{e}}^{i}\dot{\bar{\mathbf{F}}}_{\mathbf{v}}^{\,i}) \geq 0 \quad \forall\, \dot{\mathbf{F}}, \dot{q}, \dot{\bar{\mathbf{F}}}_{\mathbf{v}}^{\,i} \quad \text{with } \overline{\mathbf{F}}_{\mathbf{v}}^{\,i^{-\mathrm{T}}} : \dot{\bar{\mathbf{F}}}_{\mathbf{v}}^{\,i} = 0\end{aligned} \tag{4.12}$$

The restriction $\overline{\mathbf{F}}_{\mathbf{v}}^{\,i^{-\mathrm{T}}} : \dot{\bar{\mathbf{F}}}_{\mathbf{v}}^{\,i} = 0$ is due to the incompressible assumption on the viscous flow that can take the following forms: $\det(\overline{\mathbf{F}}_{\mathbf{v}}^{\,i}) = 1$ or $\overline{\mathbf{F}}_{\mathbf{v}}^{\,i^{-\mathrm{T}}} : \dot{\bar{\mathbf{F}}}_{\mathbf{v}}^{\,i} = 0$ or

$\dot{\bar{\mathbf{C}}}_{\mathbf{v}}^{\ \mathbf{i}} : \bar{\mathbf{C}}_{\mathbf{v}}^{i^{-1}} = 0$.

Assuming that the intrinsic dissipation is only due to the evolution of the viscous internal variables, we can deduce from eq. (4.12) the following constitutive equations:

$$\mathbf{\Pi} = \left(\bar{\mathbf{\Pi}}_{eq} + \sum_{i=1}^{n} \bar{\mathbf{\Pi}}_v^i\right) : \mathbb{P} - \rho_0 \frac{\partial \beta}{\partial J} J\mathbf{F}^{-\mathrm{T}} \tag{4.13}$$

$$\frac{\partial \varphi}{\partial q} = \frac{\partial \beta}{\partial q} \tag{4.14}$$

where $\bar{\mathbf{\Pi}}_{eq} = \rho_0 2\bar{\mathbf{F}}\partial\varphi/\partial\bar{\mathbf{C}}$ is the fully relaxed stress (equilibrium) and $\bar{\mathbf{\Pi}}_v^i = \rho_0(2\bar{\mathbf{F}}_{\mathbf{e}}^i \partial\varphi/\partial\bar{\mathbf{C}}_{\mathbf{e}}^i)\overline{\mathbf{F}}_{\mathbf{v}}^{\ i^{-\mathrm{T}}}$ is the i^{th} viscous stress. Equation (4.14) gives a compressibility law that allows the definition of a constitutive relation between q and J. With these definitions, the remaining terms in the intrinsic dissipation are expressed by:

$$\Phi = \sum_{i=1}^{n} \underbrace{\bar{\mathbf{\Pi}}_v^i : (\bar{\mathbf{F}}_{\mathbf{e}}^i \dot{\bar{\mathbf{F}}}_{\mathbf{v}}^{\ i})}_{\Phi_v^i} \geq 0 \quad \forall \dot{\bar{\mathbf{F}}}_{\mathbf{v}}^{\ i} \quad \text{with } \overline{\mathbf{F}}_{\mathbf{v}}^{\ i^{-\mathrm{T}}} : \dot{\bar{\mathbf{F}}}_{\mathbf{v}}^{\ i} = 0 \tag{4.15}$$

The i^{th} viscous contribution can also be rewritten as:

$$\Phi_v^i = \left(2\rho_0 \overline{\mathbf{F}}_{\mathbf{v}}^{\ i^{-1}} \bar{\mathbf{C}}_{\mathbf{e}}^i \frac{\partial \varphi}{\partial \bar{\mathbf{C}}_{\mathbf{e}}^i} \overline{\mathbf{F}}_{\mathbf{v}}^{\ -\mathrm{T}}\right) : \left(\overline{\mathbf{F}}_{\mathbf{v}}^{\ i^{\mathrm{T}}} \dot{\bar{\mathbf{F}}}_{\mathbf{v}}^{\ i}\right) \tag{4.16}$$

By a symmetry property of the first term between parenthesis in eq. (4.16), we also have:

$$\Phi_v^i = \left(\rho_0 \overline{\mathbf{F}}_{\mathbf{v}}^{\ i^{-1}} \bar{\mathbf{C}}_{\mathbf{e}}^i \frac{\partial \varphi}{\partial \bar{\mathbf{C}}_{\mathbf{e}}^i} \overline{\mathbf{F}}_{\mathbf{v}}^{\ -\mathrm{T}}\right) : \dot{\bar{\mathbf{C}}}_{\mathbf{v}}^{\ \mathbf{i}} \tag{4.17}$$

After some calculus, one can show that $\overline{\mathbf{F}}_{\mathbf{v}}^{\ i^{-1}} \bar{\mathbf{C}}_{\mathbf{e}}^i (\partial\varphi/\partial\bar{\mathbf{C}}_{\mathbf{e}}^i)\overline{\mathbf{F}}_{\mathbf{v}}^{\ -\mathrm{T}} = -\partial\varphi/\partial\bar{\mathbf{C}}_{\mathbf{v}}^i$ and eq. (4.17) can also be rewritten by:

$$\Phi_v^i = \left(-\rho_0 \frac{\partial \varphi}{\partial \bar{\mathbf{C}}_{\mathbf{v}}^i}\right) : \dot{\bar{\mathbf{C}}}_{\mathbf{v}}^{\ \mathbf{i}} \tag{4.18}$$

Taking into account the incompressibility constraint on the viscous flow (that can take the following forms: $\det(\overline{\mathbf{F}}_{\mathbf{v}}^{\ i}) = 1$ or $\overline{\mathbf{F}}_{\mathbf{v}}^{\ i^{-\mathrm{T}}} : \dot{\bar{\mathbf{F}}}_{\mathbf{v}}^{\ i} = 0$ or $\dot{\bar{\mathbf{C}}}_{\mathbf{v}}^{\ \mathbf{i}} : \bar{\mathbf{C}}_{\mathbf{v}}^{i^{-1}} = 0$), eq. (4.15) can be rewritten as follows:

$$\Phi = \sum_{i=1}^{n} \left(-\rho_0 \frac{\partial \varphi}{\partial \bar{\mathbf{C}}_{\mathbf{v}}^i} : \mathbb{P}_{\bar{\mathbf{C}}_{\mathbf{v}}^i}\right) : \dot{\bar{\mathbf{C}}}_{\mathbf{v}}^{\ \mathbf{i}} \quad \forall \dot{\bar{\mathbf{C}}}_{\mathbf{v}}^{\ \mathbf{i}} \quad \text{with } \dot{\bar{\mathbf{C}}}_{\mathbf{v}}^{\ \mathbf{i}} : \bar{\mathbf{C}}_{\mathbf{v}}^{i^{-1}} = 0 \tag{4.19}$$

where $\mathbb{P}_{\bar{\mathbf{C}}_{\mathbf{v}}^i}$ is a deviatoric projector for the viscous intermediate configuration. It can be expressed by:

$$\mathbb{P}_{\bar{\mathbf{C}}_{\mathbf{v}}^i} = \left(\mathbb{I} - \frac{1}{3} \bar{\mathbf{C}}_{\mathbf{v}}^{i^{-1}} \otimes \bar{\mathbf{C}}_{\mathbf{v}}^i\right) \tag{4.20}$$

The expression in eq. (4.19) exhibits objective thermodynamics fluxes ($\dot{\bar{\mathbf{C}}}_{\mathbf{v}}^{\,\mathbf{i}}$) and forces ($-\rho_0(\partial\varphi/\partial\bar{\mathbf{C}}_{\mathbf{v}}^i) : \mathbb{P}_{\bar{\mathbf{C}}_{\mathbf{v}}^i}$) for the Lagrangian viscous flow. Using the framework of standard generalized materials (e.g. see [36]), we can define a pseudo-potential of dissipation, $\zeta(\dot{\bar{\mathbf{C}}}_{\mathbf{v}}^{\,\mathbf{i}})$, that is a convex function of the thermodynamics fluxes. Using the normality principle, we can postulate the following flow rules that automatically satisfies the Clausius-Duhem inequality:

$$-\rho_0 \frac{\partial \varphi}{\partial \bar{\mathbf{C}}_{\mathbf{v}}^i} : \mathbb{P}_{\bar{\mathbf{C}}_{\mathbf{v}}^i} = \frac{\partial \zeta}{\partial \dot{\bar{\mathbf{C}}}_{\mathbf{v}}^{\,\mathbf{i}}} \quad i = 1..n \tag{4.21}$$

Equations (4.13),(4.14) and (4.21) define a viscous model that can be viewed as a parallel assembly (in terms of stresses) of n viscous incompressible elements with a nearly incompressible hyperelastic element and therefore corresponds to a Generalized Maxwell model in a Lagrangian formalism.

4.3.2. A space-time mixed variational principle for the evolution problem

Following the work presented in [73, 72], we propose to define a rate-type mixed variational principle stating the following potential:

$$L(\dot{\mathbf{u}}, \dot{q}, \dot{\bar{\mathbf{C}}}_{\mathbf{v}}^{\,\mathbf{i}}) = \int_Q \left\{ \rho_0 \dot{\varphi}(\bar{\mathbf{C}}, q, \bar{\mathbf{C}}_{\mathbf{e}}^i) - \rho_0 \dot{\beta}(J, q) + \zeta(\dot{\bar{\mathbf{C}}}_{\mathbf{v}}^{\,\mathbf{i}}) \right\} dQ - \int_Q \mathbf{f}\dot{\mathbf{u}} dQ - \int_P \mathbf{T}\dot{\mathbf{u}} dP \tag{4.22}$$

The evolution of the displacements, viscous internal variables and pressure-like stress is determined from the following minimization principle:

$$\left\{ \dot{\mathbf{u}}, \dot{q}, \dot{\bar{\mathbf{C}}}_{\mathbf{v}}^{\,\mathbf{i}} \right\} = \text{Arg} \left\{ \inf_{\dot{u} \in \mathcal{H}^u} \sup_{\dot{q} \in \mathcal{H}^q} \inf_{\dot{\bar{\mathbf{C}}}_{\mathbf{v}}^{\,\mathbf{i}}} L(\dot{\mathbf{u}}, \dot{q}, \dot{\bar{\mathbf{C}}}_{\mathbf{v}}^{\,\mathbf{i}}) \right\} \tag{4.23}$$

Considering the variation of the potential previously defined in eq. (4.22), we can find the Euler equations associated with the previous variational principle:

$$\delta_{\dot{\mathbf{u}}} L \equiv \int_Q \mathbf{\Pi} : \mathbf{F}(\delta\dot{\mathbf{u}}) dQ - \int_Q f \delta\dot{\mathbf{u}} dQ - \int_P \mathbf{T}\delta\dot{\mathbf{u}} dP = 0 \tag{4.24}$$

$$\delta_{\dot{\mathbf{q}}} L \equiv \int_Q \rho_0 \left(\frac{\partial \varphi}{\partial q} - \frac{\partial \beta}{\partial q} \right) \delta\dot{q} dQ = 0 \tag{4.25}$$

$$\delta_{\dot{\bar{\mathbf{C}}}_{\mathbf{v}}^{\,\mathbf{i}}} L \equiv \int_Q \left(\rho_0 \frac{\partial \varphi}{\partial \bar{\mathbf{C}}_{\mathbf{v}}^i} : \mathbb{P}_{\bar{\mathbf{C}}_{\mathbf{v}}^i} + \frac{\partial \zeta}{\partial \dot{\bar{\mathbf{C}}}_{\mathbf{v}}^{\,\mathbf{i}}} \right) : \delta\dot{\bar{\mathbf{C}}}_{\mathbf{v}}^{\,\mathbf{i}} dQ = 0 \quad i = 1..n \tag{4.26}$$

Using the divergence theorem and traction boundary condition allows us to see that eq. (2.1) corresponds to the local form of the space-time variational. Eqs. (4.24) and (4.25) correspond to the constitutive compressibility relation and eq. (4.26) corresponds to the i^{th} Maxwell viscous flow rule. These relations, as well as

the local constitutive eq. (4.13) for the stress, constitute a mixed form of $n+2$ fields of a quasi-static, non-linear, viscous space-time problem formulated in terms of the rate of the unknowns of the problem.

4.3.3. IGA space-time discretization

We consider the discretisation of the space-time cylinder with NURBS functions. Using the matrix/vector representation of the tensorial description of the space-time cylinder, we consider the approximations of the unknown fields $\mathbf{u}, q, \bar{\mathbf{C}}^i_{\mathbf{v}}$. For the sake of simplicity, we consider a 1D problem:

$$\begin{aligned}
&\mathbf{u}_h(\xi,\eta) = \mathbf{N^u}(\xi,\eta)\mathbf{d^u} \\
&q_h(\xi,\eta) = \mathbf{N^q}(\xi,\eta)\mathbf{d^q} \\
&\bar{\mathbf{C}}^1_{\mathbf{v_h}}(\xi,\eta) - \mathbf{1} = \mathbf{N^c}(\xi,\eta)\mathbf{d^{c1}} \\
&\vdots \\
&\bar{\mathbf{C}}^n_{\mathbf{v_h}}(\xi,\eta) - \mathbf{1} = \mathbf{N^c}(\xi,\eta)\mathbf{d^{cn}}
\end{aligned} \tag{4.27}$$

where $\mathbf{N^u}$, $\mathbf{N^q}$ and $\mathbf{N^c}$, for fields $\mathbf{u}$, q and $\bar{\mathbf{C}}^i_{\mathbf{v}}$ respectively. $\mathbf{d^u}$, $\mathbf{d^q}$ and $\mathbf{d^{ci}}$ are the vectors of degrees of freedom. The continuous space-time approximation allows us to define the rate of the unknowns from the first derivative of the approximation functions. In the matrix/vector representation, we have:

$$\begin{aligned}
&\dot{\mathbf{u}}_h(\xi,\eta) = \mathbf{B^u_t}(\xi,\eta)\mathbf{d^u} \\
&\dot{q}_h(\xi,\eta) = \mathbf{B^q_t}(\xi,\eta)\mathbf{d^q} \\
&\dot{\bar{\mathbf{C}}}_{\mathbf{v_h}}{}^{\mathbf{1}}(\xi,\eta) = \mathbf{B^c_t}(\xi,\eta)\mathbf{d^{c1}} \\
&\vdots \\
&\dot{\bar{\mathbf{C}}}_{\mathbf{v_h}}{}^{\mathbf{n}}(\xi,\eta) = \mathbf{B^c_t}(\xi,\eta)\mathbf{d^{cn}}
\end{aligned} \tag{4.28}$$

The discretized variational principle defined at eq. (4.23) then reads

$$\left\{\mathbf{d^u}, \mathbf{d^q}, \mathbf{d^{c1}}, \ldots, \mathbf{d^{cn}}\right\} = \mathrm{Arg}\left\{\mathrm{stat}_{\mathbf{d^u},\mathbf{d^q},\mathbf{d^{ci}}} L_h(\dot{\mathbf{u}}_h, \dot{q}_h, \dot{\bar{\mathbf{C}}}_{\mathbf{v_h}}{}^{\mathbf{i}})\right\} \tag{4.29}$$

We therefore obtain a discrete non-linear system to resolve that consists of cancelling the following residue: (again for a 1D problem)

$$\mathbf{R}(\mathbf{d^u}, \mathbf{d^q}, \mathbf{d^{c1}}, \ldots, \mathbf{d^{cn}}) = \begin{bmatrix} \mathcal{A}_e \int_{Q_e} \mathbf{B}_{xt}^{u^{\mathrm{T}}} \mathbf{\Pi} dQ - \mathcal{A}_e \int_{Q_e} \mathbf{B}_{\mathbf{t}}^{\mathbf{u}^{\mathrm{T}}} \mathbf{f} dQ \\ \qquad\qquad - \mathcal{A}_e \int_{S_e} \mathbf{B}_{\mathbf{t}}^{\mathbf{u}^{\mathrm{T}}} \mathbf{T} dP \\ \mathcal{A}_e \int_{Q_e} \rho_0 \mathbf{B}_t^{q^{\mathrm{T}}} \left(\dfrac{\partial \varphi}{\partial q} - \dfrac{\partial \beta}{\partial q} \right) dQ \\ \mathcal{A}_e \int_{Q_e} \mathbf{B}_t^{c^{\mathrm{T}}} \left(\rho_0 \dfrac{\partial \varphi}{\partial \bar{\mathbf{C}}_{\mathbf{v}}^1} : \mathbb{P}_{\bar{\mathbf{C}}_{\mathbf{v}}^1} + \dfrac{\partial \zeta}{\partial \dot{\bar{\mathbf{C}}}_{\mathbf{v}}^{\mathbf{1}}} \right) dQ \\ \quad \vdots \\ \mathcal{A}_e \int_{Q_e} \mathbf{B}_t^{c^{\mathrm{T}}} \left(\rho_0 \dfrac{\partial \varphi}{\partial \bar{\mathbf{C}}_{\mathbf{v}}^n} : \mathbb{P}_{\bar{\mathbf{C}}_{\mathbf{v}}^n} + \dfrac{\partial \zeta}{\partial \dot{\bar{\mathbf{C}}}_{\mathbf{v}}^{\mathbf{n}}} \right) dQ \end{bmatrix} \tag{4.30}$$

The operator $\mathbf{B}_{xt}^u$ corresponds to the gradient of the rate of the displacement such that:

$$\nabla_{\mathbf{X}} \dot{\mathbf{u}}_h = \mathbf{B}_{xt}^u(\xi, \eta) \mathbf{d}^u \tag{4.31}$$

A standard Newton scheme can be used to solve the system defined in eq. (4.53). This process consists of an iterative update of the degrees of freedom:

$$\begin{bmatrix} \tilde{\mathbf{d}}^u \\ \tilde{\mathbf{d}}^q \\ \tilde{\mathbf{d}}^c \end{bmatrix} \Leftarrow \begin{bmatrix} \tilde{\mathbf{d}}^u \\ \tilde{\mathbf{d}}^q \\ \tilde{\mathbf{d}}^c \end{bmatrix} - \begin{bmatrix} \mathbf{K}_{uu} & \mathbf{K}_{uq} & \mathbf{K}_{uc} \\ \mathbf{K}_{qu} & \mathbf{K}_{qq} & \mathbf{K}_{qc} \\ \mathbf{K}_{cu} & \mathbf{K}_{cq} & \mathbf{K}_{cc} \end{bmatrix}^{-1} \begin{bmatrix} \tilde{\mathbf{R}}_u \\ \tilde{\mathbf{R}}_q \\ \tilde{\mathbf{R}}_c \end{bmatrix} \tag{4.32}$$

The tilde upper-script denotes degrees of freedom that are not prescribed by a Dirichlet boundary condition and the tilde over the residue denotes a modified residue to take into account of the Dirichlet boundary conditions (initial conditions for the evolution problems correspond to Dirichlet boundary conditions on the space-time domain). The terms of the tangent matrix, $\mathbf{K}$, are defined by:

$$\mathbf{K}_{uu} = \mathcal{A}_e \int_{Q_e} \mathbf{B}_{xt}^{u^{\mathrm{T}}} \mathcal{C}_u^h \mathbf{B}_x^u dQ \tag{4.33}$$

$$\mathbf{K}_{uq} = \mathcal{A}_e \int_{Q_e} \mathbf{B}_{xt}^{u^{\mathrm{T}}} \left(-\rho_0 \frac{\partial \beta^2}{\partial J \partial q} \left[J \mathbf{F}^{-\mathrm{T}} \right] \right) \mathbf{N}^q dQ \tag{4.34}$$

$$\mathbf{K}_{uc} = \mathcal{A}_e \int_{Q_e} \mathbf{B}_{xt}^{u^{\mathrm{T}}} \mathcal{C}_c^h \mathbf{N}^c dQ \tag{4.35}$$

$$\mathbf{K}_{qu} = \mathcal{A}_e \int_{Q_e} \rho_0 \mathbf{B}_t^{q^{\mathrm{T}}} \left(\frac{\partial \varphi^2}{\partial q \partial \mathbf{F}} - \frac{\partial \beta^2}{\partial q \partial J} \left[J\mathbf{F}^{-\mathrm{T}} \right] \right) \mathbf{B}_x^u dQ \tag{4.36}$$

$$\mathbf{K}_{qq} = \mathcal{A}_e \int_{Q_e} \rho_0 \mathbf{B}_t^{q^{\mathrm{T}}} \left(\frac{\partial \varphi^2}{\partial^2 q} - \frac{\partial \beta^2}{\partial^2 q} \right) \mathbf{N}^q dQ \tag{4.37}$$

$$\mathbf{K}_{qc} = \mathcal{A}_e \int_{Q_e} \rho_0 \mathbf{B}_t^{q^{\mathrm{T}}} \left(\frac{\partial \varphi^2}{\partial q \partial \bar{\mathbf{C}}_{\mathbf{v}}^i} \right) \mathbf{N}^c dQ \tag{4.38}$$

$$\mathbf{K}_{cu} = \mathcal{A}_e \int_{Q_e} \mathbf{B}_t^{c^{\mathrm{T}}} \mathcal{G}_u \mathbf{B}_x^u dQ \tag{4.39}$$

$$\mathbf{K}_{cq} = \mathbf{0} \tag{4.40}$$

$$\mathbf{K}_{cc} = \mathcal{A}_e \int_{Q_e} \left(\mathbf{B}_t^{c^{\mathrm{T}}} \mathcal{G}_c \mathbf{N}^c + \mathbf{B}_t^{c^{\mathrm{T}}} \frac{\partial \zeta^2}{\partial^2 \dot{\bar{\mathbf{C}}}_{\mathbf{v}}^{\mathbf{i}}} \mathbf{B}_t^c \right) dQ \tag{4.41}$$

The operator $\mathbf{B}_x^u$ corresponds to the gradient of the approximation of the displacement field such that:

$$\nabla_{\mathbf{X}} \mathbf{u}_h = \mathbf{B}_x^u \mathbf{d}^u \tag{4.42}$$

The matrix terms $\mathcal{C}_u^h$ and $\mathcal{C}_c^h$ are issued from the matrix/vector representation of the constitutive tangent operator $\mathcal{C}_u$ and $\mathcal{C}_c$ defined by:

$$\mathcal{C}_u = \frac{\partial \mathbf{\Pi}}{\partial \mathbf{F}} \tag{4.43}$$

$$\mathcal{C}_c = \frac{\partial \mathbf{\Pi}}{\partial \bar{\mathbf{C}}_{\mathbf{v}}^i} \tag{4.44}$$

In a similar way, the terms $\mathcal{G}_u^h$ and $\mathcal{G}_c^h$ come from the matrix/vector representation of the following derivatives:

$$\mathcal{G}_u = \rho_0 \frac{\partial}{\partial \mathbf{F}} \left(\frac{\partial \varphi}{\partial \bar{\mathbf{C}}_{\mathbf{v}}^i} : \mathbb{P}_{\bar{\mathbf{C}}_{\mathbf{v}}^1} \right) \tag{4.45}$$

$$\mathcal{G}_c = \rho_0 \frac{\partial}{\partial \bar{\mathbf{C}}_{\mathbf{v}}^i} \left(\frac{\partial \varphi}{\partial \bar{\mathbf{C}}_{\mathbf{v}}^i} : \mathbb{P}_{\bar{\mathbf{C}}_{\mathbf{v}}^1} \right) \tag{4.46}$$

4.3.4. Application with invariant-based free energies (generalized Maxwell model)

We consider here invariant-based energies used to model rubber viscoelasticity. The hybrid free energy is assumed to be as follows:

$$\rho_0 \varphi = c_{10}(I_1(\bar{\mathbf{C}}) - 3) + c_{01}(I_2(\bar{\mathbf{C}}) - 3) + \sum_{i=1}^{n} \frac{\mu_i}{2}(I_1(\bar{\mathbf{C}}_{\mathbf{e}}^i) - 3) - k \left(\exp(\frac{q}{k}) - 1 \right) + q \tag{4.47}$$

where $I_1(\bullet) = \mathrm{tr}(\bullet)$ and $I_2(\bullet) = 1/2(I1(\bullet)^2 + \mathrm{tr}(\bullet : \bullet))$ are the two first invariants of a deformation tensor. The compressibility potential β is defined by:

$$\beta = q\frac{1-J}{\rho_0} \tag{4.48}$$

and the dissipation potential ζ is chosen such that:

$$\zeta = \sum_{i=1}^{n} \frac{\eta_i}{2} \dot{\bar{\mathbf{C}}}_{\mathbf{v}}^{\mathbf{i}} : \dot{\bar{\mathbf{C}}}_{\mathbf{v}}^{\mathbf{i}} \tag{4.49}$$

This model corresponds to a generalized Maxwell model written in the Lagrangian configuration. The set of material parameters is: $\{c_{10}, c_{01}, k, \mu_1, ..., \mu_n, \eta_1, ..., \eta_n\}$. Using eq. (4.13), the first Piola Kirchoff stress can be computed:

$$\mathbf{\Pi} = \left(2c_{10}\bar{\mathbf{F}} + 2c_{01}\bar{\mathbf{F}}(I_1(\bar{\mathbf{C}})\mathbf{1} - \bar{\mathbf{C}}) + \sum_{i=1}^{n} \mu_i \bar{\mathbf{F}}\bar{\mathbf{C}}_{\mathbf{v}}^{i-1}\right) : \mathbb{P} + qJ\mathbf{F}^{-\mathrm{T}} \tag{4.50}$$

The compressibility relation is given by eq. (4.14):

$$-\exp\left(\frac{q}{k}\right) = -J \tag{4.51}$$

and the i^{th}viscoelastic flow rule is obtained from eq. (4.21):

$$\frac{\mu_i}{2}\left(\bar{\mathbf{C}}_{\mathbf{v}}^{i-1}\bar{\mathbf{C}}\bar{\mathbf{C}}_{\mathbf{v}}^{i-1}\right) : \mathbb{P}_{\bar{\mathbf{C}}_{\mathbf{v}}^{i}} = \eta_i \dot{\bar{\mathbf{C}}}_{\mathbf{v}}^{\mathbf{i}} \tag{4.52}$$

At last, the residual system (eq. (4.53)) can be rewritten such that:

$$\mathbf{R}(\mathbf{d^u}, \mathbf{d^q}, \mathbf{d^{c1}}, \ldots, \mathbf{d^{cn}}) = \begin{bmatrix} \mathcal{A}_e \int_{Q_e} \mathbf{B}_{xt}^{u^{\mathrm{T}}} \mathbf{\Pi} dQ - \mathcal{A}_e \int_{Q_e} \mathbf{B}_{\mathbf{t}}^{\mathbf{u}^{\mathrm{T}}} \mathbf{f} dQ \\ \qquad\qquad - \mathcal{A}_e \int_{S_e} \mathbf{B}_{\mathbf{t}}^{\mathbf{u}^{\mathrm{T}}} \mathbf{T} dP \\ \mathcal{A}_e \int_{Q_e} \mathbf{B}_t^{q^{\mathrm{T}}} \left(-\exp\left(\frac{q}{k}\right) + J\right) dQ \\ \mathcal{A}_e \int_{Q_e} \mathbf{B}_t^{c^{\mathrm{T}}} \left(-\frac{\mu_1}{2}\left(\bar{\mathbf{C}}\right) : \mathbb{P}_{\bar{\mathbf{C}}_{\mathbf{v}}^{1}} + \eta_1 \dot{\bar{\mathbf{C}}}_{\mathbf{v}}^{\mathbf{1}}\right) dQ \\ \quad \vdots \\ \mathcal{A}_e \int_{Q_e} \mathbf{B}_t^{c^{\mathrm{T}}} \left(-\frac{\mu_n}{2}\left(\bar{\mathbf{C}}\right) : \mathbb{P}_{\bar{\mathbf{C}}_{\mathbf{v}}^{n}} + \eta_n \dot{\bar{\mathbf{C}}}_{\mathbf{v}}^{\mathbf{n}}\right) dQ \end{bmatrix} \tag{4.53}$$

4.4. Numerical applications

4.4.1. Homogeneous traction

We consider the case of a homogeneous cyclic tension/compression test in plane strain. The computational domain is a unit cube that corresponds to a unit square space domain on the time interval $[0, 1]$. We use symmetric boundary conditions on the space-time domain to obtain homogeneous strain and stress fields. We apply initial conditions and cyclic (harmonic) displacements on one side of the space-time domain (see Figure 4.7). To impose the sinusoidal signal, we first have to interpolate it with B-spline functions to define the correct values at control points (recall the non-interpolant behavior of the B-spline basis). We followed algorithms given in [82].

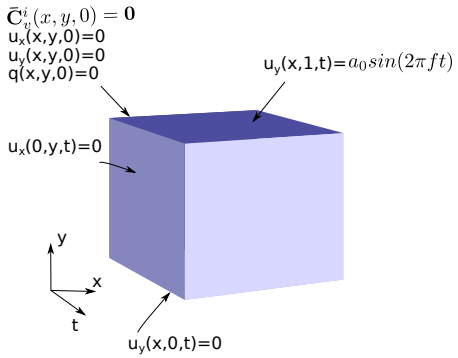

Figure 4.7. – Boundary and initial conditions on the space-time domain for the homogeneous traction test

For this test, a semi-analytical solution can be obtained. Using the homogeneity of the stress and strain fields, we have:

$$\mathbf{F} = \begin{bmatrix} \frac{J}{\lambda} & 0 & 0 \\ 0 & \lambda & 0 \\ 0 & 0 & 1 \end{bmatrix}, \quad \lambda(t) = 1 + a_0 sin(2\pi ft) \tag{4.54}$$

Therefore, the left Cauchy-Green tensor and the first strain invariant are given by:

$$\bar{\mathbf{C}} = \begin{bmatrix} \frac{J^{4/3}}{\lambda^2} & 0 & 0 \\ 0 & \frac{\lambda^2}{J^{2/3}} & 0 \\ 0 & 0 & \frac{1}{J^{2/3}} \end{bmatrix}, \quad I_1 = (1 + \lambda^2 + \frac{J^2}{\lambda^2}) J^{-2/3} \tag{4.55}$$

The i^{th} viscous strain is assumed to be of the following form:

$$\bar{\mathbf{C}}^i_{\mathbf{v}} = \begin{bmatrix} \alpha^i_{11} & 0 & 0 \\ 0 & \alpha^i_{22} & 0 \\ 0 & 0 & \alpha^i_{33} \end{bmatrix} \tag{4.56}$$

The non-zero component of the first Piola-Kirchoff stress can be obtained from eq.

(4.50) and using the traction boundary conditions, $\mathbf{\Pi}_{xx} = 0$, one can obtain the following expression for q:

$$q = \frac{1}{3J^2\lambda^2}\left(2c_{01}(2\lambda^4 - J^2(1+\lambda^2)) + 2c_{10}J^{2/3}(-2J^2+\lambda^2+\lambda^4)\right. \\ \left. + \sum_{i=1}^{n}\mu_i J^{2/3}\left(\frac{\lambda^2}{\alpha_{33}^i} + \frac{\lambda^4}{\alpha_{22}^i} - \frac{2J^2}{\alpha_{11}^i}\right)\right. \tag{4.57}$$

Replacing q in $\mathbf{\Pi}_{yy} = 0$, one has:

$$\mathbf{\Pi}_{yy} = \frac{2}{J\lambda^3}(c_{01} + c_{10}J^{2/3})(\lambda^4 - J^2) + \sum_{i=1}^{n}\mu_i\left(\frac{\lambda}{\alpha_{22}^i J^{1/3}} - \frac{J^{5/3}}{\alpha_{11}^i\lambda^3}\right) \tag{4.58}$$

Considering the compressibility relation defined in eq. (4.51) into eq. (4.57), one obtains a non-linear equation that relates $J, \lambda, \alpha_{11}^i, \alpha_{22}^i, \alpha_{33}^i$. Additionally to this non-linear equation, we can obtain the i^{th} differential system that corresponds to the viscous flow defined at eq. (4.52):

$$\dot{\alpha}_{11}^i = \frac{\mu_i}{2\eta_i}\left(\frac{2}{3}J^{4/3}\lambda^{-2}\alpha_{11}^{i^{-2}} - \frac{1}{3}J^{-2/3}\alpha_{11}^i(\lambda^2\alpha_{22}^{i^{-3}} + \alpha_{33}^{i^{-3}})\right) \tag{4.59}$$

$$\dot{\alpha}_{22}^i = \frac{\mu_i}{2\eta_i}\left(\frac{2}{3}J^{-2/3}\lambda^2\alpha_{22}^{i^{-2}} - \frac{1}{3}J^{-2/3}\alpha_{22}^i(J^2\lambda^{-2}\alpha_{11}^{i^{-3}} + \alpha_{33}^{i^{-3}})\right) \tag{4.60}$$

$$\dot{\alpha}_{33}^i = \frac{\mu_i}{2\eta_i}\left(\frac{2}{3}J^{-2/3}\alpha_{33}^{i^{-2}} - \frac{1}{3}J^{-2/3}(J^2\alpha_{11}^{i^{-3}} + \lambda^4\alpha_{22}^{i^{-3}})\right) \tag{4.61}$$

The previous system of equations was implemented with Mathematica [101] using the function NDSolve.

Adopting the material parameters given in table 4.1, we compute the first four periods of the stress response with the following loading parameters: $a_0 = 0.3$ and $f = 4Hz$. Figure 4.8 shows a comparison between the solution obtained with Mathematica, the one obtained with standard FE, and the one obtained with the ST-IGA. For the FE model, we used a backward Euler scheme to integrate the viscous flow rules. For ST-IGA and FE, as the solution is homogeneous in space, we only used one element (of order 2 for both models in space). We vary the mesh size in time for ST-IGA ($dt = 1/40$ means 40 elements in the $[0, 1]$ time interval) and with the time increment for FE. As expected, the stress response is smoothly captured with the ST-IGA. If we consider the solution computed with Mathematica to be the reference, we can compute the following L_2 error:

$$\text{err}^{ST-IGA,FE} = \int_0^{4/f}\left(\mathbf{\Pi}_{yy}^{Mathematica}(t) - \mathbf{\Pi}_{yy}^{ST-IGA,FE}(t)\right)^2 dt \tag{4.62}$$

Figure 4.9 clearly shows a faster convergence of ST-IGA compared to the standard backward Euler FE scheme: for this problem, the convergence rate is 6 times higher with ST-IGA (with p=2) than with the standard backward FE Euler scheme.

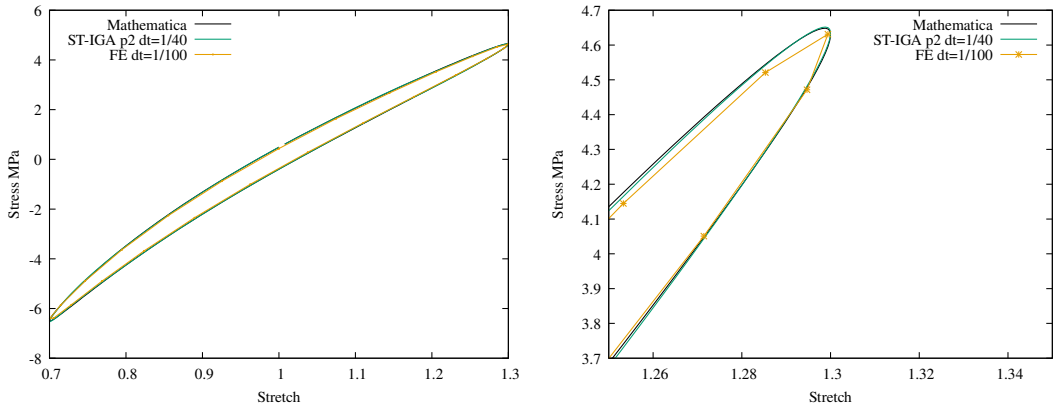

(a) 4^{th} hysteresis cycle (b) zoom on the 4^{th} hysteresis cycle

Figure 4.8. – Comparisons of the hysteresis computed with Mathematica, FE with backward Euler time integrator and ST-IGA.

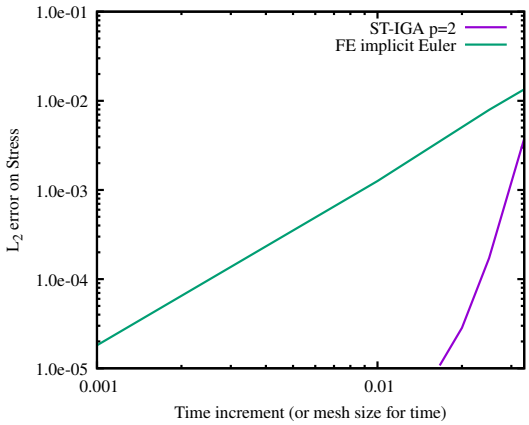

Figure 4.9. – L_2 error on the stress response computed from a reference obtained with Mathematica

4.5. Conclusion

In this chapter, the viscoelastic problem was treated by considering the unknown of this problem as internal variables: a deformation field was considered, which is different from the strategy found in literature, for which the viscosity is considered as an extra part of the displacement field. Thanks to this strategy, we solved the viscoelastic problem of Zener's viscoelastic model for linear and non-linear cases. Small and finite strain cases were considered in this study. In the linear case,

c_{10} (MPa)	c_{01} (MPa)	k (MPa)	μ_1 (MPa)	μ_2 (MPa)	η_1 (MPa.s)	η_2 (MPa.s)
1.0	0.1	10000	0.8	1.9	0.01	0.09

Table 4.1. – Material parameters

accurate numerical results were obtained. GAC stabilizing terms were added to the formulation when the solution needed to be stabilized. Moreover, at finite strains, a comparison of convergence was made between the ST IGA method and the finite element method with backward Euler time scheme. We showed on this simple test that the convergence rate obtained with the ST IGA is 6 times higher than the one obtained with the standard backward FE Euler scheme. All these results show that the space-time method is a good candidate for solving viscoelastic problems. The extension to more complicated viscoelastic models should be further studied. Moreover, applications to viscoplastic model could be carried out in future. In the case of generalized Maxwell behavior, it would be interesting to study asynchroneous strategies to see if there is an interest of such methods when characteristic times of viscosity are different (long term and short term of relaxation).

Conclusion

In this work, we propose a preliminary study of the numerical performances of the space-time isogeometric method in the context of multi-field mechanical formulations. This was done using an existing Java object-oriented hierarchy initially designed for solving multi-field coupled problems at finite strains.

First, a detailed state of art was given for the space-time method based on FE and IGA schemes. We gave references where the space-time method was used for the solving of different kinds of problems: elastodynamics problems [48, 47], thermomechanical problems [65, 59], fluid flow problems [91, 93], heat transfer problems [39, 77], viscoelastic problems [83, 67], etc. We showed that the references concerned the space-time method used on one hand in a context of finite element interpolation or with an isogeometric interpolation, and on the other hand using the continuous or the discontinuous Galerkin method. We also showed that in the literature, only few applications exist for the space-time method combined with the IGA. This may be due to the fact that these two methods are considered to have high numerical cost, especially when combined. The global efficiency of ST IGA is an issue, but it could be overcomed with the power of massively parallel computers available nowadays, especially with the emergence of many techniques of parallel time integration that solve the complete system in parallel, making it possible to adopt the space-time methods without any difficulty.

Second, we developed a space-time variational formulation for elastodynamics equation. We used a special form of test functions that are derived in time and a comparison of the use of regular test functions and derived ones was provided. In the context of problems where an impact is imposed in the initial conditions, extra terms are obligatory to be employed in the variational formulation in order to reduce the oscillations exhibited in the response. These are least-square terms that help in reducing the oscillations in the solution. We propose an alternative form of least-square terms that we added into the variational formulation that make the formulation straightforwardly applied in non-linear cases, which is not quite easy to do while having to implement least-square terms. We applied the space-time isogeometric method on different types of elastodynamics problems : linear ones such as problems at small strains and non-linear ones at finite strains for compressible and nearly-incompressible materials. Optimal convergence rates were obtained for high orders as well because employing the IGA allowed us to employ high order interpolation degrees in an natural and immediate way. Different comparisons were provided between the ST-IGA formulations on one hand and continuous ST-FEM ones and semi-discrete FEM simulations with the HHT scheme

on the other hand.

Third, we applied the space-time isogeometric method on mutiphysics problems : we used the method for the resolution of thermomechanical problems in both linear and non-linear cases. We showed that the method is accurate when having problems where different fields are involved, mechanical and thermal ones in this case. The variational formulations used concerned 3 fields that are the displacement, the temperature and the velocity. Optimal convergence rates were obtained for this type of problems as well. Moreover, we proved that the space-time solution remains accurate when using one order lower for the temperature field on one hand, and a smaller grid for the temperature also on the other hand. This shows that heterogeneous asynchronous schemes are possible to be built while applying the space-time methods. This feature gives important aspects for the method because it means that the method can be used with lower cost.

At last, the space-time isogeometric method was applied for problems having internal variables. The viscoelastic problem was treated at small and finite strains where the viscosity was employed being an internal variable, and new variational formulations were proposed. Accurate solutions were obtained proving once again the power of the space-time method in the resolution of different kinds of problems.

The global aim of our work was achieved in the sense that we have developed and examined trustable space-time IGA mixed formulations for elastodynamics, thermomechanical and viscoelastic problems at small and large strains. The next step would be to extend the framework to other problems having other origins of complexity. For instance, we can combine the methods developed here with phase field formulations to deal with fracture mechanics. We can also explore the potential of discontinuous formulations to deal with viscoplastic behaviors, damage or contact problems.

We think that the space-time methods may be promising in the resolution of industrial problems. Compared to classical time-stepping methods, these methods could be more effective in some cases. We proved that they help achieve more stability in numerical schemes compared to explicit solvers where the CFL condition is necessary to be fulfilled. Moreover, we showed that they can be more energy conservative than traditional schemes. They also allow to control numerical oscillations that can be encountered when solving problems with discontinuities such as impact problems. Even if it remains a lot of technical work and software developments to deal with real industrial problems, all these advantages make the space-time methods a good candidate in solving large industrial problems, especially with the development of computers and technologies of nowadays, making the use of huge parallel solvers possible.

Bibliography

[1] *1974 Bruch - Transient two-dimensional heat conduction problems solved by the finite element method.pdf - Google Search*. URL: https://www.google.com/search?q=1974+Bruch+-+Transient+two%E2%80%90dimensional+heat+conduction+problems+solved+by+the+finite+element+method.pdf&oq=1974+Bruch+-+Transient+two%E2%80%90dimensional+heat+conduction+problems+solved+by+the+finite+element+method.pdf&aqs=chrome..69i57.453j0j4&sourceid=chrome&ie=UTF-8 (visited on 03/28/2020) (cit. on p. 22).

[2] R. Abedi, B. Petracovici, and R.B. Haber. "A space–time discontinuous Galerkin method for linearized elastodynamics with element-wise momentum balance". In: *Computer Methods in Applied Mechanics and Engineering* 195.25 (May 2006), pp. 3247–3273. ISSN: 00457825. DOI: 10.1016/j.cma.2005.06.013. URL: https://linkinghub.elsevier.com/retrieve/pii/S0045782505002689 (visited on 02/20/2020) (cit. on p. 21).

[3] Hector Adelaide, Claude Bohatier, and Franck Jourdan. "New Results on Mesh Adaptation in Space-Time Finite Element Method". In: vol. 2. Jan. 2002, pp. 963–972. ISBN: 0-7918-3591-X. DOI: 10.1115/ETCE2002/STRUC-29042 (cit. on p. 22).

[4] Lucas Adelaide. "Méthode des éléments finis espace-temps : adaptation du maillage en cours d'évolution du contact". In: (Dec. 2001) (cit. on p. 22).

[5] Komla Dela Mawulawoe Ahose. "Caractérisation et modélisation du vieillissement thermique d'élastomères chargés par une approche multiphysique". Theses. Aix-Marseille Université, Dec. 2018 (cit. on p. 4).

[6] H. G. Aksoy and E. Şenocak. "Space-time discontinuous Galerkin method for dynamics of solids". In: *Communications in Numerical Methods in Engineering* 24.12 (Nov. 29, 2007), pp. 1887–1907. ISSN: 10698299. DOI: 10.1002/cnm.1075. URL: http://doi.wiley.com/10.1002/cnm.1075 (visited on 09/26/2019) (cit. on p. 20).

[7] J H Argyris and D W Scharpf. "NUCLEAR ENGINEERING AND DESIGN 10 (1969) 456-464. NORTH-HOLLAND PUBLISHING COMPANY, AMSTERDAM". In: (), p. 9 (cit. on p. 15).

[8] Abdul Kadir Aziz and Peter Monk. "Continuous finite elements in space and time for the heat equation". In: 1989 (cit. on p. 23).

[9] Czesław I. Bajer. "Triangular and tetrahedral space-time finite elements in vibration analysis". In: *International Journal for Numerical Methods in Engineering* 23.11 (Nov. 1986), pp. 2031–2048. ISSN: 0029-5981, 1097-0207. DOI: 10.1002/nme.1620231105. URL: http://doi.wiley.com/10.1002/nme.1620231105 (visited on 09/26/2019) (cit. on p. 21).

[10] Y. Bazilevs, V.M. Calo, J.A. Cottrell, et al. "Variational multiscale residual-based turbulence modeling for large eddy simulation of incompressible flows". In: *Computer Methods in Applied Mechanics and Engineering* 197.1 (Dec. 2007), pp. 173–201. ISSN: 00457825. DOI: 10.1016/j.cma.2007.07.016. URL: https://linkinghub.elsevier.com/retrieve/pii/S0045782507003027 (visited on 02/20/2020) (cit. on p. 15).

[11] Y. Bazilevs, V.M. Calo, J.A. Cottrell, et al. "Isogeometric analysis using T-splines". In: *Computer Methods in Applied Mechanics and Engineering* 199 (2010), pp. 229–263. DOI: 10.1016/j.cma.2009.02.036. URL: https://hal.archives-ouvertes.fr/hal-01517950 (cit. on p. 14).

[12] D.J. Benson, Y. Bazilevs, M.-C. Hsu, et al. "A large deformation, rotation-free, isogeometric shell". In: *Computer Methods in Applied Mechanics and Engineering* 200.13 (Mar. 2011), pp. 1367–1378. ISSN: 00457825. DOI: 10.1016/j.cma.2010.12.003. URL: https://linkinghub.elsevier.com/retrieve/pii/S0045782510003488 (visited on 02/20/2020) (cit. on p. 14).

[13] D.J. Benson, Y. Bazilevs, M.C. Hsu, et al. "Isogeometric shell analysis: The Reissner–Mindlin shell". In: *Computer Methods in Applied Mechanics and Engineering* 199.5 (Jan. 2010), pp. 276–289. ISSN: 00457825. DOI: 10.1016/j.cma.2009.05.011. URL: https://linkinghub.elsevier.com/retrieve/pii/S0045782509001820 (visited on 02/20/2020) (cit. on p. 14).

[14] D.J. Benson, S. Hartmann, Y. Bazilevs, et al. "Blended isogeometric shells". In: *Computer Methods in Applied Mechanics and Engineering* 255 (Mar. 2013), pp. 133–146. ISSN: 00457825. DOI: 10.1016/j.cma.2012.11.020. URL: https://linkinghub.elsevier.com/retrieve/pii/S0045782512003696 (visited on 02/20/2020) (cit. on p. 14).

[15] R Bonnerot and P Jamet. "Numerical computation of the free boundary for the two-dimensional Stefan problem by space-time finite elements". In: *Journal of Computational Physics* 25.2 (1977), pp. 163–181. ISSN: 0021-9991. DOI: https://doi.org/10.1016/0021-9991(77)90019-5. URL: http://www.sciencedirect.com/science/article/pii/0021999177900195 (cit. on p. 22).

[16] L. Boucinha, A. Gravouil, and A. Ammar. "Space–time proper generalized decompositions for the resolution of transient elastodynamic models". In: *Computer Methods in Applied Mechanics and Engineering* 255 (Mar. 2013), pp. 67–88. ISSN: 00457825. DOI: 10.1016/j.cma.2012.11.003. URL: https://linkinghub.elsevier.com/retrieve/pii/S0045782512003416 (visited on 09/26/2019) (cit. on p. 24).

[17] M. Buch, A. Idesman, R. Niekamp, et al. "Finite elements in space and time for parallel computing of viscoelastic deformation". In: *Computational Mechanics* 24.5 (Nov. 22, 1999), pp. 386–395. ISSN: 0178-7675, 1432-0924. DOI: 10.1007/s004660050459. URL: http://link.springer.com/10.1007/s004660050459 (visited on 09/26/2019) (cit. on pp. 22, 89).

[18] A. Buffa, C. de Falco, and G. Sangalli. "IsoGeometric Analysis: Stable elements for the 2D Stokes equation". In: *International Journal for Numerical Methods in Fluids* 65.11 (Apr. 20, 2011), pp. 1407–1422. ISSN: 02712091. DOI: 10.1002/fld.2337. URL: http://doi.wiley.com/10.1002/fld.2337 (visited on 02/20/2020) (cit. on p. 15).

[19] D. Burkhart, B. Hamann, and G. Umlauf. "Iso-geometric Finite Element Analysis Based on Catmull-Clark : ubdivision Solids". In: *Computer Graphics Forum* 29.5 (2010), pp. 1575–1584. DOI: 10.1111/j.1467-8659.2010.01766.x. eprint: https://onlinelibrary.wiley.com/doi/pdf/10.1111/j.1467-8659.2010.01766.x. URL: https://onlinelibrary.wiley.com/doi/abs/10.1111/j.1467-8659.2010.01766.x (cit. on p. 14).

[20] Rui P. R. Cardoso and J. M. A. Cesar de Sa. "Blending moving least squares techniques with NURBS basis functions for nonlinear isogeometric analysis". In: *Computational Mechanics* 53.6 (June 2014), pp. 1327–1340. ISSN: 0178-7675, 1432-0924. DOI: 10.1007/s00466-014-0977-5. URL: http://link.springer.com/10.1007/s00466-014-0977-5 (visited on 02/20/2020) (cit. on p. 15).

[21] K. S. Chung. "The fourth-dimention concept in the finite element analysis of transient heat transfer problems". In: *International Journal for Numerical Methods in Engineering* 17.3 (Mar. 1981), pp. 315–325. ISSN: 0029-5981, 1097-0207. DOI: 10.1002/nme.1620170302. URL: http://doi.wiley.com/10.1002/nme.1620170302 (visited on 03/23/2020) (cit. on p. 22).

[22] F. Costanzo and H. Huang. "Proof of unconditional stability for a single-field discontinuous Galerkin finite element formulation for linear elastodynamics". In: *Computer Methods in Applied Mechanics and Engineering* 194.18 (May 2005), pp. 2059–2076. ISSN: 00457825. DOI: 10.1016/j.cma.2004.07.011. URL: https://linkinghub.elsevier.com/retrieve/pii/S0045782504003676 (visited on 09/26/2019) (cit. on p. 20).

[23] J. Austin Cottrell, Thomas J. R. Hughes, and Yuri Bazilevs. *Isogeometric Analysis: Toward Integration of CAD and FEA*. 1st. Wiley Publishing, 2009. ISBN: 978-0-470-74873-2 (cit. on pp. 8, 14).

[24] Jiansong Deng, Falai Chen, Xin Li, et al. "Polynomial splines over hierarchical T-meshes". In: *Graphical Models* 70.4 (2008), pp. 76–86. ISSN: 1524-0703. DOI: https://doi.org/10.1016/j.gmod.2008.03.001. URL: http://www.sciencedirect.com/science/article/pii/S1524070308000039 (cit. on p. 14).

[25] M. Dittmann, M. Franke, İ. Temizer, et al. “Isogeometric Analysis and thermomechanical Mortar contact problems”. In: *Computer Methods in Applied Mechanics and Engineering* 274 (June 2014), pp. 192–212. ISSN: 00457825. DOI: 10.1016/j.cma.2014.02.012. URL: https://linkinghub.elsevier.com/retrieve/pii/S0045782514000693 (visited on 02/20/2020) (cit. on p. 15).

[26] Tor Dokken, Tom Lyche, and Kjell Fredrik Pettersen. “Polynomial splines over locally refined box-partitions”. In: *Computer Aided Geometric Design* 30.3 (2013), pp. 331–356. ISSN: 0167-8396. DOI: https://doi.org/10.1016/j.cagd.2012.12.005. URL: http://www.sciencedirect.com/science/article/pii/S0167839613000113 (cit. on p. 14).

[27] Serge Dumont, Franck Jourdan, and Tarik Madani. “4D Remeshing Using a Space-Time Finite Element Method for Elastodynamics Problems”. In: *Mathematical and Computational Applications* 23.2 (May 25, 2018), p. 29. ISSN: 2297-8747. DOI: 10.3390/mca23020029. URL: http://www.mdpi.com/2297-8747/23/2/29 (visited on 09/26/2019) (cit. on p. 21).

[28] T. Elguedj, Y. Bazilevs, V. M. Calo, et al. *B and F Projection Methods for Nearly Incompressible Linear and Nonlinear Elasticity and Plasticity using Higher-order NURBS Elements:* Fort Belvoir, VA: Defense Technical Information Center, Aug. 1, 2007. DOI: 10.21236/ADA478310. URL: http://www.dtic.mil/docs/citations/ADA478310 (visited on 02/20/2020) (cit. on p. 15).

[29] T. Elguedj and T.J.R. Hughes. “Isogeometric analysis of nearly incompressible large strain plasticity”. In: *Computer Methods in Applied Mechanics and Engineering* 268 (Jan. 2014), pp. 388–416. ISSN: 00457825. DOI: 10.1016/j.cma.2013.09.024. URL: https://linkinghub.elsevier.com/retrieve/pii/S004578251300251X (visited on 02/20/2020) (cit. on p. 15).

[30] Patrick Erbts and Alexander Düster. “Accelerated staggered coupling schemes for problems of thermoelasticity at finite strains”. In: *Computers & Mathematics with Applications* 64.8 (Oct. 2012), pp. 2408–2430. ISSN: 08981221. DOI: 10.1016/j.camwa.2012.05.010. URL: https://linkinghub.elsevier.com/retrieve/pii/S0898122112004002 (visited on 09/26/2019) (cit. on p. 85).

[31] David R. Forsey and Richard H. Bartels. “Hierarchical B-Spline Refinement”. In: *SIGGRAPH Comput. Graph.* 22.4 (June 1988), pp. 205–212. ISSN: 0097-8930. DOI: 10.1145/378456.378512. URL: https://doi.org/10.1145/378456.378512 (cit. on p. 14).

[32] David R. Forsey and Richard H. Bartels. “Surface Fitting with Hierarchical Splines”. In: *ACM Trans. Graph.* 14.2 (Apr. 1995), pp. 134–161. ISSN: 0730-0301. DOI: 10.1145/221659.221665. URL: https://doi.org/10.1145/221659.221665 (cit. on p. 14).

[33] Leopoldo Penna Franca and Eduardo Gomes Dutra Do Carmo. "The Galerkin gradient least-squares method". In: *Computer Methods in Applied Mechanics and Engineering* 74.1 (1989), pp. 41–54. ISSN: 0045-7825. DOI: https://doi.org/10.1016/0045-7825(89)90085-6. URL: http://www.sciencedirect.com/science/article/pii/0045782589900856 (cit. on p. 34).

[34] Donald A. French. "A space-time finite element method for the wave equation". In: *Computer Methods in Applied Mechanics and Engineering* 107.1 (Aug. 1993), pp. 145–157. ISSN: 00457825. DOI: 10.1016/0045-7825(93)90172-T. URL: https://linkinghub.elsevier.com/retrieve/pii/004578259390172T (visited on 09/26/2019) (cit. on pp. 19, 33).

[35] Martin J. Gander and Martin Neumüller. "Analysis of a New Space-Time Parallel Multigrid Algorithm for Parabolic Problems". In: *SIAM Journal on Scientific Computing* 38.4 (2016), A2173–A2208. DOI: 10.1137/15M1046605. eprint: https://doi.org/10.1137/15M1046605. URL: https://doi.org/10.1137/15M1046605 (cit. on p. 25).

[36] P. Germain, Q.S. Nguyen, and P. Suquet. "Continuum Thermodynamics". In: *Journal of Applied Mechanics* 50 (4b 1983), pp. 1010–1020. DOI: 10.1115/1.3167184. URL: http://dx.doi.org/10.1115/1.3167184 (cit. on p. 97).

[37] C. Hesch, S. Schuß, M. Dittmann, et al. "Variational space–time elements for large-scale systems". In: *Computer Methods in Applied Mechanics and Engineering* 326 (Nov. 2017), pp. 541–572. ISSN: 00457825. DOI: 10.1016/j.cma.2017.08.020. URL: https://linkinghub.elsevier.com/retrieve/pii/S004578251730600X (visited on 03/23/2020) (cit. on pp. 23, 24, 26, 59).

[38] Hans M. Hilber, Thomas J. R. Hughes, and Robert L. Taylor. "Improved numerical dissipation for time integration algorithms in structural dynamics". In: *Earthquake Engineering & Structural Dynamics* 5.3 (1977), pp. 283–292. DOI: 10.1002/eqe.4290050306. eprint: https://onlinelibrary.wiley.com/doi/pdf/10.1002/eqe.4290050306. URL: https://onlinelibrary.wiley.com/doi/abs/10.1002/eqe.4290050306 (cit. on pp. 15, 16, 45).

[39] Christoph Hofer, Ulrich Langer, Martin Neumuller, et al. "Time-Multipatch Discontinuous Galerkin Space-Time Isogeometric Analysis of Parabolic Evolution Problems". In: (), p. 24 (cit. on pp. 25, 26, 107).

[40] G. A. HOLZAPFEL. "ON LARGE STRAIN VISCOELASTICITY: CONTINUUM FORMULATION AND FINITE ELEMENT APPLICATIONS TO ELASTOMERIC STRUCTURES". In: *International Journal for Numerical Methods in Engineering* 39.22 (1996), pp. 3903–3926. DOI: 10.1002/(SICI)1097-0207(19961130)39:22<3903::AID-NME34>3.0.CO;2-C. eprint: https://onlinelibrary.wiley.com/doi/pdf/10.1002/%28SICI%291097-0207%2819961130%2939%3A22%3C3903%3A%3AAID-NME34%3E3.0.CO%3B2-C. URL: https://onlinelibrary.wiley.com/doi/abs/10.

1002/%28SICI%291097-0207%2819961130%2939%3A22%3C3903%3A%3AAID-NME34%3E3.0.CO%3B2-C (cit. on p. 79).

[41] L.-J. Hou and D.A. Peters. "Application of Triangular Space-Time Finite Elements to Problems of Wave Propagation". In: *Journal of Sound and Vibration* 173.5 (June 1994), pp. 611–632. ISSN: 0022460X. DOI: 10.1006/jsvi.1994.1250. URL: https://linkinghub.elsevier.com/retrieve/pii/S0022460X84712508 (visited on 11/25/2019) (cit. on p. 21).

[42] H. Huang and F. Costanzo. "On the use of space–time finite elements in the solution of elasto-dynamic problems with strain discontinuities". In: *Computer Methods in Applied Mechanics and Engineering* 191.46 (Nov. 2002), pp. 5315–5343. ISSN: 00457825. DOI: 10.1016/S0045-7825(02)00460-7. URL: https://linkinghub.elsevier.com/retrieve/pii/S0045782502004607 (visited on 09/26/2019) (cit. on p. 20).

[43] T.J.R. Hughes, J.A. Cottrell, and Y. Bazilevs. "Isogeometric analysis: CAD, finite elements, NURBS, exact geometry and mesh refinement". In: *Computer Methods in Applied Mechanics and Engineering* 194.39 (Oct. 2005), pp. 4135–4195. ISSN: 00457825. DOI: 10.1016/j.cma.2004.10.008. URL: https://linkinghub.elsevier.com/retrieve/pii/S0045782504005171 (visited on 11/30/2019) (cit. on p. 7).

[44] T.J.R. Hughes, A. Reali, and G. Sangalli. "Duality and unified analysis of discrete approximations in structural dynamics and wave propagation: Comparison of p-method finite elements with k-method NURBS". In: *Computer Methods in Applied Mechanics and Engineering* 197.49 (Sept. 2008), pp. 4104–4124. ISSN: 00457825. DOI: 10.1016/j.cma.2008.04.006. URL: https://linkinghub.elsevier.com/retrieve/pii/S0045782508001618 (visited on 02/26/2020) (cit. on p. 15).

[45] Thomas J. R. Hughes. *The finite element method: linear static and dynamic finite element analysis*. Englewood Cliffs, N.J: Prentice-Hall, 1987. 803 pp. ISBN: 978-0-13-317025-2 (cit. on p. 7).

[46] Thomas J.R. Hughes and Gregory M. Hulbert. "Space-time finite element methods for elastodynamics: Formulations and error estimates". In: *Computer Methods in Applied Mechanics and Engineering* 66.3 (Feb. 1988), pp. 339–363. ISSN: 00457825. DOI: 10.1016/0045-7825(88)90006-0. URL: https://linkinghub.elsevier.com/retrieve/pii/0045782588900060 (visited on 09/26/2019) (cit. on pp. 17, 41).

[47] Gregory M. Hulbert. "Discontinuity-capturing operators for elastodynamics". In: *Computer Methods in Applied Mechanics and Engineering* 96.3 (May 1992), pp. 409–426. ISSN: 00457825. DOI: 10.1016/0045-7825(92)90073-S. URL: https://linkinghub.elsevier.com/retrieve/pii/004578259290073S (visited on 09/26/2019) (cit. on pp. 19, 33, 107).

[48] Gregory M. Hulbert and Thomas J.R. Hughes. "Space-time finite element methods for second-order hyperbolic equations". In: *Computer Methods in Applied Mechanics and Engineering* 84.3 (Dec. 1990), pp. 327–348. ISSN: 00457825. DOI: 10.1016/0045-7825(90)90082-W. URL: https://linkinghub.elsevier.com/retrieve/pii/004578259090082W (visited on 09/26/2019) (cit. on pp. 17–20, 33, 34, 107).

[49] Alexander V. Idesman. "Solution of linear elastodynamics problems with space–time finite elements on structured and unstructured meshes". In: *Computer Methods in Applied Mechanics and Engineering* 196.9 (Feb. 2007), pp. 1787–1815. ISSN: 00457825. DOI: 10.1016/j.cma.2006.09.019. URL: https://linkinghub.elsevier.com/retrieve/pii/S0045782506003197 (visited on 09/26/2019) (cit. on p. 21).

[50] Alexander Idesman, Rainer Niekamp, and Erwin Stein. "Continuous and discontinuous Galerkin methods with finite elements in space and time for parallel computing of viscoelastic deformation". In: *Computer Methods in Applied Mechanics and Engineering* 190 (Nov. 2000), pp. 1049–1063. DOI: 10.1016/S0045-7825(99)00463-6 (cit. on p. 22).

[51] Alexander Idesman, Rainer Niekamp, and Erwin Stein. "Finite elements in space and time for generalized viscoelastic Maxwell model". In: *Computational Mechanics* 27 (Jan. 2001), pp. 49–60. DOI: 10.1007/s004660000213 (cit. on p. 23).

[52] P. Jamet and R. Bonnerot. "Numerical solution of the eulerian equations of compressible flow by a finite element method which follows the free boundary and the interfaces". In: *Journal of Computational Physics* 18.1 (1975), pp. 21–45. ISSN: 0021-9991. DOI: https://doi.org/10.1016/0021-9991(75)90100-X. URL: http://www.sciencedirect.com/science/article/pii/002199917590100X (cit. on p. 22).

[53] C Johnson and J Pitkäranta. "An Analysis of the Discontinuous Galerkin Method for a Scalar Hyperbolic Equation". In: (), p. 26 (cit. on p. 20).

[54] Claes Johnson. "Discontinuous Galerkin finite-element methods for 2nd-order hyperbolic problems". In: *Computer Methods in Applied Mechanics and Engineering - COMPUT METHOD APPL MECH ENG* 107 (Aug. 1993), pp. 117–129. DOI: 10.1016/0045-7825(93)90170-3 (cit. on p. 20).

[55] Claes Johnson, Uno Nävert, and Juhani Pitkäranta. "Finite element methods for linear hyperbolic problems". In: *Computer Methods in Applied Mechanics and Engineering* 45.1 (Sept. 1984), pp. 285–312. ISSN: 00457825. DOI: 10.1016/0045-7825(84)90158-0. URL: https://linkinghub.elsevier.com/retrieve/pii/0045782584901580 (visited on 09/26/2019) (cit. on p. 20).

[56] Reese E Jones and Panayiotis Papadopoulos. "A novel three-dimensional contact ÿnite element based on smooth pressure interpolations". In: (2001), p. 21 (cit. on p. 15).

[57] C. Kadapa, W.G. Dettmer, and D. Perić. "NURBS based least-squares finite element methods for fluid and solid mechanics: NURBS-BASED LSFEM FOR FLUID AND SOLID MECHANICS". In: *International Journal for Numerical Methods in Engineering* 101.7 (Feb. 17, 2015), pp. 521–539. ISSN: 00295981. DOI: 10.1002/nme.4765. URL: http://doi.wiley.com/10.1002/nme.4765 (visited on 02/20/2020) (cit. on p. 15).

[58] C. Kadapa, W.G. Dettmer, and D. Perić. "Subdivision based mixed methods for isogeometric analysis of linear and nonlinear nearly incompressible materials". In: *Computer Methods in Applied Mechanics and Engineering* 305 (June 2016), pp. 241–270. ISSN: 00457825. DOI: 10.1016/j.cma.2016.03.013. URL: https://linkinghub.elsevier.com/retrieve/pii/S0045782516300950 (visited on 02/20/2020) (cit. on pp. 15, 52).

[59] D.K. Khalmanova and F. Costanzo. "A space–time discontinuous Galerkin finite element method for fully coupled linear thermo-elasto-dynamic problems with strain and heat flux discontinuities". In: *Computer Methods in Applied Mechanics and Engineering* 197.13 (Feb. 2008), pp. 1323–1342. ISSN: 00457825. DOI: 10.1016/j.cma.2007.11.005. URL: https://linkinghub.elsevier.com/retrieve/pii/S0045782507004495 (visited on 09/26/2019) (cit. on pp. 24, 62, 107).

[60] J. Kiendl, Y. Bazilevs, M.-C. Hsu, et al. "The bending strip method for isogeometric analysis of Kirchhoff–Love shell structures comprised of multiple patches". In: *Computer Methods in Applied Mechanics and Engineering* 199.37 (Aug. 2010), pp. 2403–2416. ISSN: 00457825. DOI: 10.1016/j.cma.2010.03.029. URL: https://linkinghub.elsevier.com/retrieve/pii/S0045782510001064 (visited on 02/20/2020) (cit. on p. 14).

[61] J. Kiendl, K.-U. Bletzinger, J. Linhard, et al. "Isogeometric shell analysis with Kirchhoff–Love elements". In: *Computer Methods in Applied Mechanics and Engineering* 198.49 (Nov. 2009), pp. 3902–3914. ISSN: 00457825. DOI: 10.1016/j.cma.2009.08.013. URL: https://linkinghub.elsevier.com/retrieve/pii/S0045782509002680 (visited on 02/20/2020) (cit. on p. 14).

[62] Takashi Kuraishi, Kenji Takizawa, and Tayfun E. Tezduyar. "Space–time computational analysis of tire aerodynamics with actual geometry, road contact, tire deformation, road roughness and fluid film". In: *Computational Mechanics* 64.6 (Dec. 2019), pp. 1699–1718. ISSN: 0178-7675, 1432-0924. DOI: 10.1007/s00466-019-01746-8. URL: http://link.springer.com/10.1007/s00466-019-01746-8 (visited on 04/16/2020) (cit. on p. 26).

[63] U. Langer, Svetlana Matculevich, and Sergey Repin. "A posteriori error estimates for space-time IgA approximations to parabolic initial boundary value problems". In: *arXiv: Numerical Analysis* (2016) (cit. on p. 25).

[64] Ulrich Langer, Stephen E. Moore, and Martin Neumüller. "Space-Time Isogeometric Analysis of Parabolic Evolution Equations". In: *Computer Methods in Applied Mechanics and Engineering* 306 (July 2016), pp. 342–363. ISSN: 00457825. DOI: 10.1016/j.cma.2016.03.042. arXiv: 1509.02008. URL: http://arxiv.org/abs/1509.02008 (visited on 09/26/2019) (cit. on pp. 24, 25, 59).

[65] F. Larsson, P. Hansbo, and K. Runesson. "Space-time finite elements and an adaptive strategy for the coupled thermoelasticity problem". In: *International Journal for Numerical Methods in Engineering* 56.2 (2003). _eprint: https://onlinelibrary.wiley.com/doi/pdf/10.1002/nme.563, pp. 261–293. ISSN: 1097-0207. DOI: 10.1002/nme.563. URL: http://onlinelibrary.wiley.com/doi/abs/10.1002/nme.563 (visited on 04/21/2020) (cit. on pp. 23, 62, 107).

[66] Stéphane Lejeunes and Dominique Eyheramendy. "Hybrid free energy approach for nearly incompressible behaviors at finite strain". In: *Continuum Mechanics and Thermodynamics* (2018). ISSN: 1432-0959. DOI: 10.1007/s00161-018-0680-4. URL: https://doi.org/10.1007/s00161-018-0680-4 (cit. on pp. 50, 51, 78, 79).

[67] Hong Li, Zhihui Zhao, and Zhendong Luo. "A space-time continuous finite element method for 2D viscoelastic wave equation". In: *Boundary Value Problems* 2016.1 (Dec. 2016), p. 53. ISSN: 1687-2770. DOI: 10.1186/s13661-016-0563-1. URL: http://www.boundaryvalueproblems.com/content/2016/1/53 (visited on 09/26/2019) (cit. on pp. 23, 107).

[68] X. D. LI and N.-E. WIBERG. "STRUCTURAL DYNAMIC ANALYSIS BY A TIME-DISCONTINUOUS GALERKIN FINITE ELEMENT METHOD". In: *International Journal for Numerical Methods in Engineering* 39.12 (1996), pp. 2131–2152. DOI: 10.1002/(SICI)1097-0207(19960630)39:12<2131::AID-NME947>3.0.CO;2-Z. eprint: https://onlinelibrary.wiley.com/doi/pdf/10.1002/%28SICI%291097-0207%2819960630%2939%3A12%3C2131%3A%3AAID-NME947%3E3.0.CO%3B2-Z. URL: https://onlinelibrary.wiley.com/doi/abs/10.1002/%28SICI%291097-0207%2819960630%2939%3A12%3C2131%3A%3AAID-NME947%3E3.0.CO%3B2-Z (cit. on p. 21).

[69] X.D. Li and N.-E. Wiberg. "Implementation and adaptivity of a space-time finite element method for structural dynamics". In: *Computer Methods in Applied Mechanics and Engineering* 156.1 (Apr. 1998), pp. 211–229. ISSN: 00457825. DOI: 10.1016/S0045-7825(97)00207-7. URL: https://linkinghub.elsevier.com/retrieve/pii/S0045782597002077 (visited on 09/26/2019) (cit. on p. 21).

[70] Nguyen Dang Manh, Anton Evgrafov, Allan Roulund Gersborg, et al. "Isogeometric shape optimization of vibrating membranes". In: *Computer Methods in Applied Mechanics and Engineering* 200.13 (Mar. 2011), pp. 1343–1353. ISSN: 00457825. DOI: 10.1016/j.cma.2010.12.015. URL: https:

//linkinghub.elsevier.com/retrieve/pii/S0045782510003713 (visited on 02/26/2020) (cit. on p. 15).

[71] Arif Masud and Thomas J.R. Hughes. "A space-time Galerkin/least-squares finite element formulation of the Navier-Stokes equations for moving domain problems". In: *Computer Methods in Applied Mechanics and Engineering* 146.1 (July 1997), pp. 91–126. ISSN: 00457825. DOI: 10.1016/S0045-7825(96)01222-4. URL: https://linkinghub.elsevier.com/retrieve/pii/S0045782596012224 (visited on 02/20/2020) (cit. on p. 22).

[72] C. Miehe, F. Aldakheel, and S. Mauthe. "Mixed variational principles and robust finite element implementations of gradient plasticity at small strains". In: *International Journal for Numerical Methods in Engineering* 94.11 (2013), pp. 1037–1074. DOI: 10.1002/nme.4486. eprint: https://onlinelibrary.wiley.com/doi/pdf/10.1002/nme.4486. URL: https://onlinelibrary.wiley.com/doi/abs/10.1002/nme.4486 (cit. on p. 97).

[73] Christian Miehe. "Variational gradient plasticity at finite strains. Part I: Mixed potentials for the evolution and update problems of gradient-extended dissipative solids". In: *Computer Methods in Applied Mechanics and Engineering* 268 (2014), pp. 677–703. ISSN: 0045-7825. DOI: https://doi.org/10.1016/j.cma.2013.03.014. URL: http://www.sciencedirect.com/science/article/pii/S0045782513000650 (cit. on p. 97).

[74] Christian Mollet. "Stability of Petrov–Galerkin Discretizations: Application to the Space-Time Weak Formulation for Parabolic Evolution Problems". In: *Computational Methods in Applied Mathematics* 14 (2014), pp. 231–255 (cit. on p. 23).

[75] Monica Montardini, Matteo Negri, Giancarlo Sangalli, et al. *Space-time least-squares isogeometric method and efficient solver for parabolic problems*. 2018. arXiv: 1809.10026 [math.NA] (cit. on p. 26).

[76] Stephen Edward Moore. "A Stable Space-Time Finite Element Method for Parabolic Evolution Problems". In: *Calcolo* 55.2 (June 2018), p. 18. ISSN: 0008-0624, 1126-5434. DOI: 10.1007/s10092-018-0261-8. arXiv: 1706.07065. URL: http://arxiv.org/abs/1706.07065 (visited on 02/18/2020) (cit. on p. 23).

[77] Stephen Edward Moore. "SPACE-TIME MULTI-PATCH DISCONTINUOUS GALERKIN ISOGEOMETRIC ANALYSIS FOR PARABOLIC EVOLUTION PROBLEMS". In: (), p. 31 (cit. on pp. 25, 26, 107).

[78] H. Nguyen and J. Reynen. "A space-time least-square finite element scheme for advection-diffusion equations". In: *Computer Methods in Applied Mechanics and Engineering* 42.3 (1984), pp. 331–342. ISSN: 0045-7825. DOI: https://doi.org/10.1016/0045-7825(84)90012-4. URL: http://www.sciencedirect.com/science/article/pii/0045782584900124 (cit. on p. 22).

[79] Peter Nørtoft Nielsen, Allan Roulund Gersborg, Jens Gravesen, et al. "Discretizations in isogeometric analysis of Navier–Stokes flow". In: *Computer Methods in Applied Mechanics and Engineering* 200.45 (Oct. 2011), pp. 3242–3253. ISSN: 00457825. DOI: 10.1016/j.cma.2011.06.007. URL: https://linkinghub.elsevier.com/retrieve/pii/S0045782511002258 (visited on 02/20/2020) (cit. on p. 15).

[80] Matthieu Occelli. "Explicit dynamics isogeometric analysis : lr b-splines implementation in the radioss solver". PhD thesis. Nov. 2018 (cit. on p. 14).

[81] J. Tinsley Oden. "A general theory of finite elements. II. Applications". In: *International Journal for Numerical Methods in Engineering* 1.3 (1969), pp. 247–259. ISSN: 1097-0207. DOI: 10.1002/nme.1620010304. URL: https://onlinelibrary.wiley.com/doi/abs/10.1002/nme.1620010304 (visited on 09/26/2019) (cit. on pp. 15, 16, 21).

[82] L. Piegl and W. Tiller. *The NURBS Book*. Spinger, 1997 (cit. on p. 102).

[83] Adam Podhorecki. "The viscoelastic space-time element". In: *Computers & Structures* 23.4 (Jan. 1986), pp. 535–544. ISSN: 00457949. DOI: 10.1016/0045-7949(86)90096-9. URL: https://linkinghub.elsevier.com/retrieve/pii/0045794986900969 (visited on 09/26/2019) (cit. on pp. 22, 89, 107).

[84] Xiaoping Qian. "Full analytical sensitivities in NURBS based isogeometric shape optimization". In: *Computer Methods in Applied Mechanics and Engineering* 199.29 (June 2010), pp. 2059–2071. ISSN: 00457825. DOI: 10.1016/j.cma.2010.03.005. URL: https://linkinghub.elsevier.com/retrieve/pii/S0045782510000812 (visited on 02/26/2020) (cit. on p. 15).

[85] J. Réthoré, A. Gravouil, and A. Combescure. "A combined space–time extended finite element method". In: *International Journal for Numerical Methods in Engineering* 64.2 (2005). _eprint: https://onlinelibrary.wiley.com/doi/pdf/10.1002/nme.1368 pp. 260–284. ISSN: 1097-0207. DOI: 10.1002/nme.1368. URL: https://onlinelibrary.wiley.com/doi/abs/10.1002/nme.1368 (visited on 03/28/2020) (cit. on p. 24).

[86] M.A. Scott, D.C. Thomas, and E.J. Evans. "Isogeometric spline forests". In: *Computer Methods in Applied Mechanics and Engineering* 269 (2014), pp. 222–264. ISSN: 0045-7825. DOI: https://doi.org/10.1016/j.cma.2013.10.024. URL: http://www.sciencedirect.com/science/article/pii/S0045782513002764 (cit. on p. 14).

[87] Farzin Shakib and Thomas J.R. Hughes. "A new finite element formulation for computational fluid dynamics: IX. Fourier analysis of space-time Galerkin/least-squares algorithms". In: *Computer Methods in Applied Mechanics and Engineering* 87.1 (May 1991), pp. 35–58. ISSN: 00457825. DOI: 10.1016/0045-7825(91)90145-V. URL: https://linkinghub.elsevier.com/retrieve/pii/004578259190145V (visited on 11/25/2019) (cit. on p. 22).

[88] F. Sidoroff. "Variables internes en viscoÃ©lasticitÃ©, 3. milieux avec plusieurs configurations intermÃ©diaires". In: *J. MÃ©c.* 15.1 (1976), pp. 85–118 (cit. on p. 93).

[89] F. Sidoroff. "RhÃ©ologie non-linÃ©aire et variables internes tensorielles." In: *Symposium franco-polonais*. Cracovie, 1977 (cit. on p. 93).

[90] "STRUCTURAL DYNAMIC ANALYSIS BY A TIME-DISCONTINUOUS GALERKIN FINITE ELEMENT METHOD". In: (), p. 22 (cit. on p. 21).

[91] Kenji Takizawa and Tayfun E. Tezduyar. "Multiscale space–time fluid–structure interaction techniques". In: *Computational Mechanics* 48.3 (Sept. 2011), pp. 247–267. ISSN: 0178-7675, 1432-0924. DOI: 10.1007/s00466-011-0571-z. URL: http://link.springer.com/10.1007/s00466-011-0571-z (visited on 02/20/2020) (cit. on pp. 22, 107).

[92] Kenji Takizawa and Tayfun E. Tezduyar. "Space–time computation techniques with continuous representation in time (ST-C)". In: *Computational Mechanics* 53.1 (Jan. 2014), pp. 91–99. ISSN: 0178-7675, 1432-0924. DOI: 10.1007/s00466-013-0895-y. URL: http://link.springer.com/10.1007/s00466-013-0895-y (visited on 02/20/2020) (cit. on p. 26).

[93] Kenji Takizawa, Tayfun E. Tezduyar, and Yuto Otoguro. "Stabilization and discontinuity-capturing parameters for space–time flow computations with finite element and isogeometric discretizations". In: *Computational Mechanics* 62.5 (Nov. 2018), pp. 1169–1186. ISSN: 0178-7675, 1432-0924. DOI: 10.1007/s00466-018-1557-x. URL: http://link.springer.com/10.1007/s00466-018-1557-x (visited on 02/20/2020) (cit. on pp. 22, 107).

[94] R. L. Taylor. "Isogeometric analysis of nearly incompressible solids". In: *International Journal for Numerical Methods in Engineering* 87.1 (July 8, 2011), pp. 273–288. ISSN: 00295981. DOI: 10.1002/nme.3048. URL: http://doi.wiley.com/10.1002/nme.3048 (visited on 02/20/2020) (cit. on p. 15).

[95] İ. Temizer, P. Wriggers, and T.J.R. Hughes. "Contact treatment in isogeometric analysis with NURBS". In: *Computer Methods in Applied Mechanics and Engineering* 200.9 (Feb. 2011), pp. 1100–1112. ISSN: 00457825. DOI: 10.1016/j.cma.2010.11.020. URL: https://linkinghub.elsevier.com/retrieve/pii/S0045782510003440 (visited on 02/20/2020) (cit. on p. 15).

[96] İ. Temizer, P. Wriggers, and T.J.R. Hughes. "Three-dimensional mortar-based frictional contact treatment in isogeometric analysis with NURBS". In: *Computer Methods in Applied Mechanics and Engineering* 209-212 (Feb. 2012), pp. 115–128. ISSN: 00457825. DOI: 10.1016/j.cma.2011.10.014. URL: https://linkinghub.elsevier.com/retrieve/pii/S0045782511003355 (visited on 02/20/2020) (cit. on p. 15).

[97] Lonny L. Thompson and Dantong He. "Adaptive space–time finite element methods for the wave equation on unbounded domains". In: *Computer Methods in Applied Mechanics and Engineering* 194.18 (May 2005), pp. 1947–2000. ISSN: 00457825. DOI: 10.1016/j.cma.2004.07.019. URL: https://linkinghub.elsevier.com/retrieve/pii/S0045782504003639 (visited on 09/26/2019) (cit. on p. 22).

[98] Lonny L. Thompson and Peter M. Pinsky. "A space-time finite element method for structural acoustics in infinite domains part 1: Formulation, stability and convergence". In: *Computer Methods in Applied Mechanics and Engineering* 132.3 (June 1996), pp. 195–227. ISSN: 00457825. DOI: 10.1016/0045-7825(95)00955-8. URL: https://linkinghub.elsevier.com/retrieve/pii/0045782595009558 (visited on 02/20/2020) (cit. on p. 22).

[99] Wolfgang A. Wall, Moritz A. Frenzel, and Christian Cyron. "Isogeometric structural shape optimization". In: *Computer Methods in Applied Mechanics and Engineering* 197.33 (June 2008), pp. 2976–2988. ISSN: 00457825. DOI: 10.1016/j.cma.2008.01.025. URL: https://linkinghub.elsevier.com/retrieve/pii/S0045782508000509 (visited on 02/26/2020) (cit. on p. 15).

[100] Dongdong Wang, Wei Liu, and Hanjie Zhang. "Novel higher order mass matrices for isogeometric structural vibration analysis". In: *Computer Methods in Applied Mechanics and Engineering* 260 (June 2013), pp. 92–108. ISSN: 00457825. DOI: 10.1016/j.cma.2013.03.011. URL: https://linkinghub.elsevier.com/retrieve/pii/S0045782513000625 (visited on 02/26/2020) (cit. on p. 15).

[101] Inc. Wolfram Research. *Mathematica, Version 12.1*. Champaign, IL, 2020. URL: https://www.wolfram.com/mathematica (cit. on p. 103).

[102] Lei Zhang. "An isogeometric analysis approach for coupled multi-field problems at large strain". Theses. Ecole Centrale Marseille, Dec. 2016. URL: https://tel.archives-ouvertes.fr/tel-01525035 (cit. on pp. 4, 71).

Appendices

A. Heat Equation

A.1. Model Problem

The parabolic heat equation has the following form:

$$\rho C\dot{\theta} + div\mathbf{q} = \mathbf{r} \tag{.1}$$

where θ is the temperature field, the vector field $\mathbf{q}$ denotes the heat flux, $\mathbf{r}$ is the external heat supply, ρ is the material density, C is the specific heat, $q = -K_\theta grad\theta$ is the heat flux density linearly dependent of the gradient of the temperature (Fourier's law); K_θ is the conductivity.

The problem's boundary and initial conditions are the following:

$$\begin{aligned} &\theta = \mathbf{h}(\mathbf{x}, t) \text{ for } \mathbf{x} \in \Gamma_\theta, t \in [0, T] \\ &\mathbf{q}.\mathbf{n} = \bar{\mathbf{q}}(\mathbf{x}, t) \text{ for } \mathbf{x} \in \Gamma_\theta, t \in [0, T] \end{aligned} \tag{.2}$$

where $\mathbf{n}(\mathbf{x})$ is the normal to the boundary Γ_θ, $\mathbf{h}$ is the prescribed boundary temperature, $\bar{\mathbf{q}}$ is the prescribed boundary heat flux.

A.2. Space-Time Variational Formulation

We use classical test functions for this simple parabolic problem and so we have the following space-time variational formulation:

$$\begin{aligned} &\text{Find } \theta(\mathbf{x}, t)) \in \mathcal{H}^\theta, \text{ such that } \forall\ \delta\theta(\mathbf{x}, t) \in \mathcal{H}_0^\theta \\ &\int_Q \rho C\dot{\theta}\delta\theta dQ + \int_Q K_\theta grad\theta grad\delta\theta dQ - \int_0^T \int_{\Gamma_\theta} \mathbf{q}.\mathbf{n}\delta\theta dQ - \int_Q r\delta\theta dQ = 0 \end{aligned} \tag{.3}$$

A.3. Convergence Tests

We consider the space-time domain $Q = (0, 1)^2$. The parameters of the problem are chosen such that $K_\theta = 100W/(m.K)$, $C = 1\frac{kg.m^2}{K.s^2}$ and $\rho = 1kg.m^{-3}$. The right-hand side of the equation is calculated such that $\theta_{exact} = sin(2\pi x)sin(2\pi t)$, and therefore we have $\mathbf{f} = 2\pi sin(2\pi x)cos(2\pi t) + 4\pi^2 K_\theta sin(2\pi x)sin(2\pi t)$.

The domain of study is illustrated in Figure .1 with homogeneous Dirichlet boundary and initial conditions. The convergence curves concerning L^2 errors of

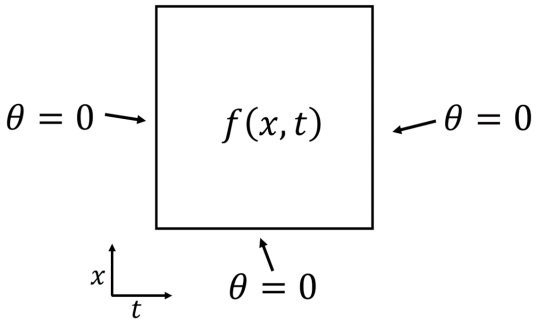

Figure .1. – Domain of study in space-time with homogeneous boundary and initial conditions for the heat equation

the temperature field for this space-time IGA problem are represented for several degrees p of B-spline functions of maximum continuity order and several values of thermal conductivity K_θ.

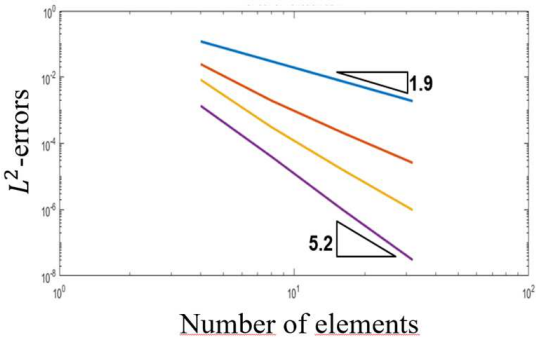

Figure .2. – Convergence curves for the L^2-errors concerning the heat equation for degrees $p = 1, 2, 3$ and 4

As it is shown in Figure .2, optimal convergence rates are obtained. In other words, we always find a slope of $p + 1$, where p is the degree of the basis functions. The formulation of the problem is convergent on the test case considered.

B. Elastodynamics

B.1. Test functions vs their derivatives in time

A numerical study is given in order to be able to compare and decide which type of test functions works better than the other and gives a more accurate response. To do so, we will first start by a simple test case where we will be taking the classical linear elastodynamics equation applied on a 1D elastic bar of length L.

Homogeneous Dirichlet initial and boundary conditions are taken for the sake of simplicity. The space-time domain is represented in Figure .3 . We impose the body load $\mathbf{f} = \rho 2sin(2\pi x)[(t-T)^2 + 4t(t-T) + t^2] + 4\pi^2 t^2 (t-T)^2 sin(2\pi x)$ such that the exact solution is: $u_{exact} = t^2(t-T)^2 sin(2\pi x)$.

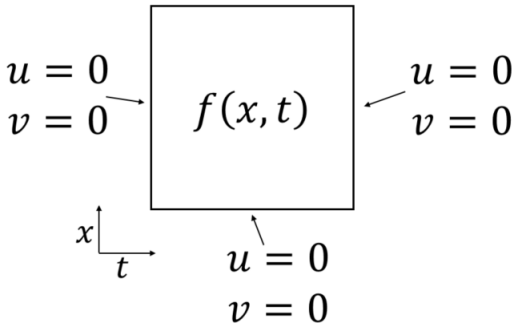

Figure .3. – The space-time domain concerning the wave propagation problem along with the corresponding boundary and initial conditions

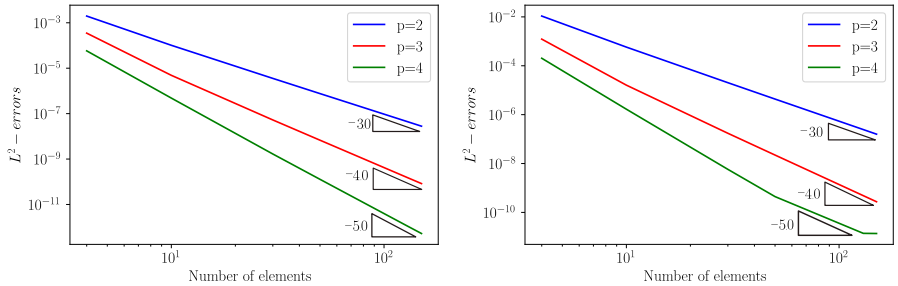

(a) Space-time errors for displacement (b) Space-time errors for velocity

Figure .4. – Convergence curves in L^2-errors for displacement and velocity concerning the elastodynamics problem for degrees $p = 1, 2$ and 3 using classical test functions

The convergence curves of this problem in norm L^2 are plotted and optimal convergence curves are obtained for both cases. Figure .4 shows the optimal convergence rates obtained for the displacement using a variational formulation containing classical test functions. Obviously, optimal convergence rates are obtained. In other words, we obtain slopes of $p + 1$ for every degree p used.

Optimal convergence curves were also obtained for the case where the variational formulation consisted on test functions derived in time. These convergence curves are plotted in Figure .5 and the figure shows that optimal convergence rates are obtained for this test case also.

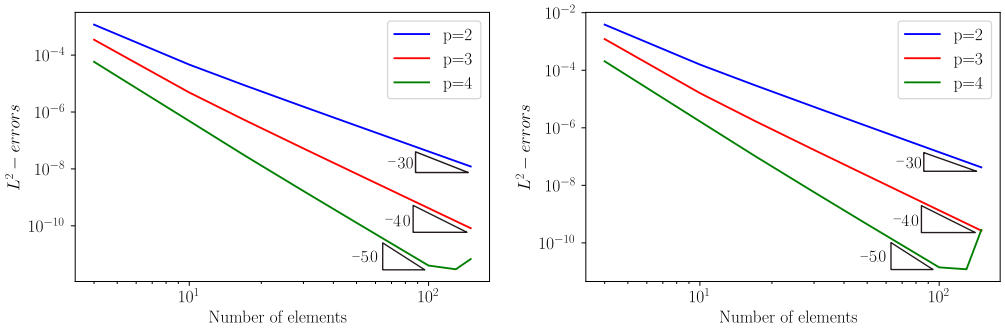

(a) Space-time errors for displacement

(b) Space-time errors for velocity

Figure .5. – Convergence curves in L^2-errors for displacement and velocity concerning the elastodynamics problem for degrees $p = 1, 2$ and 3 using test functions derived in time

It is noticed from the convergence curves that one must not use a large number of elements in the discretization, especially when using a high value of the degree p (such as $p = 4$, for example).